KERNFORSCHUNGSZENTRUM

KARLSRUHE

Juli 1977 KFK 2485

Institut für Kernphysik

A Study of the (π^-, 2n) Reaction on Nuclei of the 1p-Shell

B. Bassalleck

GESELLSCHAFT
FÜR
KERNFORSCHUNG M.B.H.

KARLSRUHE

GESELLSCHAFT FÜR KERNFORSCHUNG M. B. H.

KARLSRUHE

KERNFORSCHUNGSZENTRUM KARLSRUHE

KFK 2485

Institut für Kernphysik

A STUDY OF THE (π^-, 2n) REACTION ON NUCLEI OF THE 1p-SHELL[+)]

B. Bassalleck

[+)] von der Fakultät für Physik der Universität Karlsruhe genehmigte Dissertation

Gesellschaft für Kernforschung mbH., Karlsruhe

A STUDY OF THE (π^-, 2n) REACTION ON NUCLEI OF THE 1p-SHELL

Abstract

At the CERN-SC II the (π^-, 2n) reaction was investigated in a kinematically complete experiment. The target nuclei were ^{6}Li, ^{7}Li, ^{9}Be, ^{10}B, ^{12}C, ^{14}N and ^{16}O. The latter was studied over the widest angular range and with the highest statistics.

The two neutrons emitted were detected in coincidence by two large-area position-sensitive time-of-flight counters. The resolution achieved in excitation energy of the residual nucleus was 3-6 MeV. This is better by a factor of 3-5 than the values achieved in previous (π^-, 2n) measurements.

For definite residual states or regions in excitation energy distributions in the following variables are given: neutron energy, angle spanned by the two neutron momenta, sum and difference of the momenta of the two neutrons emitted, and angle spanned by these two momenta. All these distributions are fully corrected with respect to efficiency and geometrical acceptance. The excitation energy spectra are given in absolute rates per stopped pion.

Information has been obtained about the spectral function $S_{np}(q, E_s)$ and quantum numbers of the neutron proton pairs involved in the absorption. Conclusions on the reaction mechanism are drawn.

The results are compared with theoretical predictions as well as with other two-nucleon removal reactions.

UNTERSUCHUNG DER (π^-, 2n) REAKTION AN KERNEN DER 1p-SCHALE

Zusammenfassung

Am CERN-SC II wurde die (π^-, 2n) Reaktion in einem kinematisch vollständigen Experiment untersucht. Targetkerne waren ^{6}Li, ^{7}Li, ^{9}Be, ^{10}B, ^{12}C, ^{14}N und ^{16}O. Bei letzterem war der überstrichene Winkelbereich am größten und die Statistik am besten.

Die beiden auslaufenden Neutronen wurden in Koinzidenz nachgewiesen mittels zweier großflächiger, ortsauflösender Flugzeitzähler. Die erreichte Auflösung in der Anregungsenergie des Restkerns betrug 3-6 MeV. Dies ist um einen Faktor 3-5 besser als in früheren (π^-, 2n) Messungen.

Für bestimmte Zustände des Restkerns bzw. bestimmte Bereiche in der Anregungsenergie werden Verteilungen in folgenden Variablen gezeigt: Neutronenenergie, Winkel zwischen den Impulsen der beiden Neutronen, Summe und Differenz der beiden Neutronenimpulse und Winkel zwischen diesen beiden Impulsen. Alle diese Verteilungen sind korrigiert bezüglich Nachweiswahrscheinlichkeit der Zähler und geometrischer Akzeptanz. Die Anregungsspektren sind in absoluten Raten pro gestopptem Pion angegeben.

Information wurde erhalten über die Spektralfunktion $S_{np}(q, E_s)$ und die Quantenzahlen des Neutron-Proton Paares, das an der Absorption beteiligt war. Schlüsse über den Reaktionsmechanismus werden gezogen.

Die Ergebnisse werden mit theoretischen Vorhersagen und anderen Reaktionen verglichen.

TABLE OF CONTENTS

	- Page -
I. INTRODUCTION	2
II. KINEMATICAL QUANTITIES AND QUANTUM NUMBERS	
II. 1. Kinematical Quantities	5
II. 2. Relationship between p and q	7
II. 3. Relationship between ω and q	9
II. 4. Relationship between θ and q	10
II. 5. Recoil momentum distributions	13
II. 6. θ-distributions	17
II. 7. Angular momentum and isospin quantum numbers and selection rules	18
II. 8. Phase space	23
III. THEORY OF PION ABSORPTION	26
IV. EXPERIMENTAL SETUP AND DATA ANALYSIS	
IV. 1. Experimental setup	33
IV. 2. Neutron counters	36
IV. 3. Electronics	38
IV. 4. Off-line analysis	41
V. RESULTS AND DISCUSSION	
V. 1. ^{6}Li	44
V. 2. ^{7}Li	67
V. 3. ^{16}O	77
V. 4. ^{9}Be, ^{10}B, ^{12}C	99
V. 5. ^{14}N	99
VI. SUMMARY AND CONCLUSIONS	103
References	108
Appendix A	112

I. Introduction

For the pion as a boson true absorption takes place in nuclei. The first reaction one might consider is the absorption by one nucleon with subsequent emission of that nucleon. In case of absorption of stopped π^- the nucleus receives practically no momentum but an energy of about 140 MeV corresponding to the pion rest mass. The single nucleon would take up this amount as kinetic energy and depart with a corresponding momentum of roughly 500 MeV/c. As the pion contributes essentially no momentum, the nucleon must have had a momentum of that order before the reaction already. The probability of such momenta in the nuclear wave function is very small and, therefore, absorption by a single nucleon is largely suppressed.

As a result of these considerations the hypothesis of absorption by two correlated nucleons as the dominant process was proposed by Brueckner et al [1]. In this case, the two nucleons would share the energy available and leave the nucleus with a large angle between their momenta, the so-called back-to-back emission. Thus, the two outgoing nucleons would have a high relative momentum, $0.5|(\vec{P}_1-\vec{P}_2)|$ = 300-350 MeV/c, corresponding to a distance of roughly 0.6 fm.

Starting from these facts one hopes to learn something about shortrange nucleon-nucleon correlations by studying this process [2].

Several experiments confirmed the hypothesis of the importance of the two-nucleon mode.

The reactions investigated were mainly (π^-, 2n) [3-7] with stopped π^- as well as (π^+, 2p) [8-10] with π^+ of energies between 30 and 80 MeV. The energy resolution and statistics obtained greatly differed from experiment to experiment. So far, only two measurements [9,10] both being (π^+, 2p), allowed to investigate systematically the most important nuclei of the 1p-shell with a reasonable resolution and statistics.

Emphasis in the (π, 2 N) experiments was laid on the investigation of two-hole states in nuclei, as far as their separation energies, momenta, angular momenta and isospins are concerned [11]. Like in two-nucleon transfer or quasi-free knockout reactions of the type (d,α) and (p, pd) respectively, information obtainable from pion induced two-nucleon emission can be divided into two main categories:

a) Information on the reaction mechanism:

One interesting aspect is a possible dependence of the π NN-interaction on the quantum numbers of the two nucleons, i. e. angular momenta and associated main quantum numbers, spin and isospin. Also the influence of the pion angular momentum with respect to the target nucleons can be studied.

In this context, a comparison between (π^-, 2n) and (π^+, 2p) results might likewise yield information about the π NN-interaction. These two reactions are related via charge symmetry and lead to the same residual nucleus, but due to different initial pion states the results are not a priori identical.

b) Nuclear structure information

Results can be obtained on the distribution of separation energy of two-hole states in nuclei as well as on momentum and angular momentum distribution of nucleon pairs.

In principle, the process also provides information about nucleon-nucleon correlations. This, however, is masked to some extent by other effects and will be discussed later.

In connection with information about the reaction mechanism and nuclear structure it must not be overlooked, however, that they are not a priori completely independent of each other. For example, depending on how well the target nucleus can be expanded into two nucleons and the residual core, the reaction mechanism might change. The reaction itself is sensitive to both aspects, i. e. to the reaction mechanism as well as to the nuclear structure. Basic knowledge or assumptions concerning one aspect will help to interprete the other. A typical input used with respect to the nuclear structure are the calculated coefficients of fractional parentage (c.f.p.) for two-nucleon removal.

Only some important aspects can be indicated in the frame of this introduction. For more information and many references the reader is referred to the review articles by Koltun [12] and Hüfner [13].

II. Kinematical Quantities and Quantum Numbers

II. 1. Kinematical quantities

Fig. 1 shows the kinematical variables used in the text.

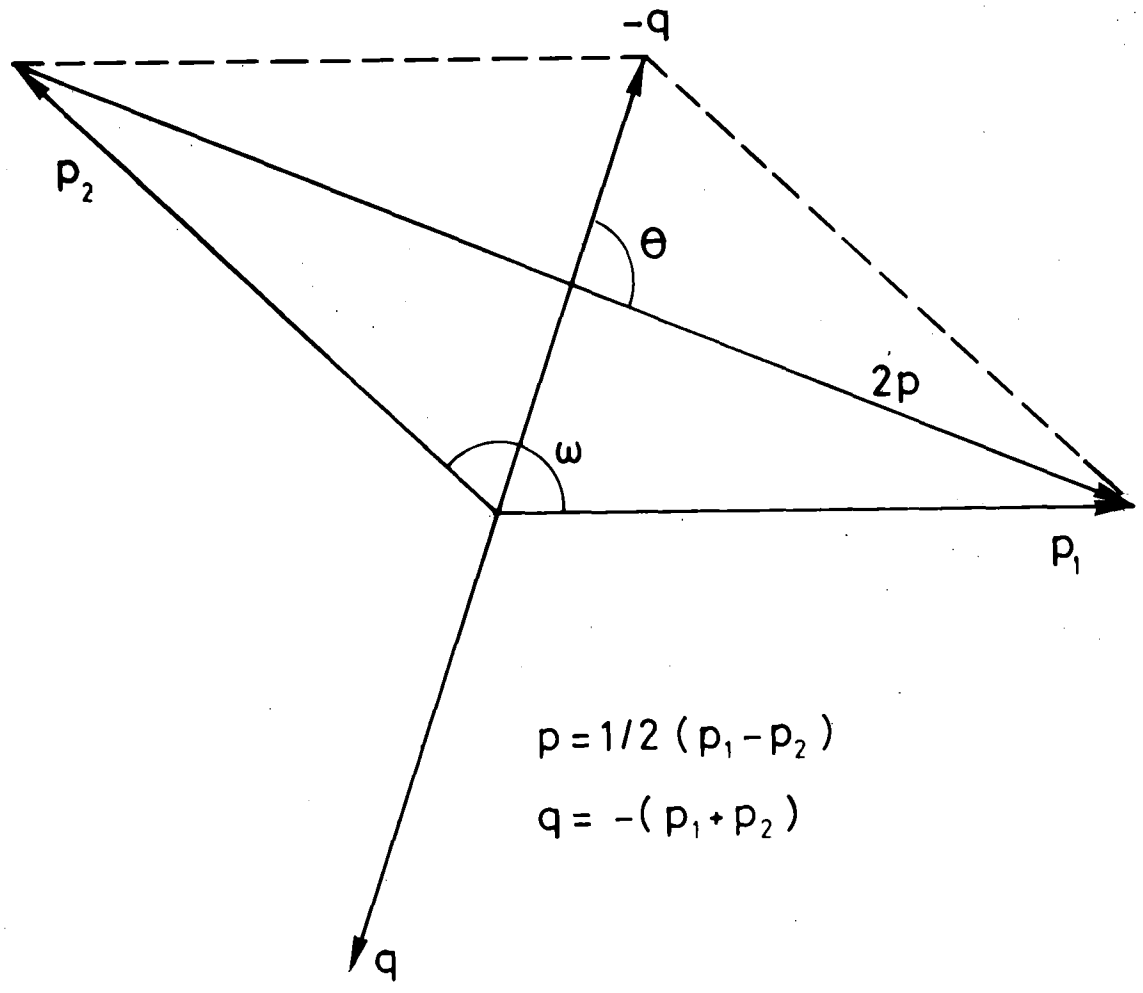

Fig. 1: Kinematical variables used in the text

We measure the time-of-flight and the directions of the two neutrons emitted. This allows to calculate the kinetic energies E_1, E_2 and the two momenta $\vec{p}_1$, $\vec{p}_2$. For stopped pions three independent variables are sufficient to determine the kinematics completely.

We then calculate the following variables:

Opening angle $\omega = \arccos \dfrac{\vec{p}_1 \cdot \vec{p}_2}{p_1 \cdot p_2}$

Recoil momentum $\vec{q} = -(\vec{p}_1 + \vec{p}_2)$; its magnitude q is equal to the momentum of the center of mass of the two nucleons with respect to the target c.m.

As the pion contributes essentially no momentum, q is also equal to the momentum of the c.m. of the absorbing nucleon pair before the absorption. Here we neglect effects of final state interactions (see II. 5.).

Relative momentum $\vec{p} = \frac{1}{2}(\vec{p}_1 - \vec{p}_2)$

Angle θ spanned by relative and c.m. momenta

$$\theta = \arccos \frac{\vec{p} \cdot \vec{q}}{p \cdot q}$$

One of the most important quantities to be calculated is the excitation energy E_x of the residual nucleus:

$$E_x = Q - E_1 - E_2 - E_R$$

with $E_R = q^2/2 \cdot M_R$, the kinetic energy of the recoiling nucleus with mass M_R.

The Q-value is defined as:

$Q = m_\pi$ - binding energy of an np-pair - $(m_n - m_p)$.

The last term takes into account the fact that the negative pion transforms a proton into a neutron $\pi^- + np \rightarrow nn$.

II. 2. Relationship between p and q

p and q are related via energy conservation. From Fig. 1 we derive:

$$p_2^2 = p^2 + \frac{1}{4} q^2 - pq \cdot \cos \theta \qquad (1)$$

and $$p_1^2 = p^2 + \frac{1}{4} q^2 + pq \cdot \cos \theta \qquad (2)$$

therefore, $$p_1^2 + p_2^2 = 2\, p^2 + \frac{1}{2} q^2 \qquad (3)$$

Using the energy conservation:

$$Q - E_x = E_1 + E_2 + E_R = (p_1^2 + p_2^2)/2\, m_n + q^2/2\, M_R$$

Together with (3) we get:

$$m_n \cdot (Q - E_x) = p^2 + \frac{1}{2} \left(\frac{1}{2} + \frac{m_n}{M_R}\right) \cdot q^2 \qquad (4)$$

For a given target nucleus A and a fixed value of E_x we thus have:

$$p^2 + aq^2 = c \qquad (5)$$

with $a = \frac{1}{2} \left(\frac{1}{2} + \frac{m_n}{M_R}\right)$ and $c = m_n\, (Q - E_x)$.

With $M_R \simeq (A - 2) \cdot m_n$ it is found that in the 1p-shell a varies from a = 3/8 (^{6}Li) to a = 2/7 (^{16}O).

For intensity reasons this experiment was mainly performed with large opening angles $\omega > 150\ ^{o}$. Therefore,

small recoil momenta q were preferred.

In Fig. 2 we present the variation of p as a function of q for representative values a = 0.3 and $Q - E_x$ = 110 MeV.

It can be seen that p is rather large and varies in a small range only; the distribution of relative momenta must be a very narrow curve. The maximum value of p is simply

$p_{max.} = \sqrt{m_n \cdot (Q - E_x)}$, it is the value for $q = 0$, which implies $\omega = 180\ ^{o}$ and $E_1 = E_2$.

In the process of pion absorption by a nucleon pair we investigate high relative momenta between the two outgoing nucleons.

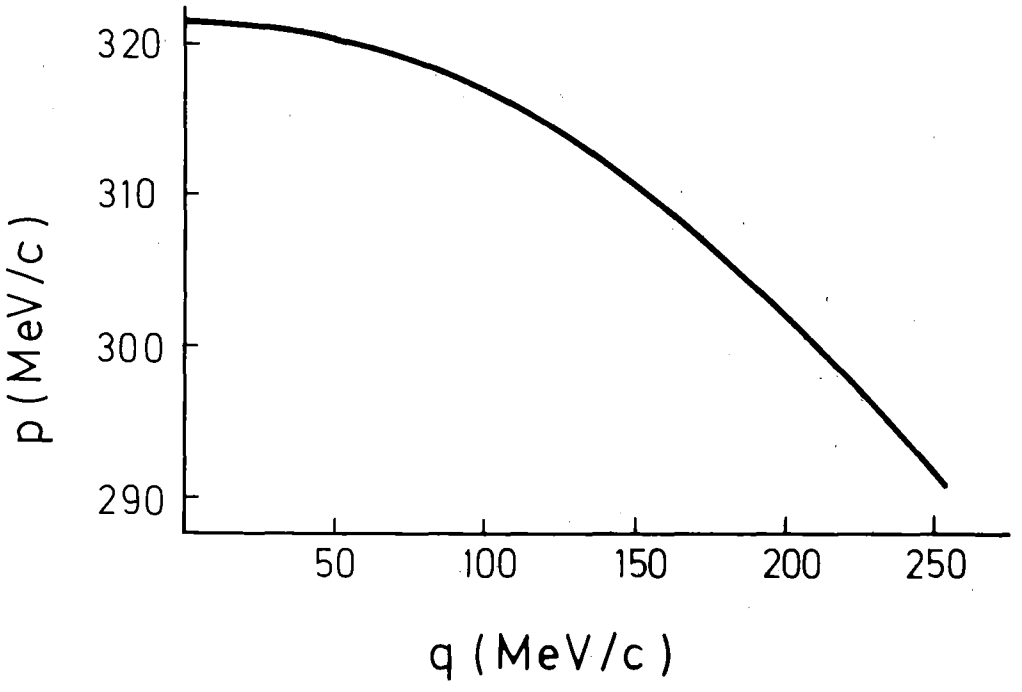

Fig. 2: Relative momentum p as a function of the c.m. momentum q

Through the uncertainty relation $p \simeq 300$ MeV/c can be related to a distance of roughly 0.65 fm which the two nucleons are assumed to have at the moment of absorption. Therefore, one can hope to learn something about the short-range behavior of two nucleons in a nucleus. In this context, it should also be mentioned that the initial state p can be different from the measured quantity p.

II. 3. Relationship between ω and q

In the plane spanned by ω and q only a certain part is allowed kinematically. For instance, $q = 0$ is possible only with $\omega = 180\ ^{o}$. For all other values of ω a minimum q exists. From Fig. 1 we derive

$$2\ p_1 p_2 \cos\omega = p_1^2 + p_2^2 - 4\ p^2 \qquad (6)$$

inserting Eqs. (1), (2) and (3) one obtains

$$\cos\omega = \frac{\frac{1}{4}\ q^2 - p^2}{\sqrt{p^2 + \frac{1}{4}\ q^2)^2 - p^2 q^2 \cos^2\theta}} \qquad (7)$$

from which we get $\omega > 90\ ^{o}$, $q < 2p$

$\omega = 90\ ^{o}$, $q = 2p$

$\omega < 90\ ^{o}$, $q > 2p$

For $\omega = 90\ ^{o}$ it follows that p and q are fixed at one value depending only on the target nucleus and on E_x:

$q = 2p$ and from Eq. (5) $\quad q\ (\omega = 90\ ^{o}) = \sqrt{\frac{c}{\frac{1}{4} + a}}$.

Inserting (5) into (7) we obtain:

$$\cos\omega = \frac{q^2 \cdot (a + \frac{1}{4}) - c}{\sqrt{[q^2 (\frac{1}{4} - a) + c]^2 - (c - aq^2)\, q^2 \cos^2\theta}} \qquad (8)$$

The extrem value of cos ω (for fixed q) follows from (8) with cos θ = 0:

$$\cos\omega_{ext} = \frac{q^2 (a + \frac{1}{4}) - c}{q^2 (\frac{1}{4} - a) + c}$$ or, equivalently:

$$q_{ext} = \sqrt{\frac{c}{a + \frac{1-\cos\omega}{4 (1+\cos\omega)}}}$$

Actually, for $\omega > 90^{\circ}$ this q_{ext} turns out to be the minimum q and for $\omega < 90^{\circ}$ the maximum q.

In Fig. 3 the shaded area indicates the allowed region, calculated for the transition

$$^{16}O\ (\pi^-,\ 2n)\ ^{14}N_{3.9\ MeV}.$$

II. 4. Relationship between θ and q

In the plane spanned by θ and q no points exist that are forbidden a priori. A restriction is imposed if the experiment is limited to a defined ω-range. In the following we limit ourselves to the case $\omega_{max} = 180^{\circ}$ and $90^{\circ} < \omega_{min} < 180^{\circ}$.

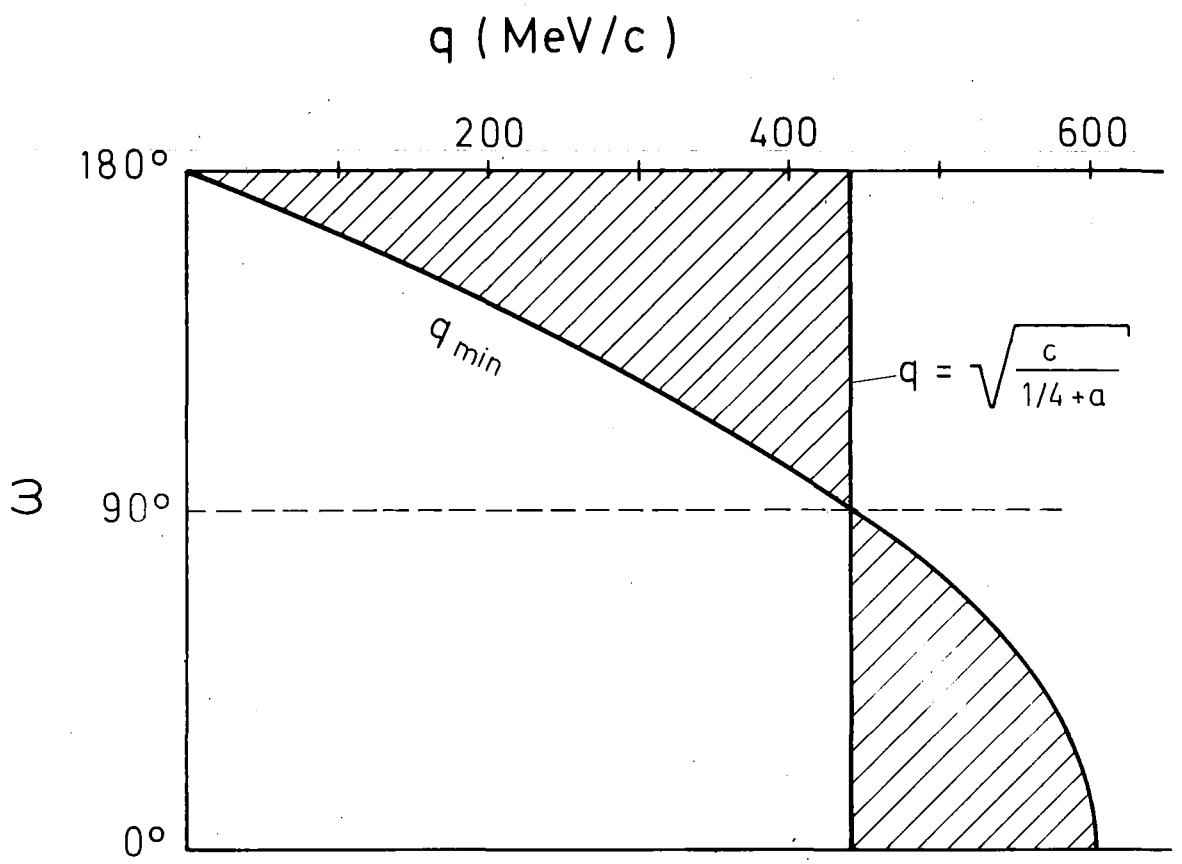

Fig. 3: Kinematically allowed region in the plane spanned by the recoil momentum q and the angle ω (see also text).

From Eq. (8) we get:

$$\cos\theta = \pm\sqrt{\frac{x - y/\cos^2\omega}{(c - aq^2)\cdot q^2}} \qquad (9)$$

with $x = [q^2(\frac{1}{4} - a) + c]^2$ and $y = [q^2(a + \frac{1}{4}) - c]^2$

The two signs in Eq. (9) reflect the fact that for reasons of symmetry the θ-distributions must be symmetrical around $\theta = 90\,^{\circ}$.

The shaded area in Fig. 4 shows the allowed region, again for the transition $^{16}O\ (\pi^-, 2n)\ ^{14}N_{3.9\ MeV}$ and $\omega_{min} = 150^o$ Because of the experimental limitation in ω recoil momenta q are completely measured only up to q = q´; see Fig. 4.

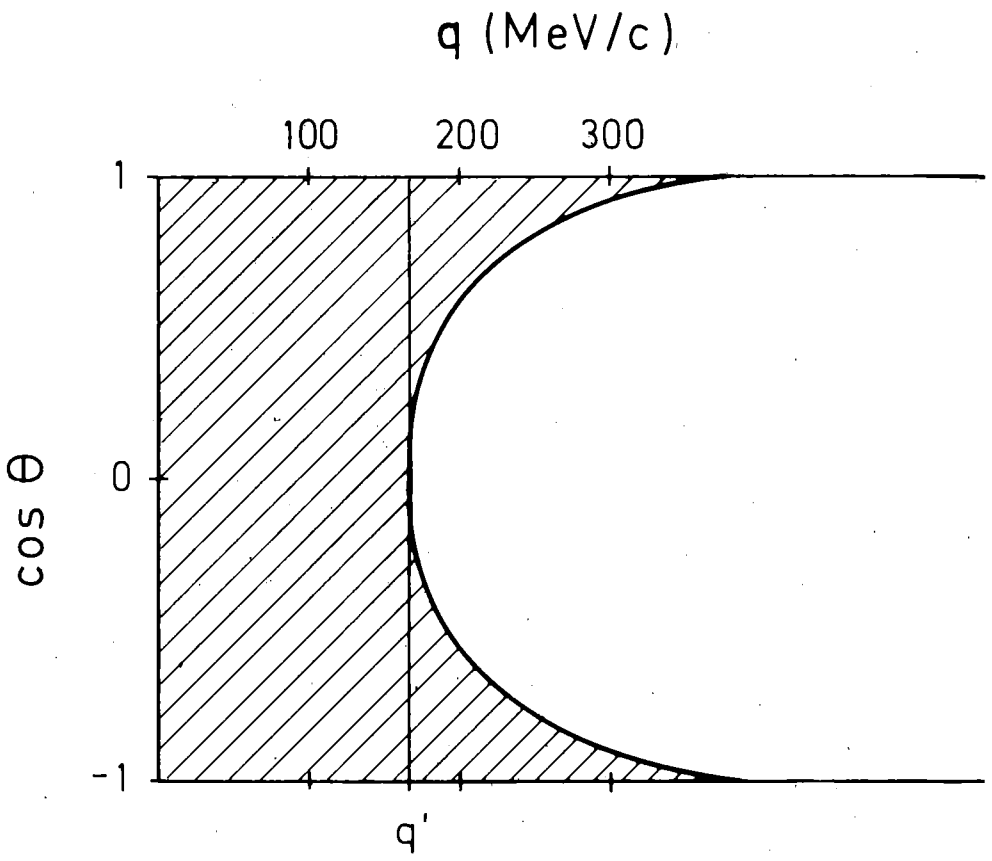

Fig. 4: Experimentally covered region in the plane spanned by the recoil momentum q and the angle θ (see also text).

Beyond that value the phase space is restricted and only on the assumption that the matrix element is independent

of θ the q-distributions at high q can be given.

Eq. (9) with $\omega = \omega_{min}$ and $\cos\theta = 0$ gives

$$q' = \sqrt{\frac{c\ (1+\cos\omega_{min})}{\cos\omega_{min}\ (a-\frac{1}{4})+a+\frac{1}{4}}} \qquad (10)$$

In our example $q' = 167$ MeV/c.

All q-distributions shown are indicated up to the highest recoil momenta measured. For $q > q'$ the assumption mentioned above regarding θ was made, see also II. 8.
All the reported θ-distributions are integrated over q up to $q = q'$.

II. 5. Recoil momentum distributions

The special importance of the measured recoil momentum distributions lies in the fact that they reflect the motion of the c.m. of the absorbing nucleon pair with respect to the c.m. of the target. As the pion contributes essentially no momentum, the q-distribution is the momentum distribution of the c.m. of the pair before absorption, except for effects of final state interactions between the nucleons and the residual core (so-called distortions).

In the following treatment we adopt the picture of a quasi-free pion absorption by a nucleon pair in the target where the residual core just acts as a spectator and we neglect final-state interactions. In a shell model description a transformation can be performed from the individual coordinates of the two nucleons to c.m. and

relative coordinates of the 2N-system, the Talmi-Moshinsky-transformation [14].

We denote the corresponding angular momenta by l_1, l_2, L and l, respectively. We then have $\vec{l}_1 + \vec{l}_2 = \vec{\Lambda} = \vec{l} + \vec{L}$. The energy conservation in the shell model gives

$$2\,(n_1 + n_2) + l_1 + l_2 = 2\,(n + N) + l + L,$$

where n_1, n_2, N, n are the corresponding principal quantum numbers. The last equation also guarantees the parity conservation

$$(-1)^{l_1 + l_2} = (-1)^{l + L}.$$

For removal of different nucleon pairs we thus obtain (see also Ref. 14 and Chapter 2 of Appendix A) the following possibilities.

For two nucleons from the 1p-shell, i. e. p^2-removal,

$l_1 = l_2 = 1$ and

we have $\Lambda = 0$, a) 2S (N=1, L=0) x 1s (n=0, l=0)

b) 1S x 2s

$\Lambda = 1$, c) 1P x 1p

$\Lambda = 2$, d) 1D x 1s

e) 1S x 1d

In all cases the parity of the residual nucleus is identical to that of the target nucleus.

For s^1p^1-removal we have

$\Lambda = 1$, f) 1P x 1s

g) 1S x 1p

and the parity of the residual nucleus is different from that of the target nucleus.

For s^2-removal we have

$\Lambda = 0$, h) 1S x 1s

and again the residual state and the target nucleus have the same parity.

Some remarks should be made on the combinations a) - h). Usually, $l = 0$ is assumed in the initial state because for $l_i \neq 0$ it seems uncertain whether the angular momentum barrier allows a sufficiently short distance between the two nucleons to make the process happen.

The calculations by Cohen and Kurath [15] and Balashov et al. [16] of the coefficients of fractional parentage (c.f.p.) for two-nucleon removal were made for reactions of the type (d, α) and (p, pd) requiring $l_i = 0$. However, the important quantity in their calculations is Λ and the results obtained by these authors are equally applicable to this experiment in which $l_i = 0$ must not be fulfilled a priori.

As this measurement was performed mainly for large angles ω, small recoil momenta q were preferred. This results in a suppression of $L \neq 0$ transitions and, therefore, in the case of $\Lambda = 2$ combination e) 1S x 1d may appear. For s^1p^1-removal combination g) 1S x 1p may be of some importance.

The transition matrix element M_{fi} for pion absorption can be related to the momentum distribution of the c.m. of the pair [17,18]

$$M_{fi} = \text{const.} \cdot \phi\ (q)$$

where $\phi\ (q)$ is the Fourier transform of the c.m. wave function of the pair. The pion is assumed to be absorbed

from the P orbit and the absorption should occur at zero range between the two nucleons. In general, i. e. without the zero range approximation, the Fourier transform of the relative wave function has also to be taken into account [18]

$$M_{fi} = \text{const.} \cdot \phi\ (q) \cdot \zeta(p).$$

The wave function of the c.m. motion of the pair can be evaluated using e. g. a harmonic oscillator or a square well potential. If there is an experimental preference for a small q or if for different reasons, like surface absorption, the contribution from small radii is suppressed, the square well potential should give better results. Contrary to the harmonic oscillator potential, it does not become infinite for large radii and thus describes more reasonably the asymptotic part of the wave function. This asymptotic part is essentially determined by the binding energy of the particles.

The change of the momentum distributions with increasing separation energy was pointed out by the authors of Ref. 18. In this case, the average radii will be smaller and, hence, the average momenta larger.

In any case we expect for $L = 0$ q-distributions with their maxima at $q = 0$ and for $L \neq 0$ with a minimum at $q = 0$; see also Fig. 2 in Appendix A. Various effects will modify the shape of the q-distributions. We mention here initial state correlations, rescattering (see Chapter III.), and final-state interactions.

If the contribution from the internal parts of the nuclei is higher, like in the case of absorption by two s-shell nucleons, the distortion is expected to have a bigger effect on the observed q-distribution.

II. 6. θ-distribution

The importance of the angle θ was emphasized by Koltun [19]. In the quasi-free picture with a two-nucleon impulse approximation the θ-distribution allows conclusions to be drawn on the angular momentum structure of the nucleon pairs involved. The angular momentum and isospin selection rules, which will be elaborated in Chapter II. 7., have to be taken into account too.

The excitation energy E_x, recoil momentum q, and angle θ form a complete set of variables. For a fixed E_x the distribution of events may be expressed as

$$\frac{d^2R(q,\theta)}{dq\ d\cos\theta} = \text{const.} \cdot \text{PSF} \cdot |M(q,\theta)|^2.$$

The phase space factor PSF will be calculated in II. 8. For fixed q the θ-distribution F (θ) can then be expanded in a series of Legendre polynomials:

$$F(\theta) = \text{const.}\ \Sigma a \cdot P_r(\cos\theta)$$

where according to Koltun [19]

$$|L_f - L_f'| \leq r \leq |L_f + L_f'| \quad \text{and} \quad |l_f - l_f'| \leq r \leq |l_f + l_f'| \ .$$

The index f refers to final-state values of the angular momenta.

It follows that for $L_f = 0$ $F(\theta) = \text{const.}$ We shall see that $F(\theta) = \text{const.}$ is frequently observed in the experiment. It was already mentioned that for reasons of symmetry $F(\theta)$ must be symmetrical around $\theta = 90^o$, i. e. r can only be even.

II. 7. Angular momentum and isospin quantum numbers and selection rules

The transformation from l_1, l_2 to L and l was mentioned in II. 5. We keep the model of direct, quasi-free absorption ("two nucleon impulse approximation") and use the notation of Fig. 5 for the angular momenta.

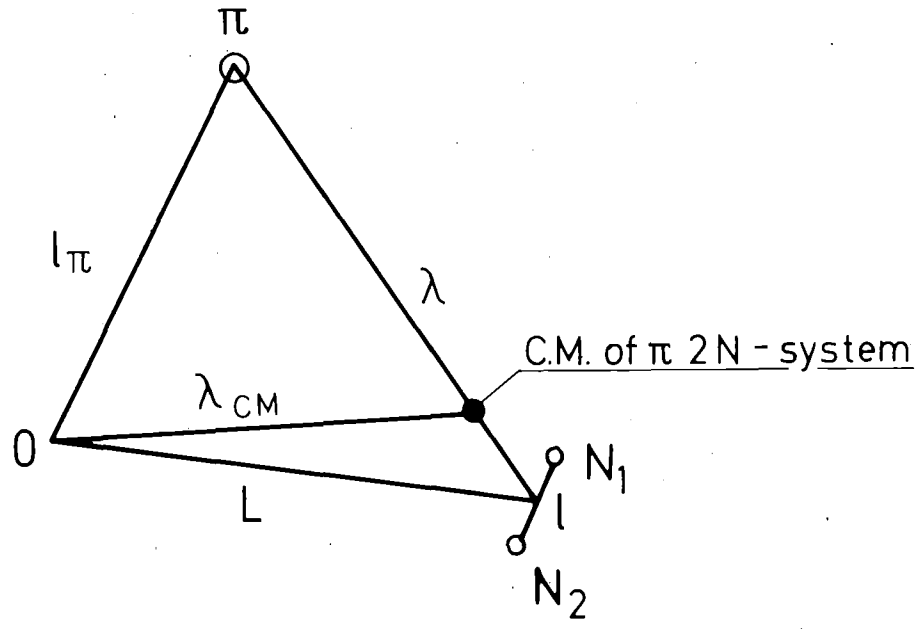

Fig. 5: Angular momenta used in the text

The origin 0 is in the c.m. of the target nucleus; l_π is the orbital angular momentum of the pion (we take only atomic S- or P-absorption). L and l have already been defined, λ is the pion angular momentum with respect to the c.m. of the two nucleons, and λ_{cm} the angular momentum of the c.m. of the π 2N-system.

a) Conclusions from $l_\pi = 0$ or 1

In the quasi-free model angular momentum and parity have to be conserved within the π 2N-system, i. e. λ is the relevant quantity rather than l_π. Similar to the transformation $l_1, l_2 \rightarrow l$, L mentioned previously we can make a transformation $l_\pi, L \rightarrow \lambda, \lambda_{cm}$.
Then we have the conditions

$$\vec{l}_\pi + \vec{L} = \vec{\lambda} + \vec{\lambda}_{cm} \quad \text{and} \quad (-1)^{l_\pi + L} = (-1)^{\lambda + \lambda_{cm}}.$$

For $l_\pi = 0$ (S-wave pions) one obtains the following possibilities:

$$L = 0, \quad \lambda, \lambda_{cm} = 0, 0$$
$$L = 1, \quad \lambda, \lambda_{cm} = 0, 1 \text{ or } 1, 0$$
$$L = 2, \quad \lambda, \lambda_{cm} = 0, 2 \text{ or } 2, 0$$

For $l_\pi = 1$ (P-wave pions) more possibilities exist for $\vec{l}_\pi + \vec{L}$:

$$L = 0, \quad \lambda, \lambda_{cm} = 0, 1 \text{ or } 1, 0$$
$$L = 1, \quad \lambda, \lambda_{cm} = 0, 0 \text{ or } 1, 1 \text{ or } 2, 2$$
$$L = 2, \quad \lambda, \lambda_{cm} = 0, 1 \text{ or } 1, 0 \text{ or } 1, 2 \text{ or } 2, 1$$

For L = 1 and L = 2 only the lowest possible values of λ and λ_{cm} are listed.

For most of the nuclei studied here $l_\pi = 1$ is known to be dominant and combined with the geometrically favoured L = 0 the relevant angular momentum λ can be 0 or 1. But due to the fact that $m_{2N} >> m_\pi$, the c.m. of the π 2N-system is very close to the c.m. of the nucleon pair, i. e. $\lambda_{cm} = L$ in a first approximation and then $\lambda = l_\pi$.

b) Koltun's selection rule $\Delta L = 0$ [19]

As we regard only pions moving slowly with respect to the target nucleus, it seems plausible to assume that there will be no angular momentum transfer to the c.m. of the two-nucleon system, i. e. $\Delta L = 0$.

This can be put in more quantitative terms. Let $\vec{q}$ and $\vec{p}_\pi$ be the momentum of the c.m. of the two nucleons and the pion momentum, respectively, both with respect to the target c.m. Then the relative momentum between the pion and the nucleon pair is

$$\vec{P}_{rel} = \frac{m_\pi \vec{q} - 2m_N \vec{p}_\pi}{2m_N + m_\pi} .$$

Its magnitude can be estimated:

$$P_{rel} \leq \frac{m_\pi q + 2m_N p_\pi}{2m_N + m_\pi} \simeq 17 \text{ MeV/c} = 0.08 \text{ fm}^{-1}$$

for q = 200 MeV/c and $p_\pi \simeq 3$ MeV/c for absorption from the atomic 2P-level in ^{12}C (n = 2, Z = 6).

For a distance d = 1 fm we get

$$\Delta L \leq P_{rel} \cdot d \simeq 0.08 \text{ (in units of } \hbar)$$

and thus $\Delta L = 0$ seems to be preferred indeed, at least for light nuclei.

In the case of $\Delta L = 0$ it is clear that the pion angular momentum and parity can affect only the "internal" quantum numbers l and S of the two nucleons, the latter being the two-nucleon total spin.

c) Transition rules for the two nucleons

We first assume $\Delta L = 0$ and restrict ourselves to $(\pi^-, 2n)$ or $(\pi^+, 2p)$ where the isospin of the two nucleons in the final state must be unity, $T_f = 1$. Because of the negative intrinsic parity of the pion $P_\pi = (-1)^{\lambda+1}$. The notation $J = l + S$ is used in the following paragraphs.

For s-absorption of the pion ($\lambda = 0$) we then have

$$\Delta l = 1, \quad \Delta J = 0 \qquad (11)$$

and this gives the following isospin selection rules.

i) For l_i = odd $T_i = 0$ is forbidden:

From the Pauli principle we derive in this case $S_i = 0$. Eq. (11) implies $\Delta S = 1$ and therefore $S_f = 1$ and l_f even. The Pauli principle would require $T_f = 0$ which is not allowed for two identical nucleons.

ii) For l_i = even both $T_i = 0,1$ are allowed:

The case l_i = even and $T_i = 0$ implies $S_i = 1$, generating, generally, more possibilities of combining l_i and S_i such that $\Delta l = 1$, $\Delta J = 0$ is possible without a change of S. The case l_i = even and $T_i = 1$ implies $S_i = 0$ and with $\Delta S = 1$ we get $S_f = 1$, l_f = odd. This imposes $T_f = 1$ which is correct.

Examples: $^{TS}l_J = {}^{01}S_1 \rightarrow {}^{11}P_1$

$${}^{10}S_0 \rightarrow {}^{11}P_0$$

For <u>p-wave absorption</u> ($\lambda = 1$) we obtain

$$\Delta l = 0,2 \quad \text{and} \quad \Delta J = 1. \qquad (12)$$

iii) For l_i = even we now find $T_i = 1$ forbidden:

l_i = even and $T_i = 1$ imply $S_i = 0$. Using Eq. (12) we find $\Delta S = 1$, i. e. $S_f = 1$ and l_f = even. This in turn implies $T_f = 0$ which is not allowed.

iv) For l_i = odd both $T_i = 0,1$ are allowed:

If l_i = odd, $T_i = 0$ we have $S_i = 0$. Then $\Delta S = 1$, i. e. $S_f = 1$ and l_f = odd, implying $T_f = 1$. In the case l_i = odd, $T_i = 1$ we have $S_i = 1$ and this spin 1 can easily make $\Delta J = 1$ without change of S.

Examples: ${}^{00}P_1 \rightarrow {}^{11}P_0, {}^{11}P_2$

$${}^{11}P_0 \rightarrow {}^{11}P_1 \text{ or } {}^{11}P_1 \rightarrow {}^{11}P_0, {}^{11}P_2$$

As a summary, for $\Delta L = 0$ one obtains the following isospin selection rules:

S-wave pion ($\lambda = 0$), for l_i = odd only $T_i = 1$ is allowed, whereas for l_i = even $T_i = 0$ and 1 are allowed.

P-wave pion ($\lambda = 1$), for l_i = even only $T_i = 0$ is allowed, whereas for l_i = odd $T_i = 0$ and 1 are allowed.

If $l_i = 0$ is assumed on the basis of the close correlation and the Koltun rule $\Delta L = 0$ is respected, the following transitions should be the most important ones:

For S-wave pions ($\lambda = 0$) $^{10}S_0 \rightarrow {}^{11}P_0$

and $^{01}S_1 \rightarrow {}^{11}P_1$

For P-wave pions ($\lambda = 1$) $^{01}S_1 \rightarrow {}^{10}S_0$

$\searrow$ $^{10}D_2$

For the case $\Delta L = 1$, which is in principle allowed but should be much less frequent, one obtains:
In case of S-wave absorption ($\lambda = 0$) $\Delta l = 0,2$ and $\Delta J = 1$ in order to conserve parity and angular momentum. Therefore, we have the same selection rules as for the case $\Delta L = 0$ and $\lambda = 1$. In case of p-wave absorption ($\lambda = 1$) $\Delta l = 1$ and $\Delta J = 0$ in order to conserve parity and angular momentum. Therefore, the selection rules are identical to the case $\Delta L = 0$ and $\lambda = 0$.

In connection with the isospin selection rules above it should be mentioned that for target nuclei with $T = 0$ T_i will be the same as T of the residual state. For example, if $T_i = 1$ is forbidden, no levels with $T = 1$ should be excited in the residual nucleus.

II. 8. Phase space

Except for multiplicative constants, the phase space factor is given by

$$PSF = \int \delta (\vec{p}_1 + \vec{p}_2 + \vec{q}) \cdot \delta(E_f - E_i)\, d^3p_1 \cdot d^3p_2 \cdot d^3q =$$

$$\int \delta (E_f - E_i)\, d^3p_1 \cdot d^3p_2$$

$$E_f = E_1 + E_2 + E_R = (p_1^2 + p_2^2)/2m_n + q^2/2M_R = \frac{p^2}{m_n} + \frac{q^2}{4m_n} + \frac{q^2}{2M_R}$$

$E_i = Q - E_x$, see II. 2.

Now we transform from the variables $\vec{p}_1$, $\vec{p}_2$ to $\vec{p}$ and $\vec{q}$, $\vec{p}_1 = \frac{-1}{2}\vec{q} + \vec{p}$ and $\vec{p}_2 = -\frac{1}{2}\vec{q} - \vec{p}$.

The corresponding Jacobian turns out to be unity:

$$\left| \frac{\partial(\vec{p}_1, \vec{p}_2)}{\partial(\vec{q}, \vec{p})} \right| = 1.$$

Therefore $$\begin{aligned} PSF &= \int \delta(E_f - E_i) \cdot d^3p \cdot d^3q = \\ &= \int \delta(E_f - E_i) \cdot p^2 \cdot dp \cdot d\Omega_p \cdot q^2 \cdot dq \cdot d\Omega_q = \\ &= 4\pi \int \delta(E_f - E_i) \cdot p^2 \cdot q^2 \cdot dp \cdot dq \cdot d\Omega_q \end{aligned}$$

The integration over $d\Omega_p$ has been performed and for the integration over $d\Omega_q$ the direction of $\vec{p}$ is chosen as the z-axis, in which case $d\Omega_q = d\cos\theta \cdot d\phi$. Integration over $d\phi$ gives another constant of 2π and so we obtain

$$\begin{aligned} PSF &= \text{const.} \int \delta(E_f - E_i)\, p^2 \cdot q^2 \cdot dp \cdot dq \cdot d\cos\theta \\ &= \text{const.} \int \delta(E_f - E_i) \cdot dE_f \cdot \left(\frac{dE_f}{dp}\right)^{-1} \cdot p^2 \cdot q^2 \cdot dq \cdot d\cos\theta \\ &= \text{const.} \int p \cdot q^2 \cdot dq \cdot d\cos\theta. \end{aligned}$$

Therefore, the transition rate as a function of q and θ takes a particularly simple form:

$$\frac{d^2R}{dq \cdot d\cos\theta} = \text{const.} \cdot p \cdot q^2 \cdot \left|M(q, \theta)\right|^2$$

In case that the matrix element is independent of θ, integration over θ is trivial and one obtains for the recoil momentum distribution

$$\frac{dR}{dq} = \text{const.} \cdot p \cdot q^2 \cdot \left| M\ (q) \right|^2 .$$

It should be mentioned that in case of an experimental limitation, like a ω_{min}, the phase space factor calculated here has to be modified for $q > q'$, q' being defined in II. 4. We have determined this modified phase space by means of a Monte Carlo program.

III. THEORY OF PION ABSORPTION

Only the most important aspects of the many theoretical calculations shall be mentioned here. The already cited review articles [12,13] and the one by Kopaleishvili [20] give a general survey and many references. Most theoretical attemps have been undertaken using the model of quasi-free absorption by a nucleon pair. In the following points a) - e) the main difficulties will be described.

a) Pion wave function

For stopped pions hydrogen-like wave functions are normally used and optical potential effects are neglected. For pions in flight a plane wave is the usual assumption.

b) Realistic wave function of the target nucleus

Most authors start with shell model wave functions or, for very light nuclei like ^{6}Li or ^{7}Li, with cluster model wave functions. The target nucleus wave function $\Psi_A\ (\vec{r}_1, \ldots\ldots \vec{r}_A)$ is then expanded in all possible states of the residual nucleus (A-2) plus the motion of the two nucleons

$$\Psi_A\ (\vec{r}_1, \ldots\ldots\ldots, \vec{r}_A) = \Sigma\ C \cdot \Psi_{A-2}\ (\vec{r}_1, \ldots\ldots\ldots, \vec{r}_{A-2}) \cdot \Psi_2\ (\vec{r}_{A-1}, \vec{r}_A).$$

C are the relevant coefficients of fractional parentage (c.f.p.). They depend on all internal quantum numbers of the two subsystems. The summation extends over these quantities, i. e. excitation energy, angular momentum, spin and isospin. The initial state 2N wave function can be separated into relative and c.m. parts [14]:

$$\Psi_2(\vec{r}_{A-1}, \vec{r}_A) = \phi(\vec{r}) \cdot \Phi(\vec{R})$$

where $\vec{r} = \frac{1}{2} \cdot (\vec{r}_{A-1} - \vec{r}_A)$ and $\vec{R} = \vec{r}_{A-1} + \vec{r}_A$.

For a detailed comparison with our measured excitation energy spectra knowledge of the distribition of two-hole states in Ψ_A is very important. Such c.f.p. calculations for two nucleon removal are available [15,16], but only for removal from the 1p-shell. Only very few detailed theoretical predictions exist regarding the excitation energy spectrum in pion induced reactions [21-23].

The c.f.p. contain pure nuclear structure information and as the pion absorption reaction mechanism, in principle, selects special pairs of nucleons, one can expect interesting information from a detailed comparison between experimental pion results and the c.f.p. predictions. Therefore, such a comparison will be made here.

c) Correlation between the two nucleons before the absorption

A long time ago it was realized that a pure shell model description underestimates by several orders of magnitude [2] the experimentally observed total absorption rates of bound pions. A way out of this problem was the inclusion of short-range correlations (SRC) that modify the nucleon pair relative wave function $\phi(\vec{r})$ at short distances. The form of these correlations is in most cases a multiplicative factor, the so-called Jastrow factor, containing a single parameter function supposed to describe effects of the hard core on $\phi(\vec{r})$. Chung et al. [24], for instance, used the following factor:

$f(r) = 1-j_0(qr)$, j_0 = spherical Bessel function. q is in this case the momentum exchanged by the two otherwise independent nucleons. Correlation factors of the type

$$f(r) = 1-\exp(-ar^2)$$

with a correlation parameter have been used by many authors [25-28]. The factors are always such that they become zero for $r \to 0$ and 1 for $r \to \infty$, i. e. for large r $\phi(r)$ remains unchanged.

Finally, it should be pointed out that not all authors agree on the necessity of SRC and on the way this aspect of pion absorption should be treated; see for instance Ref. 29.

d) π NN-interaction operator

For the description of pion induced nuclear reactions the bound nucleons have to be treated non-relativistically, i. e. the non-relativistic form of the π N-interaction is required. Mostly the so-called Galilei-invariant Chew-Low Hamiltonian

$$H_{\pi N} = f\cdot\vec{\sigma}_N(\vec{v}_\pi-\vec{v}_N)(\tau_N\cdot\Phi_\pi) \to \frac{f'}{m_\pi}\cdot\vec{\sigma}_N(\nabla_\pi-\frac{m_\pi}{m_N}\nabla_N)(\tau_N\cdot\Phi_\pi)$$

has been used where f, f' are coupling constants, $\vec{\sigma}_N$ and τ_N are nucleon spin- and isospin operators, and Φ_π is the pion wave function. The first term in $H_{\pi N}$, with $\vec{v}_\pi$ or $\dot{\nabla}_\pi$, corresponds to the limiting case of a fixed nucleon (static case) and the second term, with $\vec{v}_N$ or ∇_N, takes into account a moving nucleon (Fermi-movement or recoil) and ensures the Galilei invariance of $H_{\pi N}$. Regarding the atomic

1S and 2P pion wave functions (see for instance Ref. 24) one realizes that the first term practically drops for 1S-absorption because in a first approximation $\nabla_\pi \Phi_\pi^{1S} = 0$ within the nuclear radius. On the other hand, for 2P-absorption the second term becomes negligible because $\Phi_\pi^{2P} << \Phi_\pi^{1S}$ within the nucleus. Therefore, in a first approximation the first term of $H_{\pi N}$ describes P-wave absorption, whereas the second describes S-wave absorption.

In the quasi-free two-nucleon model summation over just two nucleons is carried out for calculation of matrix elements:

$$\left\langle f \left| \frac{f'}{m_\pi} \sum_{j=1}^{2} [\vec{\sigma}_N (\nabla_\pi - \frac{m_\pi}{m_N} \nabla_N) \cdot (\tau_N \Phi_\pi)]_j \right| i \right\rangle$$

$H_{\pi N}$ is the simplest, Galilei-invariant expression for the πN-interaction and it can also be derived from the Lorentz-invariant, pseudoscalar πN-interaction (γ_5-coupling) as the non-relativistic limiting case. However, this reduction to the non-relativistic case is ambiguous; see for instance Ref. 30.

Apart from the Hamiltonian just described a phenomenological ansatz for two nucleon absorption was developed [31]. It assumes zero range approximation and contains 4 independent coefficients fixed by pion production data.

An important addition to $H_{\pi N}$ was proposed by Koltun and Reitan [32], namely s-wave scattering of the pion by one nucleon before absorption by the second nucleon (so-called rescattering formalism). They incorporate normal

and charge exchange scattering on the first nucleon. In case of absorption by the free deuteron they found the charge exchange scattering and the d-state (l = 2) admixture to be important.
Applying their theory to the reaction $^{6}Li\ (\pi^{-}, 2n)^{4}He$ Koltun and Reitan [33] emphasized the importance of rescattering on absolute rates and momentum distribution of the quasi-deuteron. Again the l = 2 contribution to $\phi(\vec{r})$ played a role. Kopaleishvili and Machabeli [34] argued that when taking into account rescattering the final state nucleon-nucleon interaction (see part e) of this chapter) may be neglected.

Also in recent calculations by Hachenberg et al. [29] rescattering has been used.

e) Interaction of the outgoing particles

In the final state of the (π, 2n) reaction we have at least three interacting particles. This fact makes the theoretical description very complicated as it requires Faddeev equations or something equivalent. For two nucleons and the residual core we have the NN-interaction and the interaction between nucleons and the core, the distortions.

There is no agreement in the literature on the relative significance of these two effects but in most treatments the distortions have been neglected and $\Phi_f(\vec{R})$ has been approximated by a plane wave.

Concerning the NN final state interaction (FSI) many authors used an asymptotic form for $\phi_f(\vec{r})$ derived from

experimental NN scattering data. Strictly speaking, this approximation is only valid outside of the interaction region. A second possibility is the exact solution of the Schrödinger equation for NN scattering with a realistic potential (Hamada-Johnston for example) and for a relative energy corresponding to the kinematics. This method was used for instance by Koltun and Reitan [33], Kopaleishvili [35] or Elsaesser and Eisenberg [36]. Different results were obtained from inclusion of this more realistic form of the NN interaction. Kopaleishvili found a relative increase in p^2-removal as compared to s^1p^1 and s^2-removal. Elsaesser and Eisenberg found an increased emission at large opening angles.

There are at the moment only few theoretical attempts that include NN final state interactions and distortion. Kaushal and Waghmare [37] used an optical potential for the distortion and concluded that they are even more important than the NN-FSI. They also showed that the recoil momentum distribution is modified by the distortions.

Theoretical works with a complete three body description of the final state are Refs. 27 and 28. Garcilazo and Eisenberg [27] solved the Faddeev equations with separable potentials whilst Morris and Weber [28] used a coupled channel formalism with realistic potentials. The most important conclusions drawn by Morris and Weber are:

1) The NN soft core FSI broadens the energy and angular distributions and produces a relative minimum at $\omega = 180^{o}$. The last statement is in clear disagreement with known experiments.

2.) SRC's are absolutely necessary to explain the (π, NN) reaction. In agreement with Morris and Weber, Garcilazo and Eisenberg confirm the importance of the distortions and the necessity of the initial state SRC for the reproduction of the 180° correlation observed.

Summarizing it can be said that for the time being no theory exists that considers in a satisfactory way all aspects mentioned under a) - e). It is not clear which effects (short-range correlations, rescattering, final state interactions) are the most important and what is their individual influence on experimentally obtained results.

As to the old motivation for (π, NN) experiments, namely to learn something about short-range correlations, the following statement can be made. It is certainly not easy, if at all possible, to get this information because in the experimental results their effects are masked by the final-state interactions. Only if the latter can be treated appropiately, one can hope to obtain information about SRC.

For a more detailed comparison with the experiment theoretical predictions on the excitation energy spectrum are needed, including high E_x, i.e. removal of s-shell nucleons. Energy, momentum and angular distributions should be calculated for certain excited states or regions in excitation energy.

IV. EXPERIMENTAL SET-UP AND DATA ANALYSIS

IV. 1. Experimental set-up

The experiment was performed at the low energy pion channel of the CERN-SC II in 1975/76. The internal proton beam intensity was 1-2 μA. The pion of 70 MeV kinetic energy were degraded in Teflon plates and stopped in targets of $\sim$5 g/cm^2 thickness. The stopping rates were of the order of 1.5 x 10^5 sec^{-1}. About 40 % of the beam consisted of pions, the rest being muons and electrons.

Fig. 6 shows schematically the experimental setup. All counters were plastic scintillators. Stopped pions were detected in counters CI - CV and the hodoscope with a conventional 1, 2, 3, hodoscope, 4, $\overline{5}$ logic. CV served as an anti-counter. CII, with the dimensions 12 x 12 x 1 cm, gave the start signals for the two neutron times-of-flight. For optimum time resolution it had a pair of twisted-strip light-guides and one RCA 8850 photomultiplier on each end. The measured time resolution of this counter for minimum ionizing particles, i. e. pulses of 2 MeV, was 300 psec.

Apart from the logic signal also the pulse height of CIII was registered for each valid event in order to get some idea about the pion stopping point in the target in the beam direction. For each run and corresponding degrader thickness the pulse height of CIII was calibrated by inserting ^{12}C plates of various thicknesses as targets and recording the pulse height distribution.

The hodoscope between C III and C IV consisted of 4 strips of 2.5 cm width each, mounted on SEN 1045

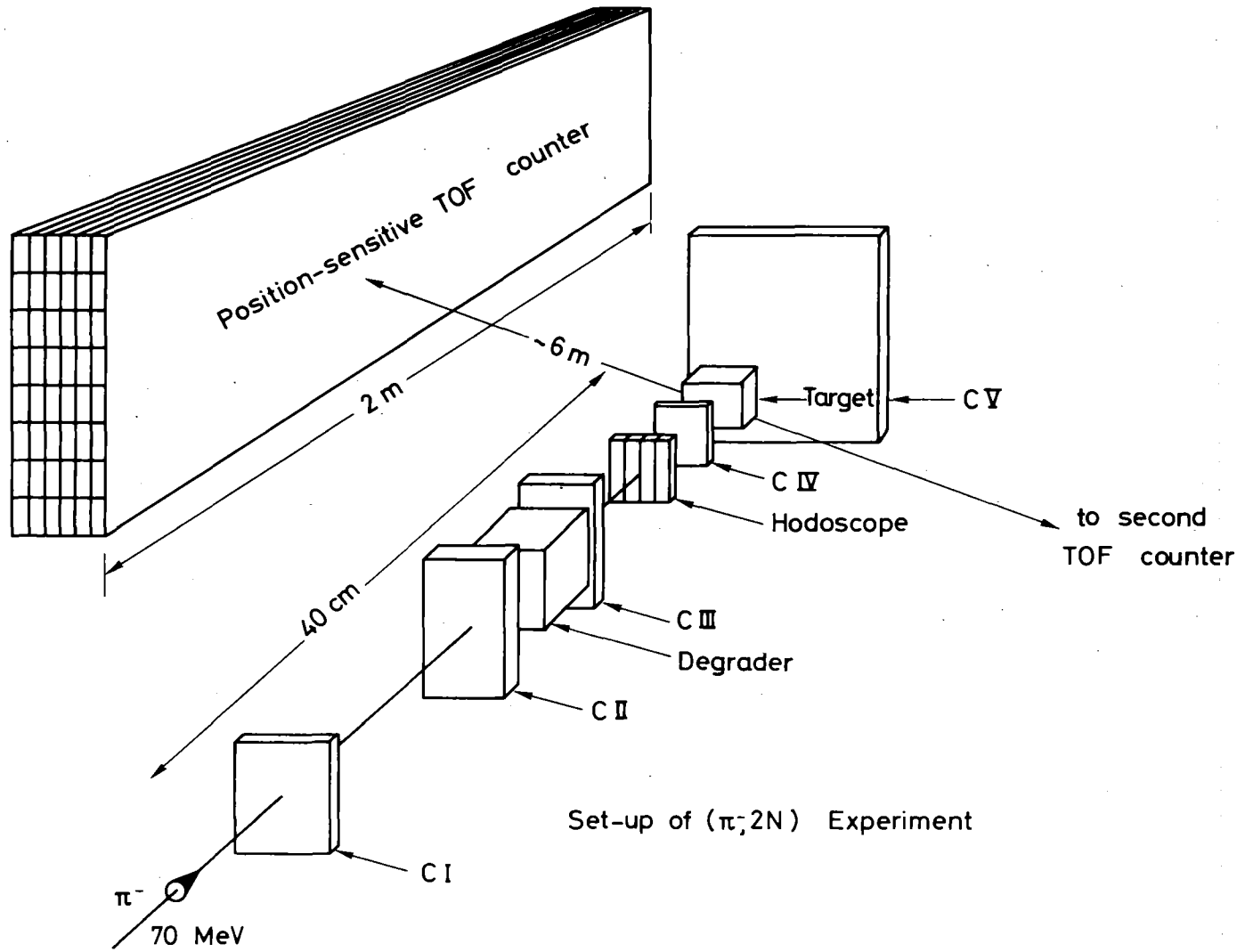

Fig. 6: Experimental set-up

photomultiplier assemblies. It determined with an accuracy of about ±1.5 cm the pion stopping point in the target perpendicular to the beam direction. C IV was a very thin (0.5 mm) scintillator and rejected the pions which had stopped in the hodoscope and not in the target.

The anti-counter V was relatively large in area, 30 x 25 cm, and like C II and C III it had a pair of twisted-strip light-guides and RCA 8850 photomultipliers. The threshold of its discriminator was kept as low as possible in order to ensure high efficiency.

For the detection of the two neutrons we used two large-area, position-sensitive time-of-flight counters with the dimensions 200 x 48 x 9 cm. They will be described in IV. 2.

For the targets ^{9}Be, ^{10}B, ^{12}C and ^{14}N the distance from the target to the neutron counters was 4.5 m and the angle between the lines connecting the center of the counters with the target was 160°. In the case of ^{6}Li, ^{7}Li and ^{16}O they were 5.8 m and 169°, respectively. With ^{16}O an independent measurement was performed at 4.5 m distance and an angle of 140°. The covered range for the angle ω was 140-180°, 150-180° and 125-160°, respectively, for the three cases just mentioned.

IV. 2. Neutron counters

The picture below shows one of the two neutron counters used. Their design is based on a smaller prototype counter. Its construction and testing is described in Refs. 38 and 39. Therefore, only the most important features will be explained here.

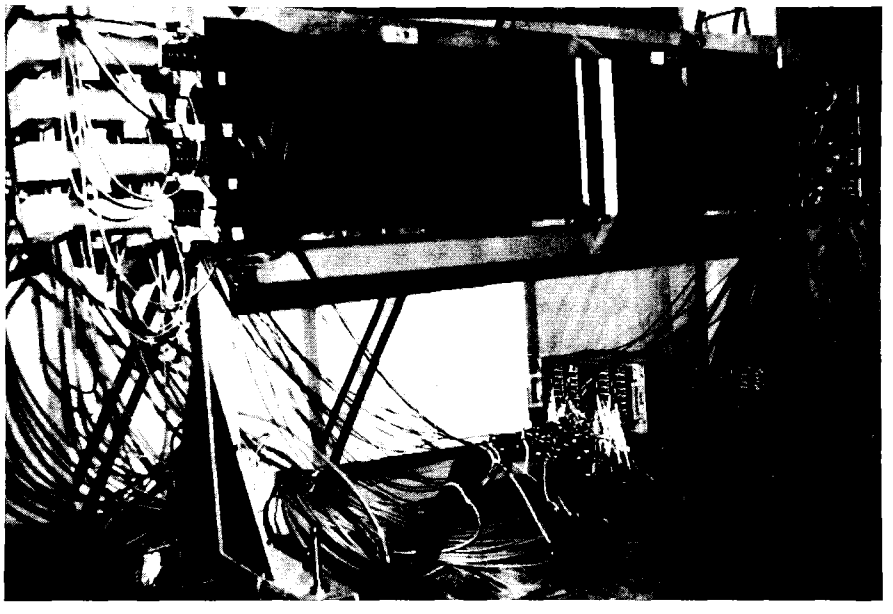

Each of the two counters used in this experiment consists of 4 moduls mounted on top of each other. Each module is subdivided into 12 scintillator rods, 6 in depth and 2 in height. The whole counter is assembled from 48 optically isolated rods of 200 x 6 x 1.5 cm each.

The material is NE 110. The total thickness of 9 cm was chosen as a compromise between efficiency and unwanted number of double-scattering events. The subdivision in depth allowed a better localization of the neutron interaction point and thus improved the resolution.

A pair of 56 DVP photomultipliers was attached to each module. They provided the information on time-of-flight and on the time difference between the arrival of the light signals at both ends and on pulse height. From the time difference the neutron impact point along the counter was determined.

Apart from the eight 56 DVP's 30 small tubes, SEN 1045, were mounted on each counter. For each valid event the pattern of all phototubes producing a signal was recorded. Later, in the off-line program, this allowed to recognize those rods that had emitted light and thus determined the neutron impact point vertically and in depth.

A more detailed description of the counters can be found in Refs. 38 and 39.

The time resolution obtained with minimum ionizing electrons, generating 20 MeV pulses in the counter, was typically 800 psec. This includes 300 psec from the start counter. It was measured between one side of the neutron counter and the start counter with particles hitting the neutron counter only in the center.

The spatial resolution was about ±4.5 cm along the counter, resulting in an angular resolution of about ±0.5° for a flight path of 5.8 m.

The resolution finally achieved in excitation energy of the residual nucleus was 3-6 MeV, depending on the pulse height threshold, the flight path, and the excitation energy. This is at least by a factor of three better than in all previous (π^-, 2n) experiments.

Calibration of the counters, i. e. adjustment of high voltages for the phototubes, adjustment of discriminator thresholds, and calibration of slope and zero offset of the time encoders was done before each data acquisition run. For this purpose, both counters were positioned in the direct beam of the low-energy pion channel. Light propagation velocity and light attenuation in the modules were also determined in the beam. Knowledge of the effective light propagation velocity is necessary to determine the neutron impact point along the counter from the measured time difference between the left and right ends of the counter. Light attenuation plays a role in determining the software pulse height threshold used in the off-line analysis in order to take into account the efficiency.

IV. 3. Electronics

Fig. 7 shows a block diagram of the electronics for the (π^-, 2n) experiment. The electronic set-up of the two counters is symmetric and therefore only the electronics associated with the neutron counter 1 (NC 1) has been represented.

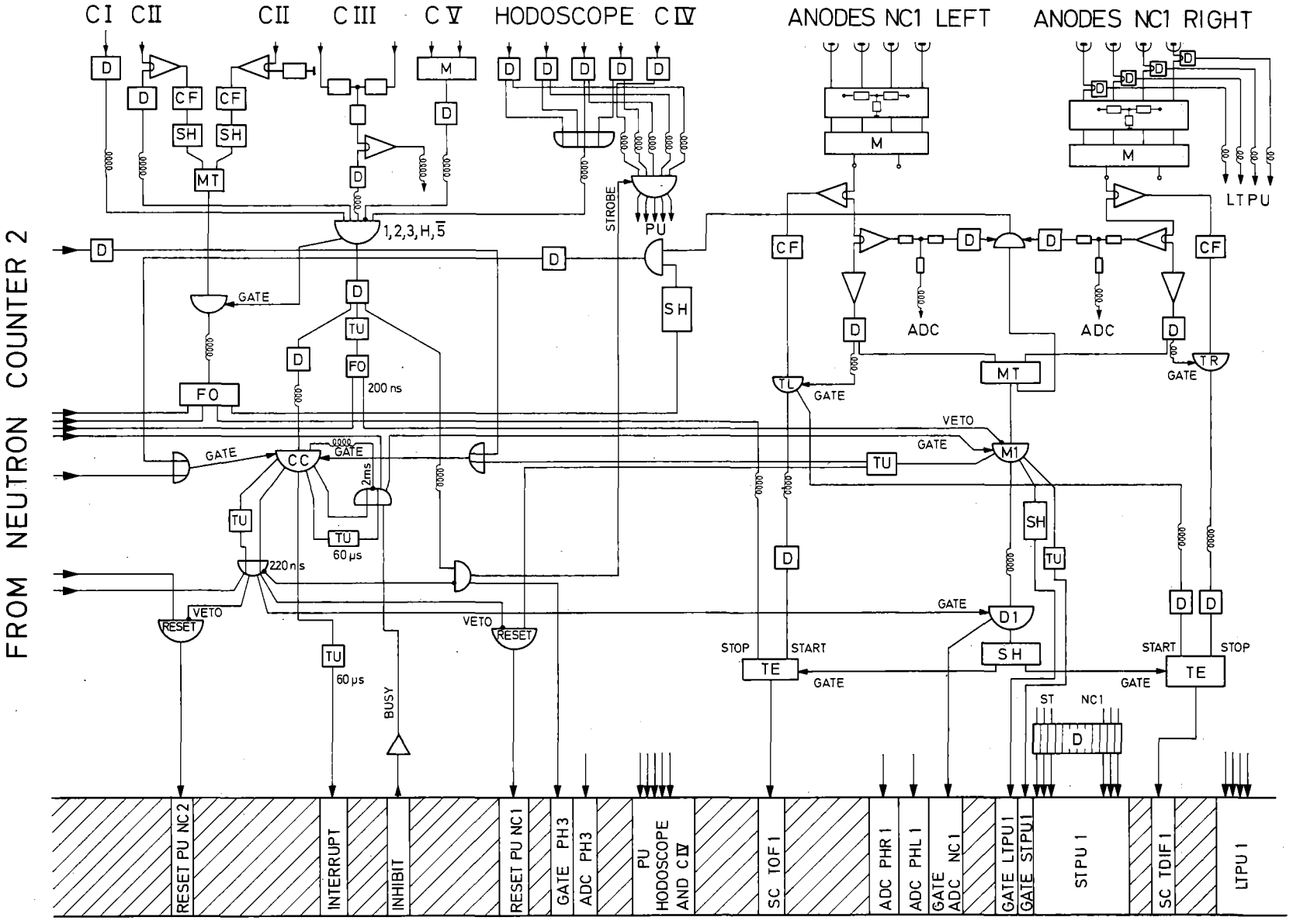

Fig. 7: Block diagram of the electronics

Notation: D=Discriminator, M=Mixer, CF=constant fraction discr., SH=Shaper, MT=mean timer, FO=Fan out, TU=Timing unit, PU=Pattern unit, TE=Time encoder, SC=Scaler, NC=Neutron counter, CC=central coinc., D1=delayed coinc. NC1, LTPU=large tube PU, STPU=small tube PU, TL(R)=time left (right), M1=Master coinc. NC1, ST=Small tubes, PHR(L)=pulse height right (left), TOF= time of flight, TDIF=time difference

After the stop coincidence (1, 2, 3, hodoscope, $\overline{5}$) had registered a stopped pion a gate of about 200 nsec width was generated. During this time both neutron counters had to give a signal (so-called master coincidences M1 and M2) in order to indicate a valid event. In this case, the central coincidence (CC) would be open and via the so-called delayed coincidences (D1 and D2) gate signals would be generated for the pulse height and time information from both counters. The corresponding signals were delayed until the gate was present. The logic signals from all small tubes and from one big tube per module were fed without delay into pattern units. In case of no valid event these units were reset.

For each valid event the following quantities were recorded:
four pulse heights (left and right sides of each neutron counter), four time informations (two times-of-flight and two time differences), for both counters the pattern of all big and small tubes with a signal, the pulse height of C III, and the hodoscope information. In addition, several flags were set, for instance for the thin counter C IV or for a second stop signal within a certain time after the first.

Each valid event generated an interrupt and the on-line PDP 8L computer read out the CAMAC crate and transferred the information into a buffer. 31 events were written on magnetic tape as one block. During the whole readout and transmission cycle of 2 msec the electronics was blocked against events by means of veto

signals. Despite this relatively long time interval, the dead time turned out to be completely negligible as the valid event rate was of the order of 0.2/sec.

Separate scalers registered the following rates: pion stop rate, the most important coincidences like master, central, delayed and also chance coincidence rates for which additional coincidences were set up.

IV. 4. Off-line analysis

The very extensive off-line data analysis was performed on the CERN CDC 7600, to a large extent parallel to data acquisition. Only the most important points will be mentioned here.

In order to achieve the desired high resolution in excitation energy, the time resolution of the neutron counters required special care. In particular, the so-called walk effect (dependence of the triggering time on pulse height) had to be treated very carefully. We used ORTEC 473 constant fraction discriminators for this purpose, but their residual walk turned out to be still too great. Therefore, we determined for each constant fraction discriminator the "walk-curves", i. e. we measured with the counters in the pion beam the dependence of the signal time on pulse height. The necessary variation in pulse height was achieved by changing the high voltages. The resulting "walk-curves" were incorporated into the evaluation program and for each

event analyzed the time-of-flight and time difference were corrected accordingly. In this way, the resolution in E_x could be improved by 2-3 MeV.

For the determination of absolute rates the efficiency of the neutron counters has to be known. It depends critically on the pulse height threshold. For big counters, as we used them, also the light attenuation has to be taken into account in order to have a pulse height threshold independent of the position along the counter. In case of exponential light attenuation the geometrical mean value of the pulse heights on both ends, $(PH_{left} \cdot PH_{right})^{0.5}$, is independent of the position. Therefore, in the course of data analysis a software pulse height threshold was set on that quantity. This threshold was in general 4-5 MeV electrons equivalent and was checked to be higher than the hardware threshold of the discriminators. The efficiency was calculated according to the Kurz code [40] which had been tested on the prototype counter by comparison with an experimental efficiency determination [39]. Relatively good agreement was found. Unless stated otherwise, all distributions shown here are corrected for neutron counter efficiency.

As we restrict ourselves to nn-coincidences, the events with at least one charged particle had to be rejected. The big counters are of course also sensitive to charged particles. They were identified (mainly protons) by means of the known relationship between the energy and pulse height and, in addition, by taking into account that charged particles trigger in any case the first layer of rods in the counter.

Apart from the neutron counter efficiency, the data had to be corrected for geometrical acceptance. By this we mean that the detection efficiency is a function of the angle ω, the position and the size of the two counters. With a Monte Carlo simulation program this dependence was determined and used for data evaluation. Unless stated otherwise all distributions shown are corrected for this geometrical acceptance.

Events with at least one low energy neutron, i. e. E_n < 12-15 MeV, were rejected; the same applies for events from the last 12 cm on each counter end because of nonuniformity in the light propagation velocity.

Within the covered ω-range and for E_n > 12-15 MeV all of our distributions represent the transition rates, i. e. they are fully corrected and can, therefore, be directly compared with theoretical predictions.

Recoil momentum distributions are in general divided by the three-body phase space factor (see II. 8.) and thus represent the dependence of the matrix element on q. For q > q´ (see II. 4.) the restriction in phase space due to the geometry has been taken into account. For the θ-distributions q has been integrated up to q = q´.

The errors given are statistical errors that take into account the event by event correction factor for counter efficiency and geometrical acceptance as well as the number of events. The estimated error for the quoted absolute rates is $\pm^{60}_{30}$ %. This includes possible losses

of events during data acquisition, rejection of events during off-line analysis, uncertainties in the pion stop rate and in the efficiency of the counters.

V. RESULTS AND DISCUSSION

V. 1. ^{6}Li

^{6}Li is probably the best studied nucleus as far as pion absorption experiments are concerned. The special interest in this target nucleus centers around the following facts:

a) It is known from many theoretical and experimental investigations of quasi-free scattering reactions, such as (p, pd) [18,41], (p, pα) [42], (d, 2d) [43], (d, dα) [44,45], (α, 2α) [46,47] and also quasi-free electron scattering [48], that the α-d cluster structure is an important part of the ^{6}Li g. s. configuration. In this picture the separation energy of a deuteron in ^{6}Li is only 1.47 MeV, which means that the two clusters are on the average rather separated in space. Therefore, the quasi-free description of π-absorption is expected to work well in this case.

b) Due to the large number of investigations the ^{6}Li wave function is fairly well known which is important for theoretical calculations and comparisons with experimental results.

c) In contrast to heavier 1p-shell nuclei a not negligible number of pions are absorbed from the 1S atomic orbit. So far more theoretical effort has gone into S-wave absorption than into P-wave absorption.

d) Since there are only 2 nucleons in the 1p-shell, considerable absorption by the s-shell nucleons is expected which leads to highly excited states of the residual nucleus ^{4}He.

e) The distortion effects on these ejected s-shell nucleons should be less important than in heavier nuclei.

Several authors have so far investigated experimentally the ^{6}Li (π^-, 2n) ^{4}He reaction [4,5,6]. Only in the case of Ref. 6 more than one peak could be resolved in the excitation energy spectrum, but the statistics was very poor (284 events in total). The analogous ^{6}Li (π^+, 2p) ^{4}He reaction was studied with a significantly better resolution [8,9,10], using π^+ of 31 to 76 MeV kinetic energy. The excitation energy distributions were dominated by two large peaks, a narrow one centered at 0 MeV and corresponding to the transition leaving ^{4}He in its ground state, and a much wider peak between 20 and 40 MeV excitation energy.

Our measured excitation energy spectrum in shown in Fig. 8. It is in very good agreement with the aforementioned (π^+, 2p) results. For the first time in a (π, 2N) experiment the peak between 20 and 40 MeV provides indications of fine structure. It, obviously, consists of

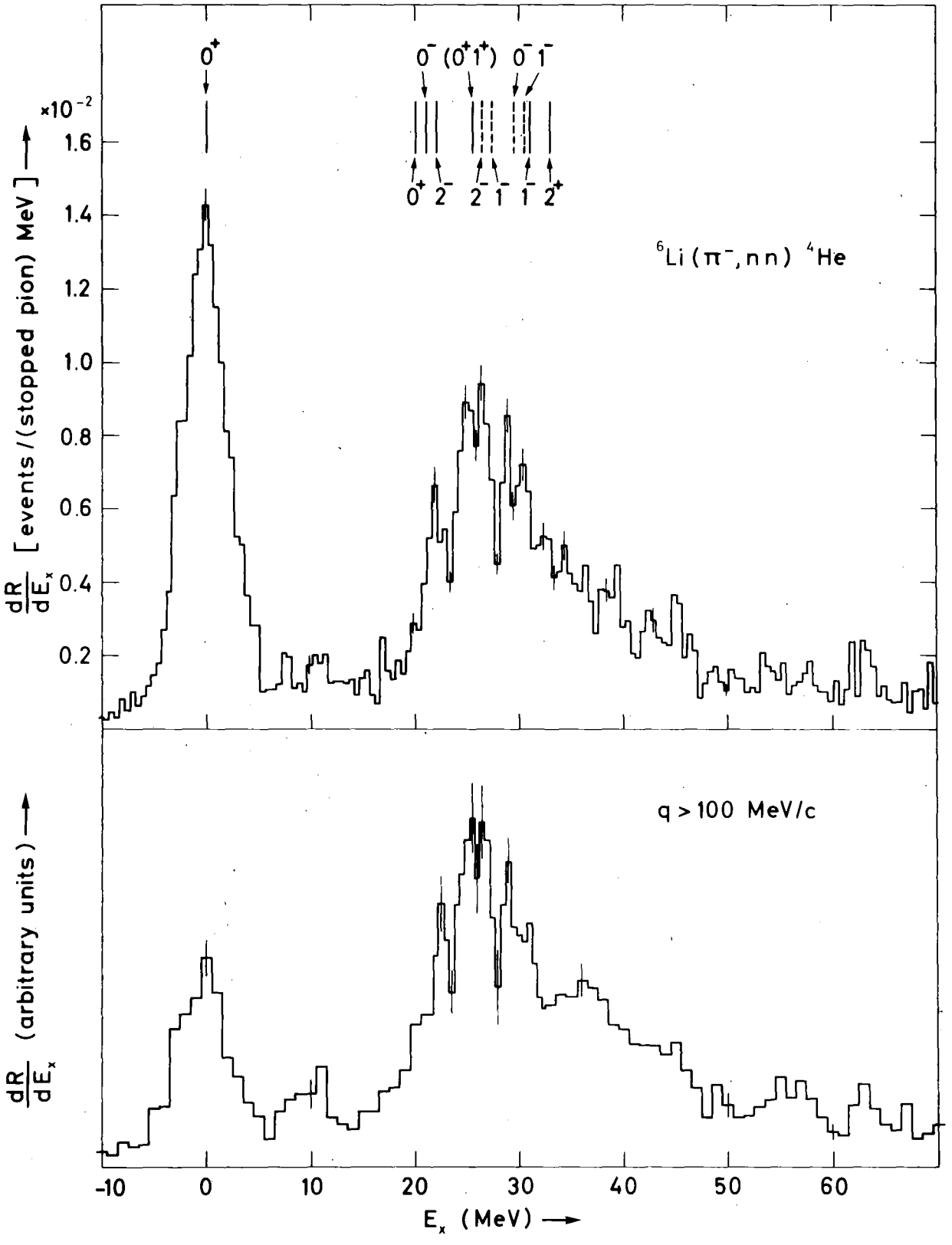

Fig. 8: Excitation energy spectra of ^{4}He. Top: all data (positions and quantum numbers of the known levels are also indicated). Bottom: events with large recoil momenta.

several of the known excited states [49] of ^{4}He which are also indicated in Fig. 8.

This spectrum can be interpreted in the following way. Absorption by the two $p_{3/2}$-shell nucleons of ^{6}Li gives ^{4}He in its ground state, whereas the structure at higher excitation energies results from absorption by two nucleons at least one of them stemming from the s-shell. We denote the three possibilities by p^{-2}, $s^{-1}p^{-1}$ and s^{-2}.

In a cluster model description the ground state transition corresponds to absorption by the d-cluster in ^{6}Li. In this picture the events at higher excitation energies are due to capture on either one nucleon from the d- and one from the α-cluster or on two nucleons from the α-cluster.

A comparison between the excitation energy spectrum without restrictions and with $q > 100$ MeV/c, also displayed in Fig. 8, shows that the ground state events are much more concentrated at smaller recoil momenta than the events with higher excitation energies. This is in agreement with the previous (π^-, 2n) experiment of Calligaris et al. [6] and with the (π^+, 2p) results given in Refs. 9 and 10. It can be explained by the different separation energies of the two regions; see Chapter II. 5. and Ref. 18.

Fig. 9 shows a density distribution as a function of the two neutron energies. The line of events corresponding to the ground state transition can be easily localized.

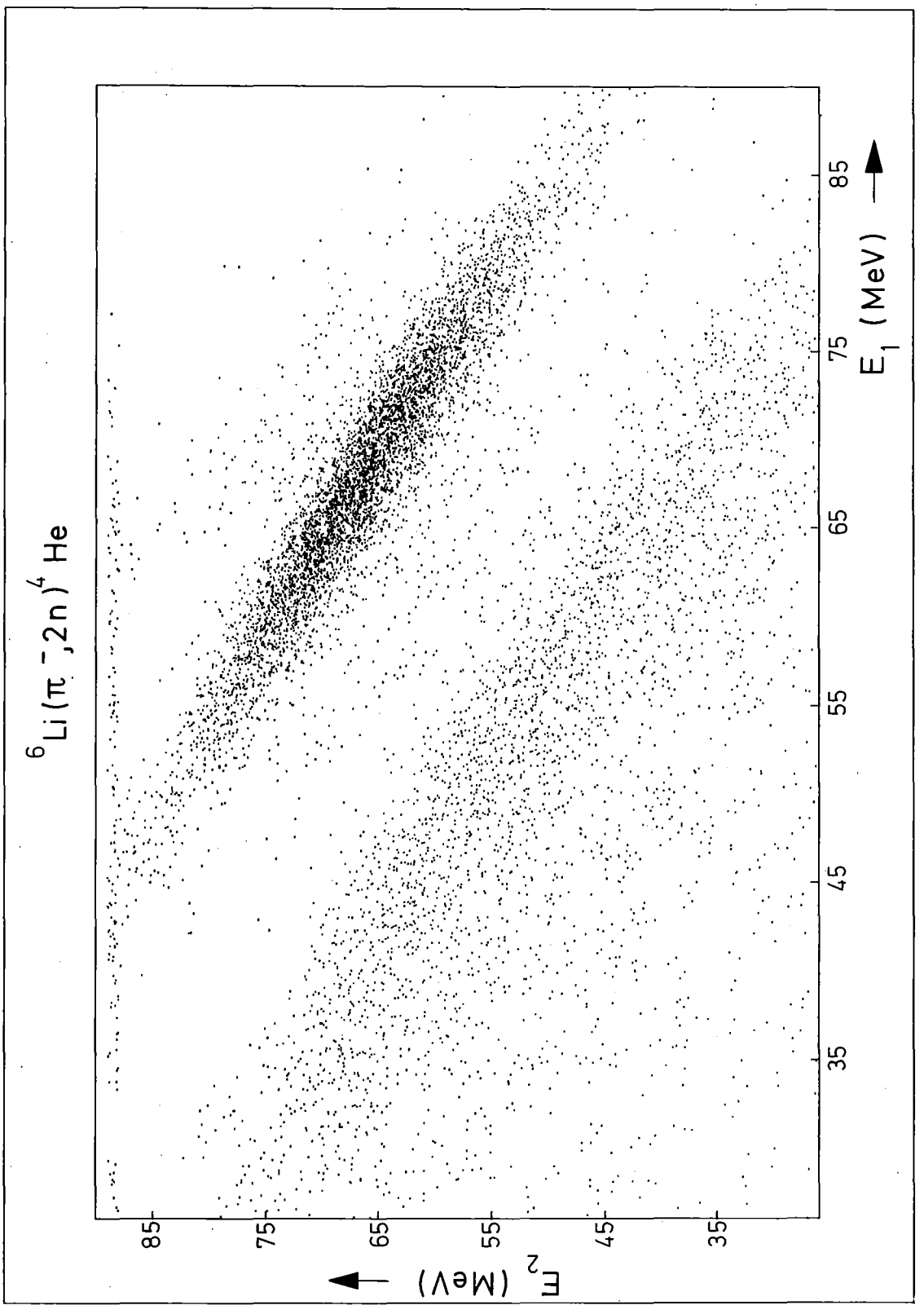

Fig. 9: Density distribution as a function of the two neutron energies

The data shown in this figure are raw data, i. e. not corrected for efficiency and geometrical acceptance. Therefore, the events with higher excitation energies are somewhat suppressed. The ground state distribution demonstrates the energy sharing between the two neutrons. The maximum occurs in the symmetric case where both nucleons emitted have the same energy. Away from this value the neutron energy distributions decrease rather quickly. Events in which one nucleon acquires a major portion of the energy and the other only little are very rare.

From many quasi-free scattering experiments and also from theoretical investigations the relative angular momentum between the α-and d-cluster in ^{6}Li is known to be L = 0. Then the quasi-deuteron must be in the $^{3}S_{1}$ state in order to give the correct ^{6}Li spin $J_{^{6}Li} = 1$.

The recoil momentum (q)-distribution for the ground state, shown in Fig. 10, indeed confirms an L = 0 transition having its maximum at q = 0 MeV/c. The very narrow width (HWHM ∿ 45 MeV/c) is due to the small separation energy of the two nucleons. This momentum distribution reflects the motion of the c.m. of the two p-shell nucleons ("deuteron-cluster") in the ^{6}Li nucleus. Similar q-distributions have been obtained by several of the already cited quasi-free scattering reactions (see Refs. 45, 47, 48, 50-53). A summary of the measured widths of these distributions can be found in Ref. 45.

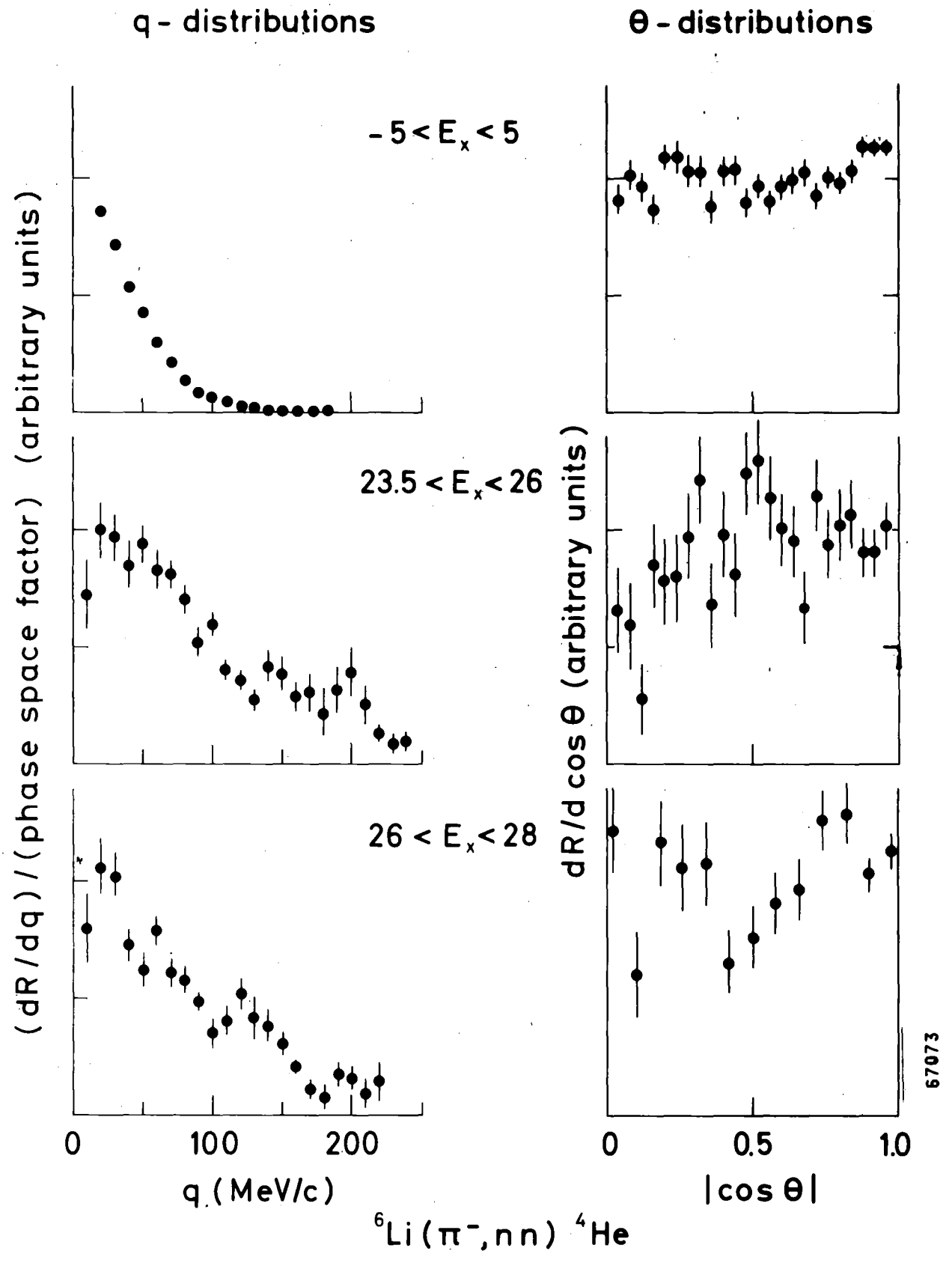

Fig. 10: q- and θ-distributions for different regions in excitation energy of ^{4}He.

Our value for the half width at half maximum (HWHM) of the q-distribution is in good agreement with the (π^+, 2p) results [9,10]. Probably because of worse resolution the value from a previous (π^-, 2n) experiment [6] is slightly higher than ours. In general, the widths resulting from pion absorption are larger than those from (x, xy) quasi-free scattering experiments.

In this context it has to be mentioned that in case of pion absorption the relative motion of the two nucleons modifies the measured recoil momentum distribution [18]. For the other reactions, like (p, pd) or (d, 2d), the quasi-deuteron stays a deuteron, whereas in the (π, 2N) reaction the π + "d" → 2N process itself affects the q-distribution.
Inclusion of the relative motion of the two nucleons (see Chapter II. 5.) makes the recoil momentum distributions broader. Also the distortion can affect the q-distributions differently for the various reactions.

In Fig. 11 we show again the measured q-distribution for the transition to the ^{4}He ground state together with some theoretical curves. The solid curve, taken from Ref. 18, is the Fourier transform squared of a 2S wave function in a square well potential. It was calculated with cut-off approximation and taking into account the relative motion and the separation energy for ^{6}Li → ^{4}He + p + n. It gives a rather good fit to the data.

The dashed curve is the corresponding 2S curve for a harmonic oscillator potential [10,33] neglecting the relative motion of the two nucleons:

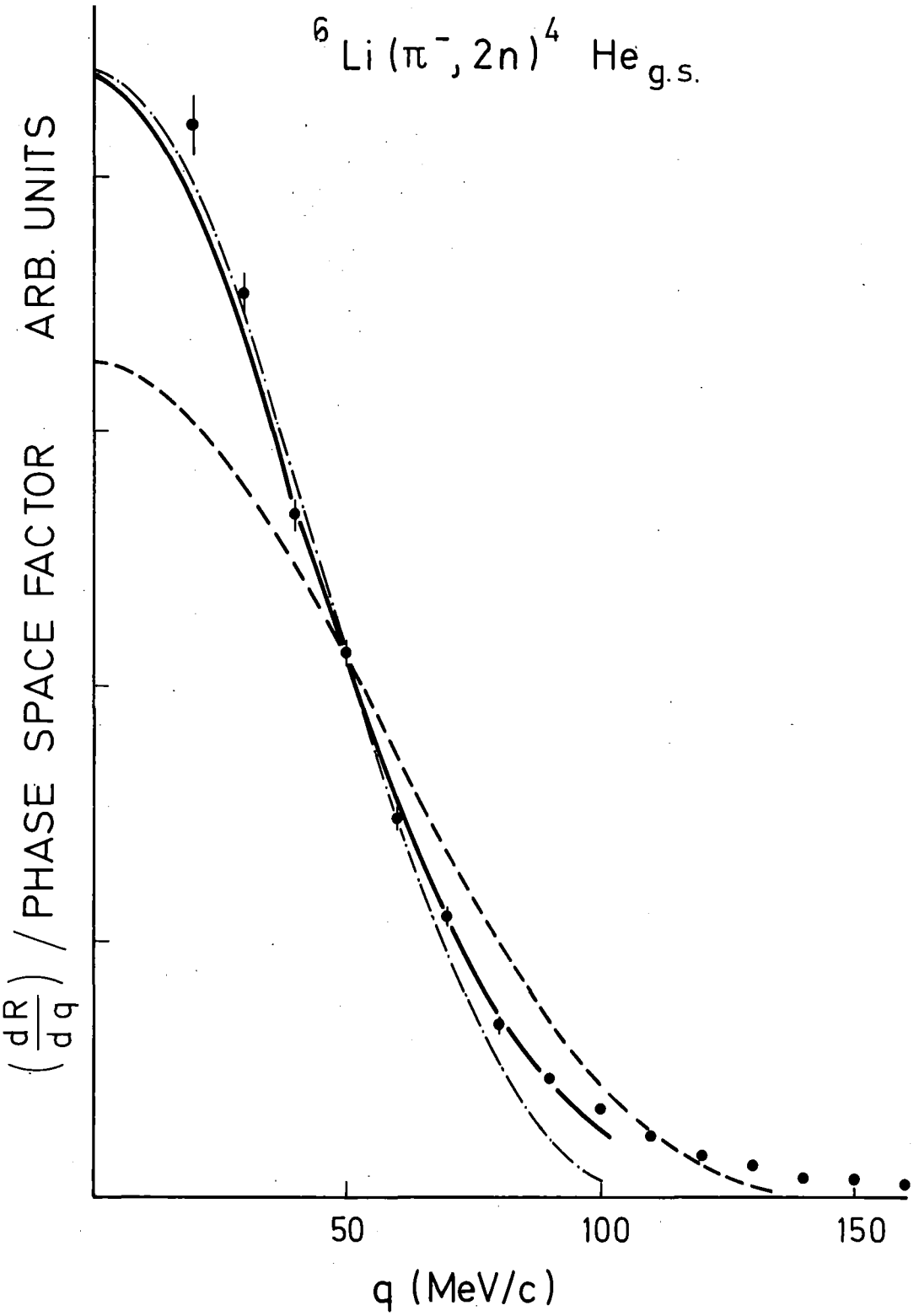

Fig. 11: Measured q-distribution for the transition to the ground state of ^{4}He. The solid line is a theoretical curve from Ref. 18 (2S-motion in a square well potential). The dashed and dot-dashed curves are calculated for 2S-motion in a harmonic oscillator potential. See also text.

$$\left|\Phi_{2S}(q)\right|^2 = \text{const.} \cdot (1 - \frac{2}{3}\ \frac{q^2}{q_0^2})^2 \cdot \exp\ (-\frac{q^2}{q_0^2})$$

The parameter q_0 is related to the harmonic oscillator length parameter r_0 which has been taken according to the r.m.s. radius obtained by electron scattering data [62].

With $q_0^2 = \mu \frac{\hbar^2}{r_0^2}$, r_0 = 1.92 fm (corresponding to an r.m.s. radius of 2.6 fm, see Ref. 62) and the reduced mass of the two nucleons and the residual ^{4}He $\mu \sim \frac{4}{3} m_n$ one obtains q_0 = 118.7 MeV/c. The curve, however, is too wide to fit the data.

By changing the parameter q_0 to q_0 = 92.4 MeV/c a better fit can be obtained; it is displayed as the dot-dashed curve. But this q_0 leads to an r.m.s. radius of 3.34 fm in clear disagreement with the electron scattering data.

Because of the extremely low separation energy of the two p-shell nucleons in ^{6}Li the correct asymptotic behavior of the wave function of their c.m. is very important. Therefore, the square well potential gives a much better reproduction of the data than the harmonic oscillator potential.

The θ-distribution for the ground state transition, also shown in Fig. 10, is independent of θ. We know that $L_i = 0$ and if we assume the validity of Koltun's rule $\Delta L = 0$ (see Chapter II. 7.) we get $L_f = 0$ and with that the measured θ-distribution is easily explained (see II. 6.).

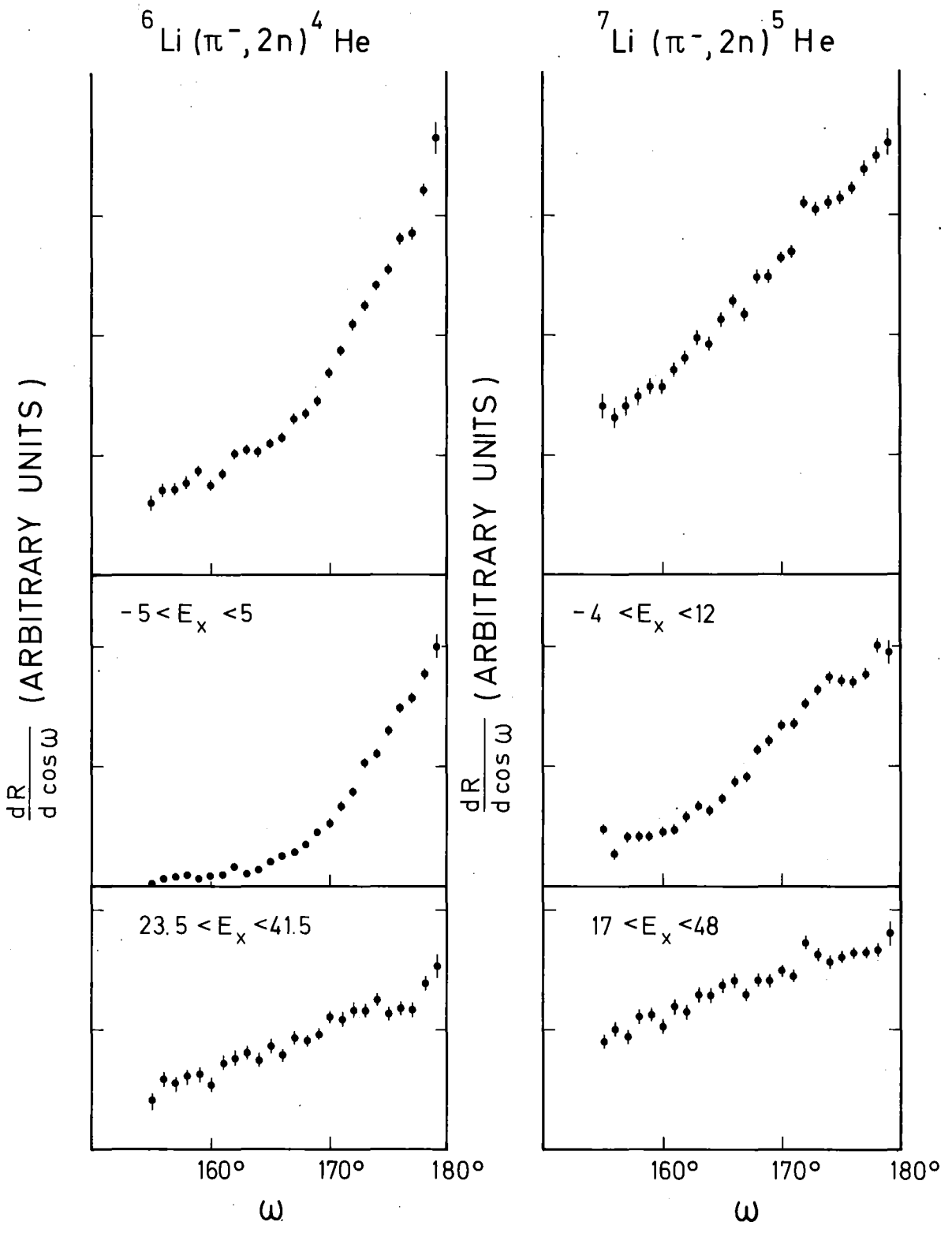

Fig. 12: ω-distribution integrated over all excitation energies (top) and for different regions in excitation energy (center and bottom) of ^{4}He and ^{5}He, respectively.

The ω-distribution for the ground state transition, shown in Fig. 12, exhibits the expected strong peaking towards 180°, thus proving the dominance of the quasi-free reaction mechanism.

Our ^{6}Li ω-distribution integrated over all excitation energies, also shown in Fig. 12, is considerably narrower than the one obtained by Nordberg et al. [5], HWHM ∿ 9° compared to ∿20°. It is more consistent with the distribution given by Davies et al. [4] although these authors have measured only very few points. In Fig. 13 we show again the same ω-distribution integrated over all excitation energies together with a theoretical prediction by Kopaleishvili and Machabeli [54], based on an α-d model of ^{6}Li and S-wave absorption of the pion.

The general tendency and width are reproduced. The same distribution calculated with a shell model of ^{6}Li is much too wide; see Ref. 54. However, the theory does not seem to be refined enough to allow final conclusions to be drawn.

Fig. 13 also shows our measured ground state ω-distribution together with two theoretical predictions. One is from Jain and Banerjee [55] who include the interaction of the outgoing neutrons with the residual nucleus (distortions), using distorted waves, and assume S-wave π-absorption. They use shell model wave functions and neglect the mutual NN interaction in the final state. There is no satisfactory agreement with our data which agree better with the calculation of Alberi and Taffara [56]. These authors employed a simple α-d model of ^{6}Li

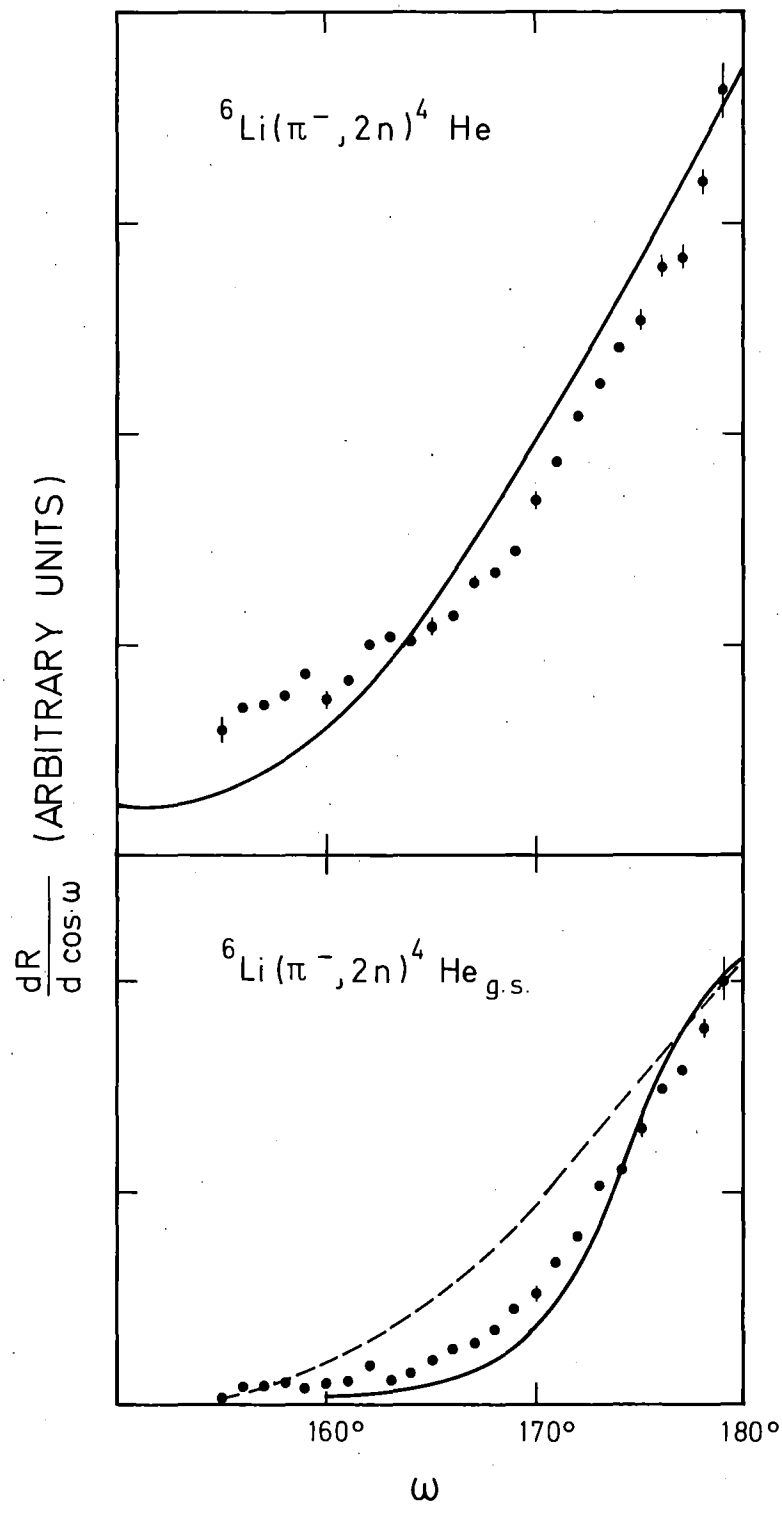

Fig. 13: ω-distributions for the residual nucleus ^{4}He. Top: all events; the solid line is a theoretical curve from Ref. 54. Bottom: events from the transition to the ground state; the solid curve is from Ref. 56 and the dashed one from Ref. 55.

and also assume S-absorption. They do not include effects of distortions.

It should be kept in mind that all these comparisons are not presented in terms of absolute rates and that the theoretical treatments usually neglected some important aspects such as P-wave absorption.

The neutron energy distribution for the ground state events, shown in Fig. 14, consists of a rather narrow symmetric peak centered at a value corresponding to half the energy available. Together with the narrow ω-distribution it forms a consistent picture of the direct quasi-free absorption by the two p-shell nucleons of ^{6}Li.

Due to the very narrow q-distribution of this transition the relative momentum p between the two neutrons emitted is restricted to a very small region around 350 MeV/c; see Fig. 14.
The maximum value of p can easily be calculated; it corresponds to q = 0 as is explained in Chapter II. 2.

As a summary for the ^{6}Li $(\pi^{-}, 2n)$ $^{4}He_{g.s.}$ transition it can be said that all distributions indicate clearly the dominance of the direct, quasi-free reaction mechanism. Due to the small separation energy and the large distance in excitation energy to the first excited state, this is a unique case for experimental and theoretical investigations. Even relatively simple theoretical calculations seem to give at least qualitative agreement with the q- and ω-distributions. This indicates that the effects of distortions and NN final state interactions can not be important.

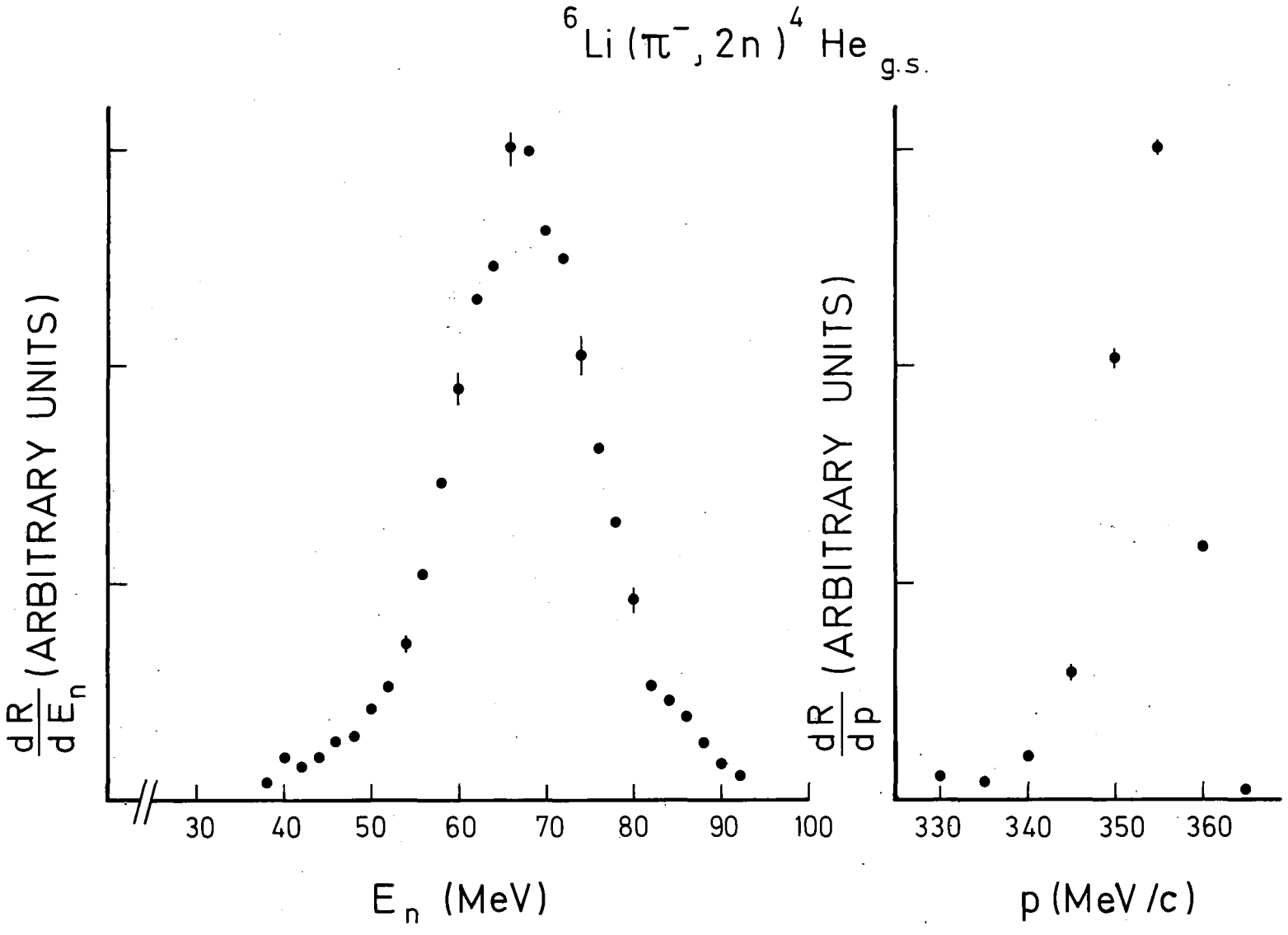

Fig. 14: E_n- and p-distribution for the transition to the ground state of ^{4}He.

^{4}He excited states

In good agreement with previous (π^+, 2p) experiments [8,9,10] we see many events with excitation energies of 20-50 MeV. The known excited levels of ^{4}He [49] start at 20.1 MeV and are all particle unstable. The possible final states and their thresholds in excitation energy are:

t + p	19.8 MeV
^{3}He + n	20.6 MeV
d + d	23.9 MeV
d + n + p	26.1 MeV
2n + 2p	28.3 MeV

An interesting question is whether and how much absorption occurs on pairs where one nucleon comes from the α-cluster (s-shell) and the other nucleon from the d-cluster (p-shell). This might lead to the final states t + p or ^{3}He + n mentioned above and would result in a negative parity final state (see also Chapter II. 5.). The corresponding excitation energies are expected to be lower than for the case of both absorbing nucleons from the α-cluster, i. e. s^2-removal.

The following is a simple argument against s^1p^1-removal. Because of the low d-α separation energy the two clusters are most of the time rather widely separated in space. Therefore, it seems unlikely that there is enough spatial correlation between one nucleon from the "d" and one from the "α" to absorb the pion. This consideration is consistent with the result of the cluster model calculation by Golovanova and Zelenskaya [23]. They predict a ratio of 1:0.2:1.5 for p^2:s^1p^1:s^2 removal.

With a sufficiently good resolution one can hope to resolve the individual excited levels of ^{4}He and then draw a conclusion from the parity with respect to s^1p^1- or s^2-removal. However, our experiment cannot distinguish between these two cases; but we do observe a relatively weak population of the first two excited levels (20.1 MeV, 0^+, T = 0 and 21.1 MeV, 0^-, T = 0). Our main strength centers around 22.5 MeV, 24-27 MeV, 30 MeV and perhaps 35-36 MeV (see Fig. 8). The only other positive parity levels known are at 25.5 MeV (0^+ or 1^+, T = 0) and 33 MeV (2^+, T = 0). As not only these two states are reached, it is very likely that we observe some negative parity states, i. e. s^1p^1-removal. One example is the apparent structure around 30 MeV.

In any case our excitation spectrum reproduces the general features of the cluster model prediction of Ref. 23. Their calculation with a shell model wave function for ^{6}Li agrees less with our spectrum than the cluster model does because it gives too much strength around E_x = 20 MeV.

In another calculation by Kopaleishvili and Machabeli [34] for the process (π^-, 2N) on ^{6}Li special attention was paid to the rescattering effect (see Chapter III.). The calculation was carried out for absorption from the atomic 1S-orbit and within the shell model. In their model it turns out that s^2-removal is negligible compared with s^1p^1-removal and therefore their detailed excitation energy prediction shows only negative parity excited

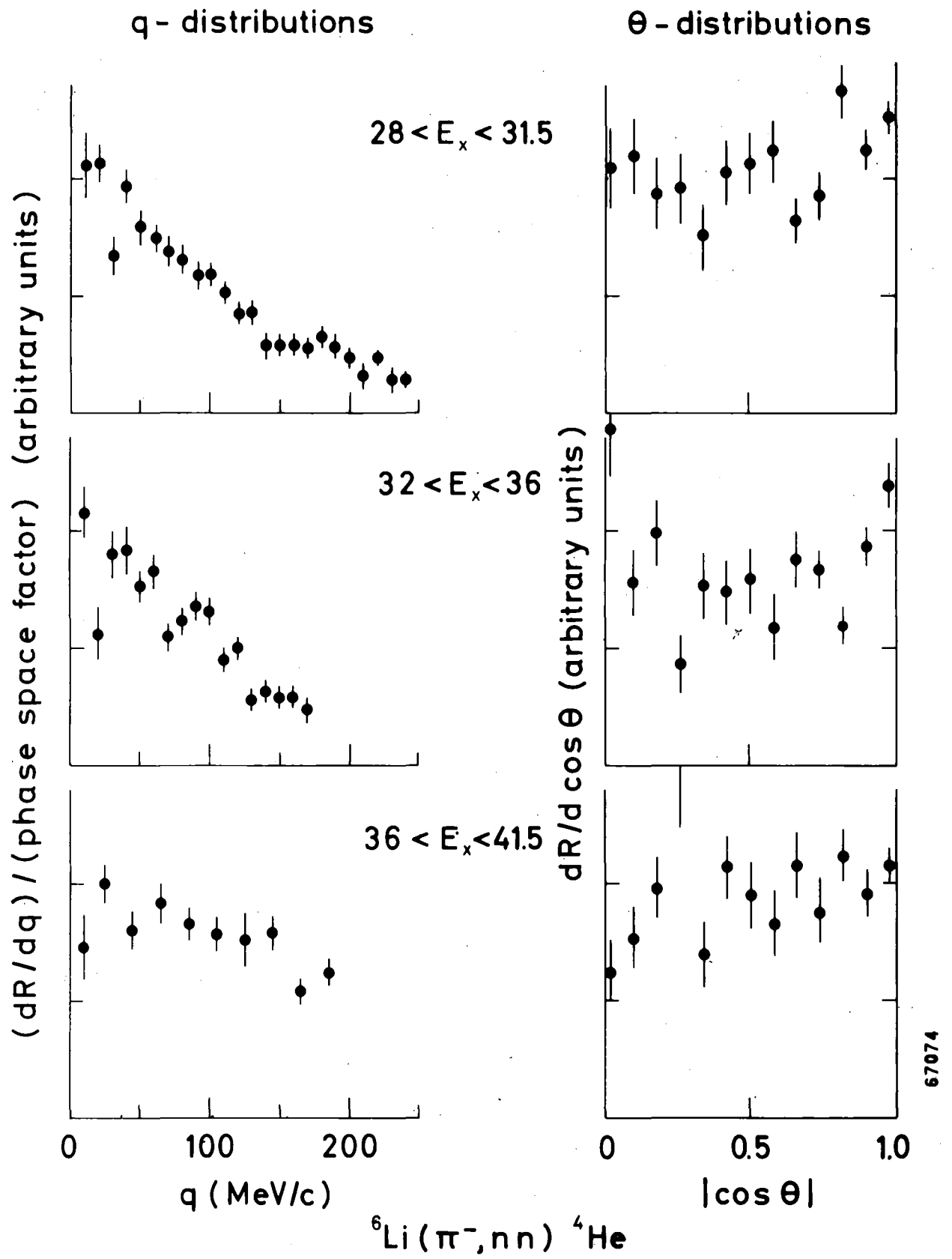

Fig. 15: q and θ-distributions for different regions in excitation energy of ^{4}He.

states of ^{4}He. It is, however, inconsistent with the known level scheme of ^{4}He [49].

Burman and Nordberg [8] interpreted their (π^+, 2p) results in terms of preferential excitation of T = 1 negative parity levels. But at that time no positive parity level in ^{4}He between 21 and 28 MeV was known.

In principle the measured q-distributions for the events with high excitation energies should help in clarifying the open questions concerning $s^{-1}p^{-1}$ and s^{-2} probabilities. Several of such q-distributions are shown in Figs. 10 and 15. Obviously, all of them are much wider than the ground state q-distribution but they all seem to have the maximum at q = 0, indicating at least an important L = 0 component. For s^2-removal a wide distribution is expected due to 1S motion. For s^1p^1-removal and l_i = 0, however, it should be 1P with a minimum at q = 0, which is not observed. Of course, in this case also 1S x 1p is allowed but this would mean l_i=1 and it is not clear if the spatial correlation between two such nucleons is strong enough.

Our geometry for this target favored L = 0 and so a possible explanation for the events characterized by high excitation energies is a major s^{-2} part plus some $s^{-1}p^{-1}$ in the 1S x 1p configuration and some $s^{-1}p^{-1}$ with 1P x 1s where the distortion or other effects have filled the minimum at q = 0.

Fig. 16 shows the q-distribution we measured for events with excitation energies between 23.5 MeV and 28 MeV

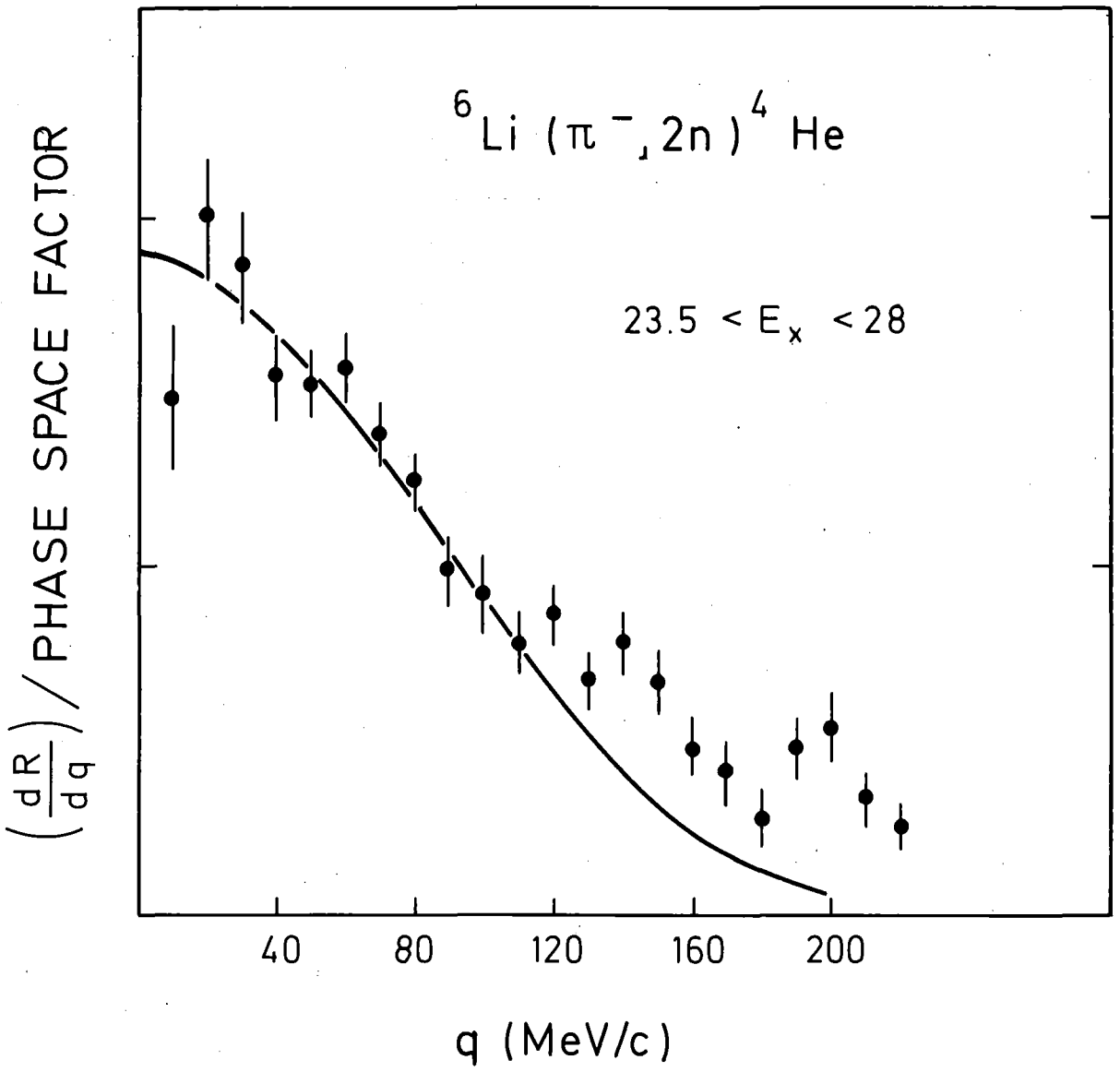

Fig. 16: Measured q-distribution for a certain region in excitation energy of ^{4}He. The solid line is a theoretical curve from Ref. 18, calculated for 1S-motion in a square well potential without cut-off and with zero range approximation (see also text).

together with a theoretical calculation by Sakamoto et al. [18] for the positive parity state around 26 MeV. The curve was calculated for a square well potential without cut-off and with zero range approximation for the two absorbing particles. In this case, the transition matrix element reduces to essentially $\Phi(q)$, the Fourier transform of the 1S wave function of the c.m. of the two nucleons. From several calculated curves by Sakamoto et al. [18], with and without cut-off and zero range approximation, the one shown here gives the best fit to our data as far as the width of 90-100 MeV/c is concerned. One notices satisfactory agreement up to recoil momenta of $\sim$110 MeV/c, but not beyond.

Also Alberi and Taffara [56] calculated a q-distribution corresponding to high excitation energies, assuming the process to result in 2n + 2d. However, the resulting distribution is wider than any of our distributions up to E_x $\sim$36 MeV.

Figs. 12 and 17 show the opening angle distribution and some neutron energy and relative momentum distributions, respectively, for the region of high excitation energies. The ω-distribution is still peaked at 180^o but it is much wider than the ground state distribution. This, of course, is related to the wider q-distributions and can also be due to more distortions for the nucleons from the inner shell.

Also the E_n-distributions are much wider than for the ground state and the p-distributions change in the same way, which is expected on the basis of the wider q-distributions.

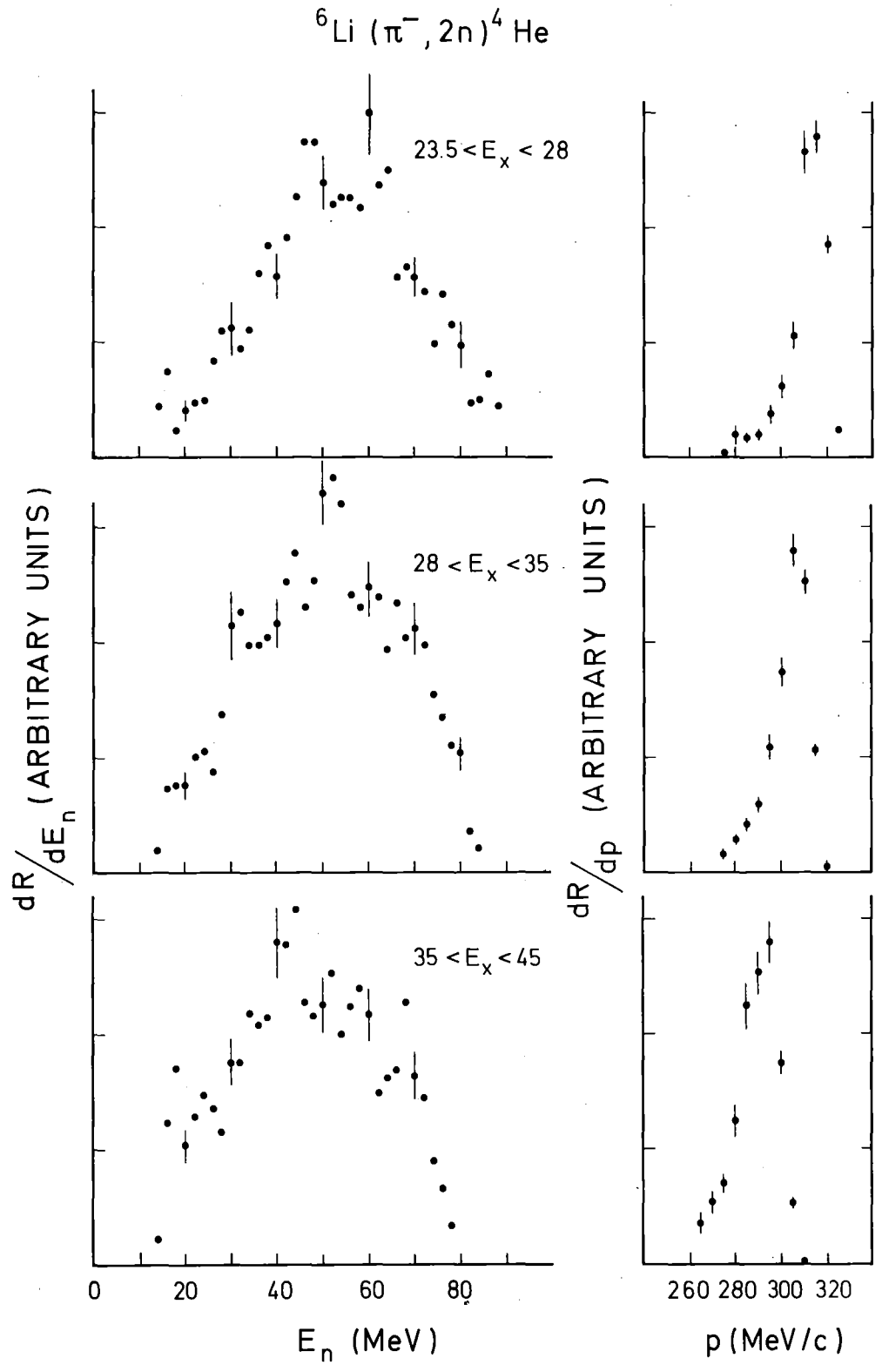

Fig. 17: E_n - and p-distributions for different regions in excitation energy of ^{4}He.

As a summary of the high excitation energy events in the ^{6}Li (π^-, 2n) ^{4}He reaction it can be said that in the shell model picture both s^1p^1 and s^2-removal very likely play a role. Their relative magnitudes are not yet clear but s^1p^1-removal does not seem to be dominant. The observed structure in excitation energy and the corresponding distributions in several variables demonstrate the importance of the direct, quasi-free mechanism involving the s-shell nucleons.

In general, cluster model descriptions of ^{6}Li give a better qualitative agreement between theoretical predictions and experimental results than shell model descriptions. This point is not restricted to high excitation energies and it is not surprising considering the well known cluster properties of ^{6}Li.

V. 2. ^{7}Li

In several respects ^{7}Li is rather similar to ^{6}Li and most of the points mentioned at the beginning of Chapter V. 1. are also applicable to ^{7}Li.

Based on cluster model calculations [57] as well as on quasi-free scattering reactions of the type (p, pt) [18] and (α, 2α) [47], the ^{7}Li ground state configuration is expected to be fairly well described by an α-t system with relative angular momentum L = 1. The triton spin $S_t = \frac{1}{2}$ couples with this L = 1 to give the ^{7}Li ground state spin $\frac{3}{2}$.

The following is an interesting aspect regarding ^{7}Li. In the triton of the α-t system we have one np-pair with antiparallel and one with parallel spin. Removing the pair in the antiparallel spin state leaves a neutron in the p-shell with spin parallel to L = 1; thus, the residual nucleus ^{5}He with spin $\frac{3}{2}$ is formed. Removing the pair in the parallel spin state leaves the neutron with spin antiparallel to L = 1, thus giving ^{5}He with spin $\frac{1}{2}$. The two residual states are easily found in the level scheme of ^{5}He [49]; they are the ground state and the first excited state, respectively. There are no other levels known in the vicinity and so we have a good opportunity to study the isospin dependence of the pion absorption mechanism. The transition to the ground state consists of T = 0 and T = 1 contributions, whereas the first excited state is reached exclusively by T = 0.

In previous measurements ^{7}Li was used as target by Davies et al. [4] and Nordberg et al. [5] for the (π^-, 2n)

reaction and by Favier et al. [9] for $(\pi^+, 2p)$. Also for the study of the two-nucleon transfer (p, ^{3}He) reaction ^{7}Li was used [58].

Fig. 18 shows the excitation energy spectra measured by us together with the few levels known of ^{5}He, all of which being particle unstable. Obviously the ground and first excited states are populated. According to Ref. 49 the first excited state ($\frac{1}{2}^-$, $T = \frac{1}{2}$) is centered around 4 MeV with a natural width of 4 MeV, whereas the ground state ($\frac{3}{2}^-$, $T = \frac{1}{2}$) has a width of 0.6 MeV. Then we observe considerable excitation from $\sim$12 MeV extending to beyond 40 MeV. The general shape of the spectrum is rather similar to the ^{6}Li case but the two dominating structures overlap more in ^{7}Li. The two previous ^{7}Li $(\pi^-, 2n)$ ^{5}He measurements either showed no excitation spectrum (Ref. 5) or was the resolution too bad (Ref. 4) to be comparable. However, our spectrum is similar to that obtained with $(\pi^+, 2p)$ [9], except that the $(\pi^+, 2p)$ result contains relatively more at higher excitation energies. This is true for the distribution integrated over all recoil momenta as well as for the one restricted to small q.

The fact that the ground state is populated to a fairly great extent proves that T = 1 absorption is of some importance. If we assume $l_i = 0$ and Koltun's rule $\Delta L = 0$, the selection rules of Chapter II. 7. show that the T = 1 contribution to this transition must have been induced by S-wave pions.

According to the c.f.p. calculation for quasi-elastic deuteron knockout [16] both transitions, the one to the

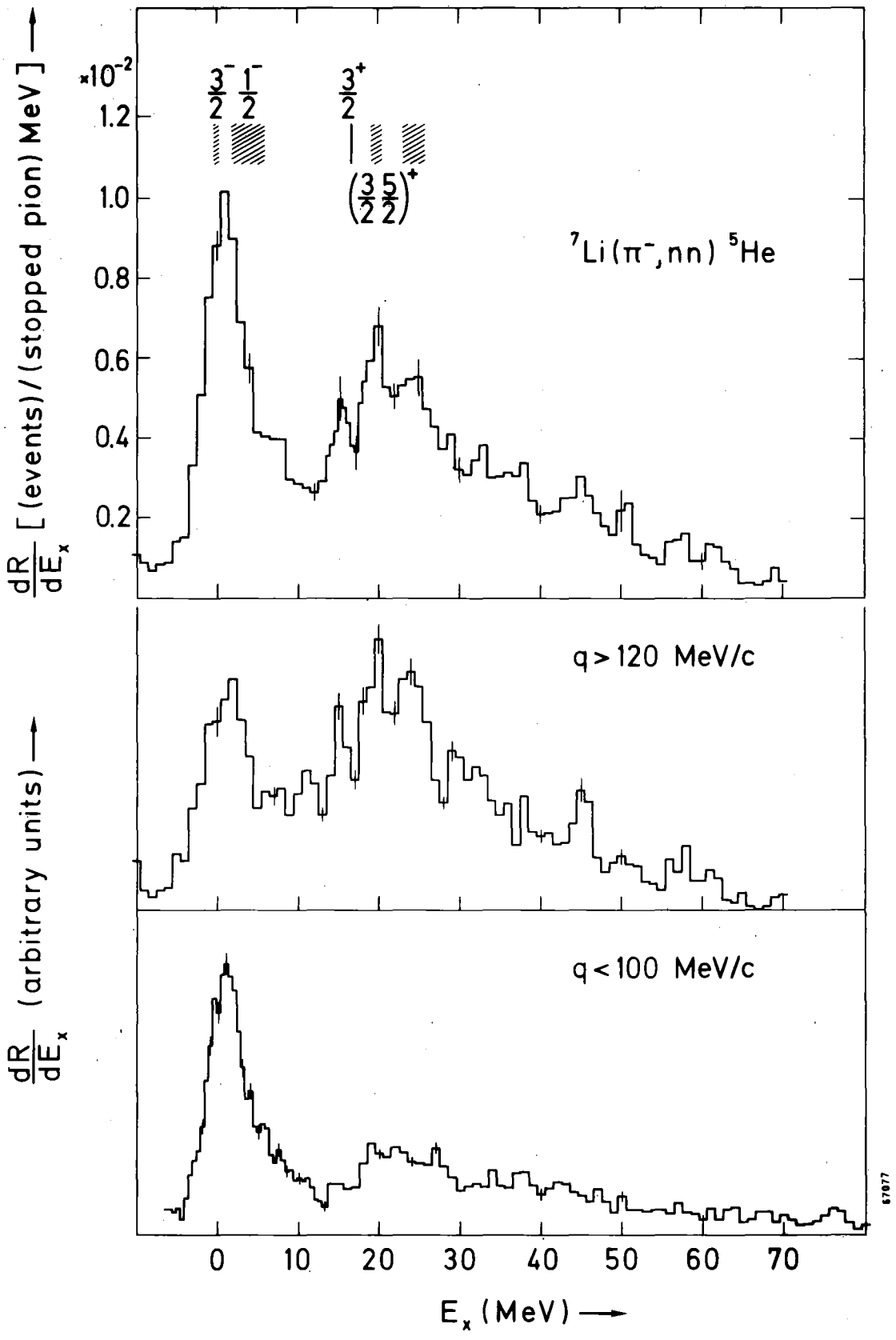

Fig. 18: Excitation energy spectra of ^{5}He. Top: all data (positions, widths and quantum numbers of the known levels are also indicated). Center and bottom: events involving restrictions on recoil momentum.

ground state as well as the one to the first excited state of ^{5}He, should have a 45 % L = 2 component, the rest being L = 0. The q-distributions we measured for these transitions, shown in Fig. 19, are somewhat biased due to the geometry ($\omega > 155^{o}$) and therefore L = 0 will dominate. Both distributions have their maximum at q = 0. The analogous (π^{+}, 2p) measurement [9] yielded a very similar recoil momentum distribution, both in terms of width (HWHM $\simeq$ 60-80 MeV/c) and in terms of a possible enhancement in the q-region 120-160 MeV/c. This shoulder can be the indication of the L = 2 component. Also the θ-distributions of Fig. 19, showing some θ-dependence, give a hint of transitions which are not exclusively $L_i = 0$, $\Delta L = 0$. The wider q-distribution of the ^{5}He ground state as compared to the ^{4}He ground state reflects the higher deuteron binding energy: 9.7 MeV in ^{7}Li, 1.47 MeV in ^{6}Li.

The opening angle, neutron energy, and relative momentum distributions for the ground plus first excited states shown in Figs. 12 and 20 emphasize the importance of the direct quasi-free absorption process, although all of them are wider than the corresponding ^{6}Li distributions.

Jain and Banerjee [55] calculated the q- and ω-distributions for ^{7}Li (π^{-}, 2n) ^{5}He and low excitation energies. As in ^{6}Li the q-distribution predicted by these authors is too wide to be compatible with our data, but for ^{7}Li the ω-distribution fits rather well. This is shown in Fig. 21.

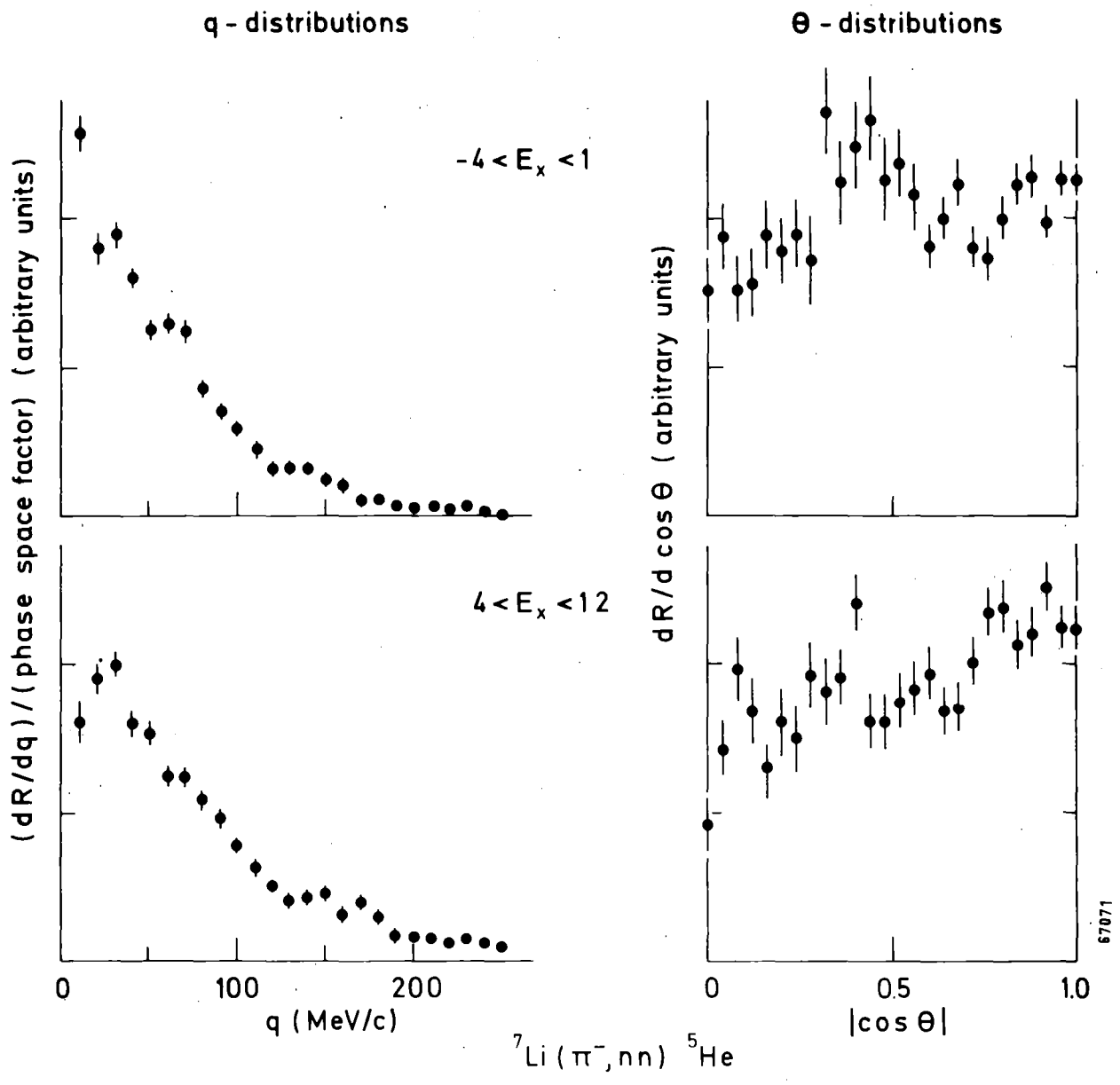

Fig. 19: q- and θ-distributions for different regions in excitation energy of ^{5}He.

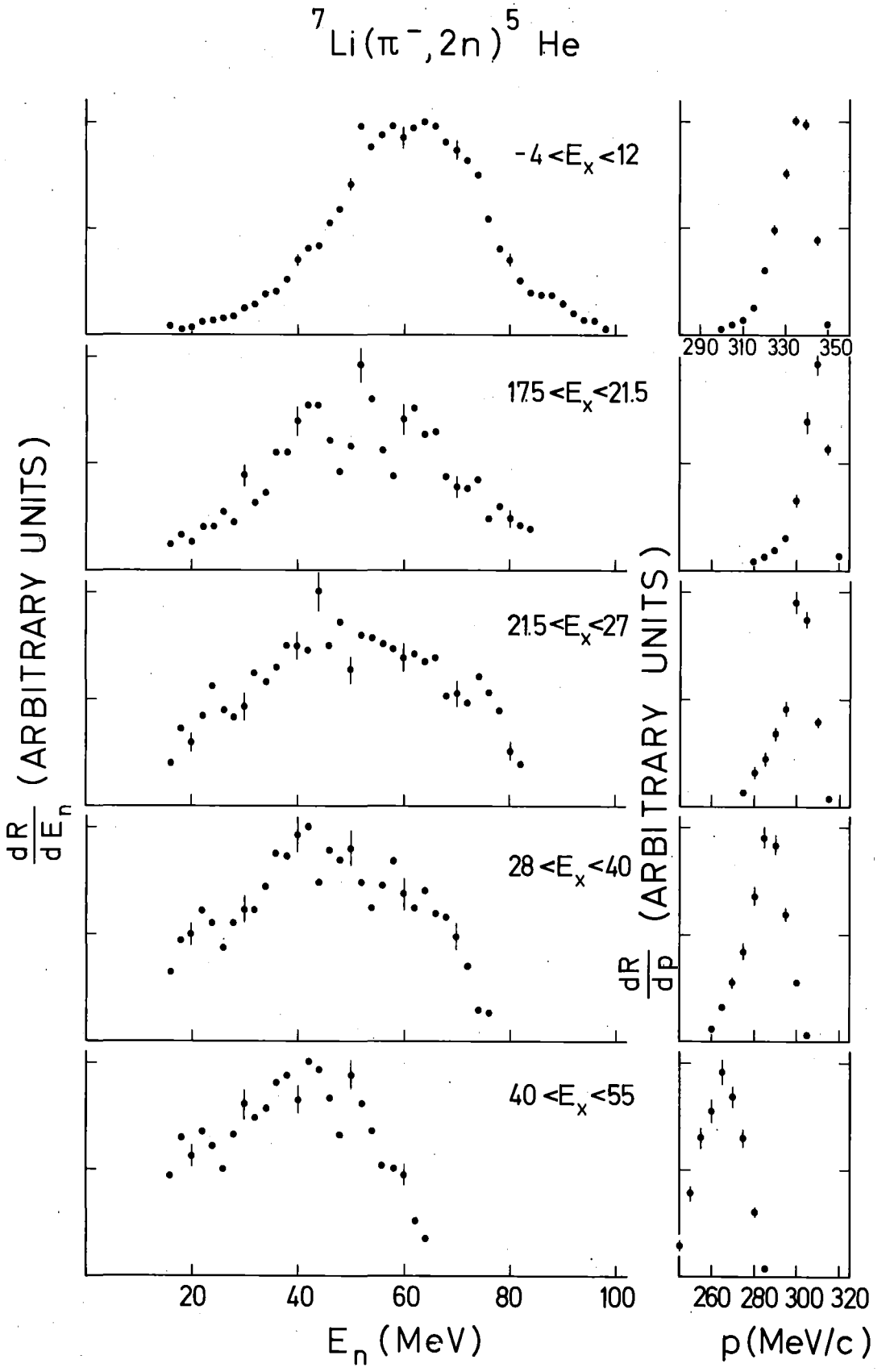

Fig. 20: E_n- and p-distributions for different regions in excitation energy of ^{5}He.

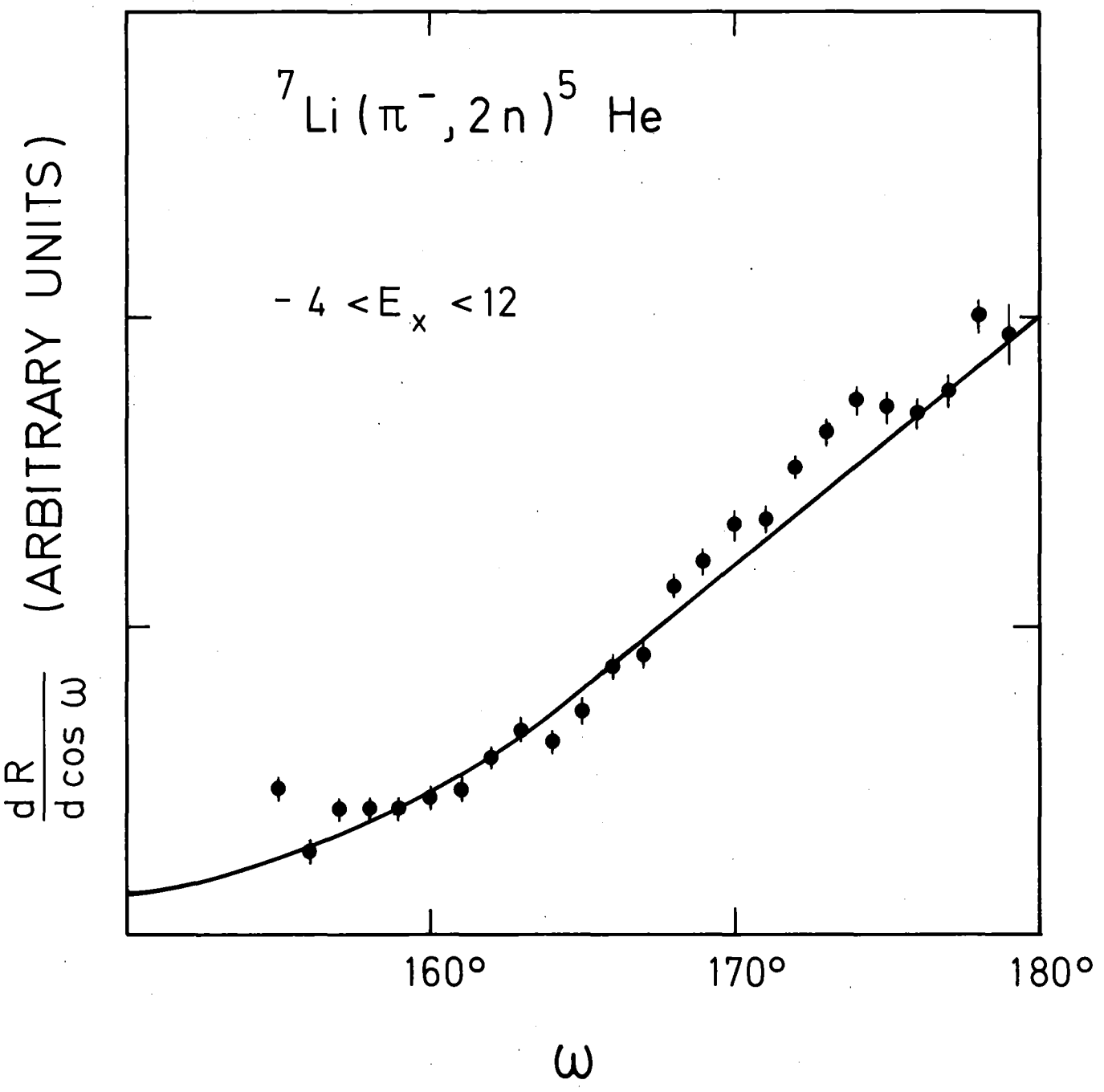

Fig. 21: Measured ω-distribution for transitions to ground and first excited state of ^{5}He. The solid line is a calculated curve from Ref. 55 (see also text).

With respect to the events at high excitation energy, corresponding to the removal of at least one s-shell nucleon, Golovanova and Zelenskaya [23] predict a strong peak at 20 MeV for s^2-removal. Again, like in ^{6}Li, the contribution from s^1p^1-removal should be negligible. The spectrum we observed, see Fig. 18, agrees with the predicted position of the strong peak. A problem arises when the positive parity of the ^{5}He levels [49] at 16.8 MeV and 19.9 MeV is considered. As ^{7}Li has a negative parity, population of these levels would mean absorption by sp-pairs, which contradicts the prediction of Ref. 23. The parity of the broad level around 24-25 MeV is not known.

Any possible ^{12}C contamination in our data (from counters surrounding the target) would be most significant in the region of the observed peak at 16 MeV. Therefore, we do not want to draw any final conclusions on this point. The observed peak is slightly shifted with respect to the 16.8 MeV level position and we conclude that a quantitative estimate of the excitation occurring at this level cannot be given. We note that this state is known to be a d-t system in relative S-motion and that it was observed in a (p, ^{3}He) reaction [58].

Kopaleishvili and Machabeli [34] in their investigation of the rescattering effect predict many excited states to be reached by s^1p^1-removal between 14 and 28 MeV, all with positive parities. The most prominent one is located at 18 MeV and its $J^P = \frac{1}{2}^+$ does not agree with the $J^P = \frac{3}{2}^+$ of the known level at 16.8 MeV.

The q-distributions we measured for the events characterized by high excitation energies, Fig. 22, generally reveal a maximum close to q = 0. Some of them also indicate admixtures of $L \neq 0$. We do not observe a q-distribution that would be immediately interpreted as L = 1 and thus be consistent with s^1p^1-removal. Again there are three points to be considered in this context. First, the geometry ($\omega > 155^o$) favored L = 0. Second, the combination 1S x 1p is theoretically possible for s^1p^1-removal. This would result in a q-distribution with a maximum at q = 0. Third, distortion and other final state interaction effects can modify a possible L = 1 q-distribution. However, we do not believe that these things have such a drastic influence on the q-distributions.

On the basis of these arguments it is clear that only experiments covering a wider ω-range and with still better resolution can finally clarify the open questions concerning s^1p^1-removal. Also a more refined theory, particularly on q-distributions, would help.
Part of the θ-distributions of Fig. 22 for the high excitation energy events contain structure and, hence, allow the conclusion that the transitions are not pure $L_i = 0 \rightarrow L_f = 0$.

In Fig. 12 we show the ω-distribution for the high excitation energy region and in Fig. 20, for completeness, some E_n- and p-distributions. They demonstrate that the characteristics of the quasi-free reaction mechanism become less pronounced the higher the excitation energy is. This is expected since non-quasi-free events, like break-up into several particles, will be located at high excitation energies.

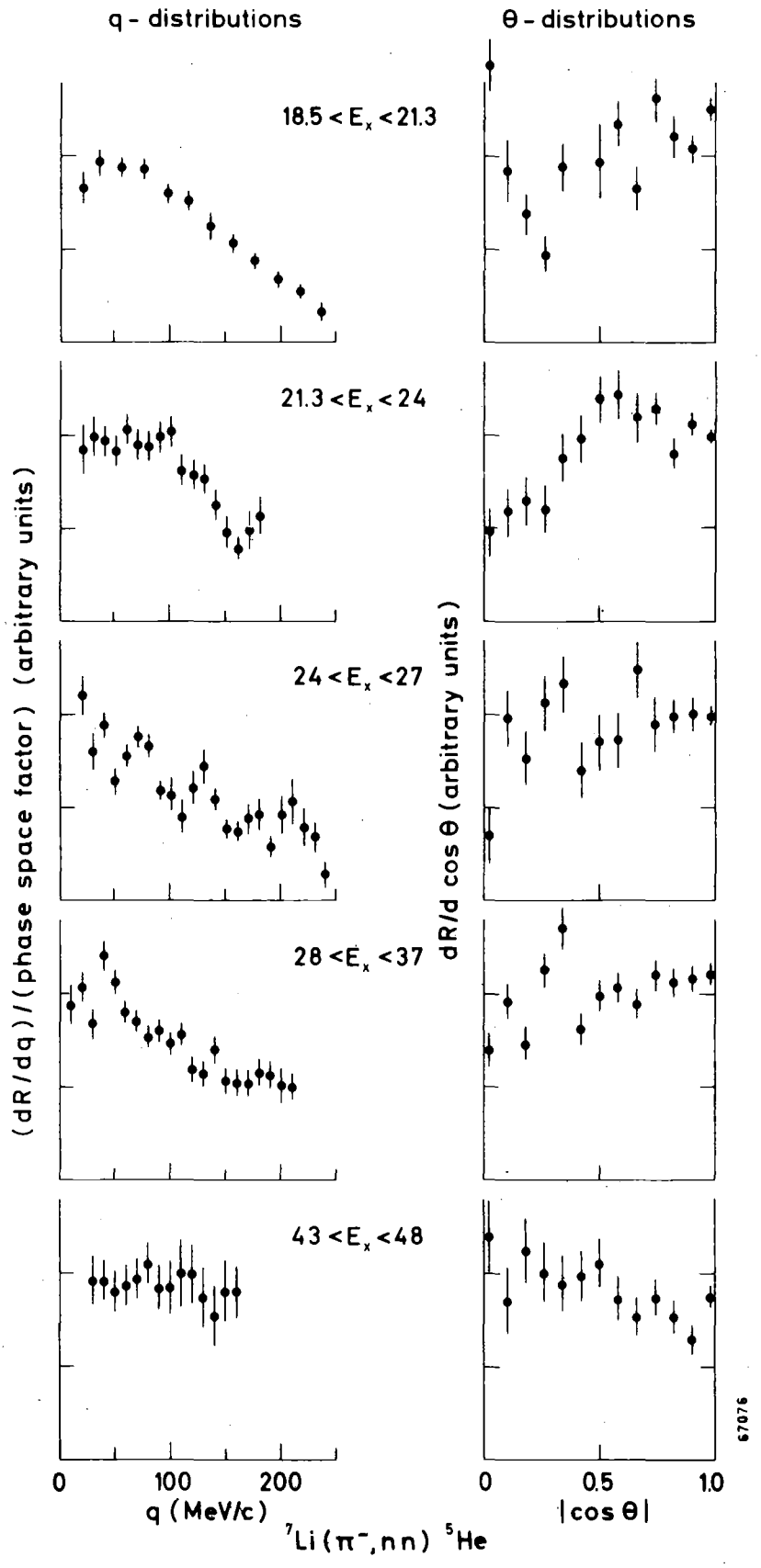

Fig. 22: q- and θ-distributions for different regions in excitation energy of ^{5}He.

V. 3. ^{16}O

The ^{16}O data shown here are of particular interest and importance because a wider range in opening angles ω and hence also in recoil momenta q has been covered. Two independent measurements were performed, one with a 5.8 m flight path and $\omega > 155^{o}$ and one with 4.5 m and $125^{o} < \omega < 160^{o}$. They will be referred to as measurements I and II, respectively. In both cases a D_2O target was used and the monoenergetic neutrons of E_n = 68 MeV from the deuteron absorption could be used as an additional check of the energy calibration.

In previous (π^-, 2n) measurements ^{16}O was used as a target only by Nordberg et al. [5] and no excitation spectrum was shown. Both major (π^+, 2p) experiments, performed by Favier et al. [9] and Arthur et al. [10], respectively, reported results on ^{16}O.

Fig. 23 shows our results from measurement I as a density distribution, depending on the two neutron energies. The events from absorption by the deuteron can be easily seen as they fall into a few channels only. Apart from the deuteron events, one strong line is observed which corresponds to a given excited state in the residual nucleus ^{14}N.

Fig. 24 shows our measured excitation spectra from measurement I. Also indicated are the positions and relative magnitudes of c.f.p. according to the calculations for two p-shell nucleon removal [15,16]. The excitation spectrum integrated over all recoil momenta is dominated by a peak around 4 MeV. There is also an indication of the transition

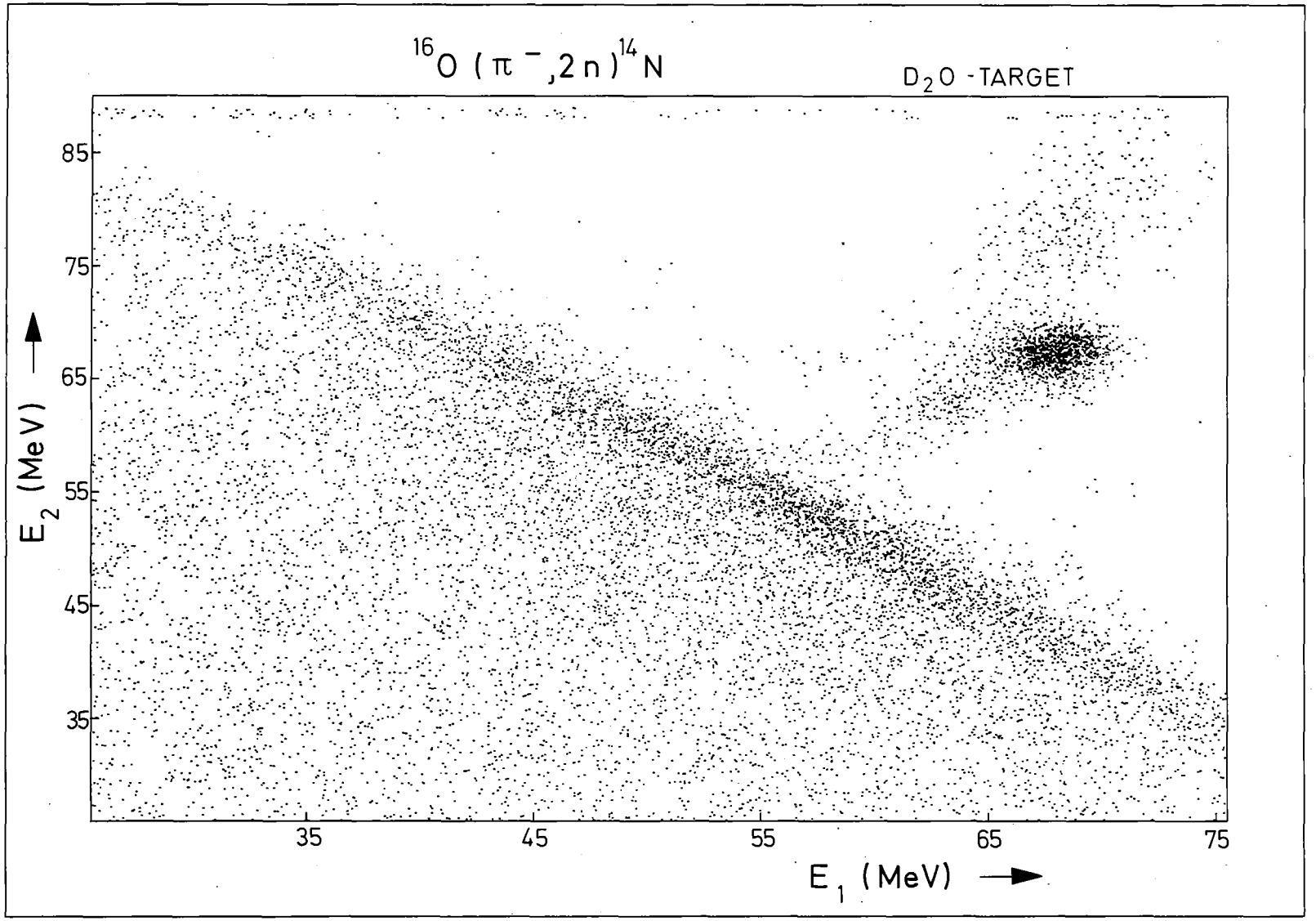

Fig. 23: Density distribution as a function of the two neutron energies.

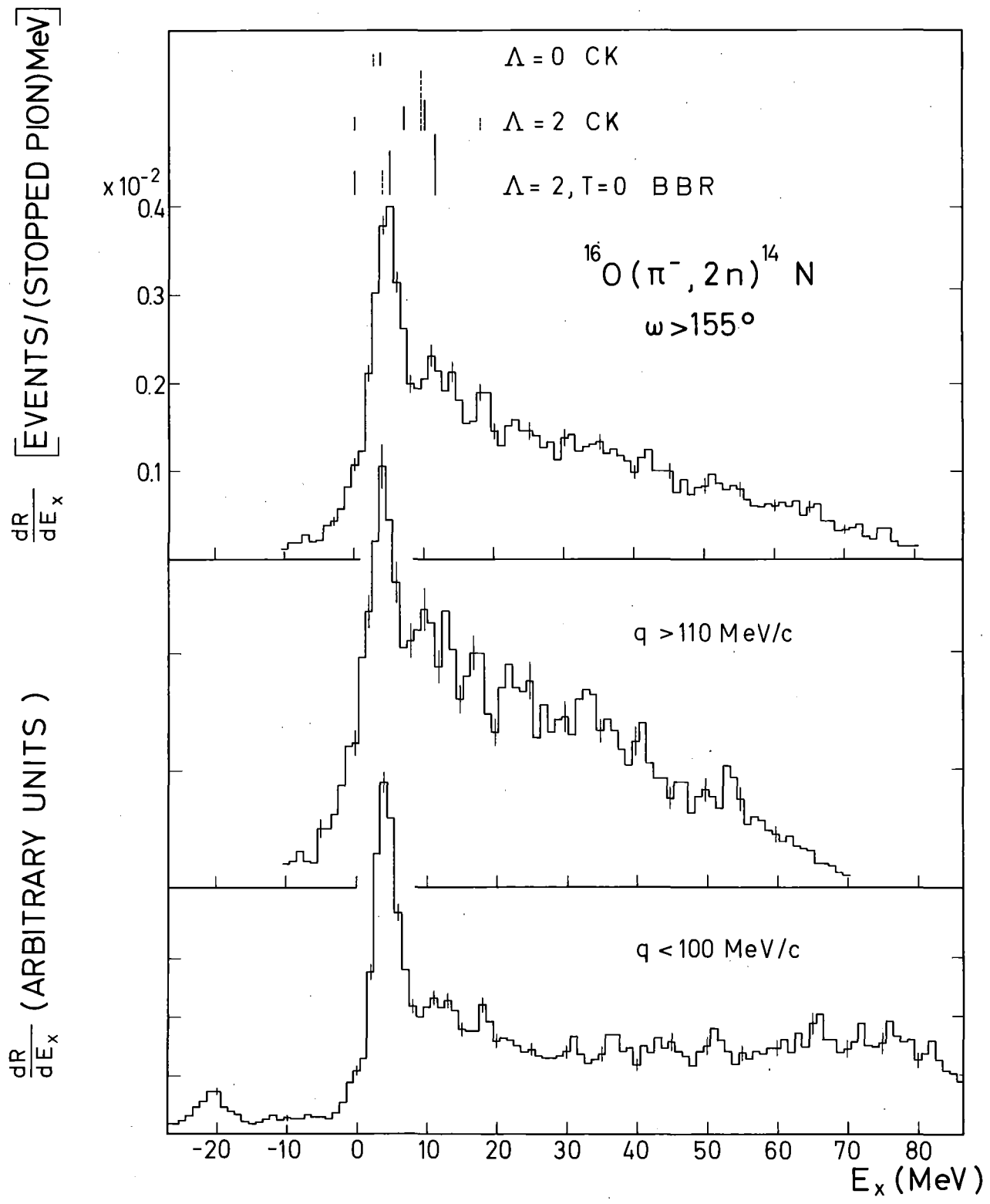

Fig. 24: Excitation energy spectra of ^{14}N from measurement I (ω>155°). Top: integrated over all recoil momenta. Center and bottom: events with restrictions on q. Results of c.f.p. calculations from Ref. 15 (CK) and Ref. 16 (BBR) are indicated in the upper part of the figure. For (CK) the solid lines refer to T=0 and dashed lines to T=1. For (BBR) the dashed line refers to Λ=0.

to the ground state (0 MeV), some structure around 11 MeV, and a possible peak at 18 MeV.

3.9 MeV level

The dominating peak at 4 MeV can be easily interpreted as the second excited state (3.945 MeV, 1^+, T = 0) of ^{14}N. This attribution is confirmed by the results of two (π^-, γ) measurements [59,60] and also suggested by the two c.f.p. calculations [15,16]. Both of them predict one of the few Δ = 0 transitions to be around 4 MeV. Measurement I favored these transitions and so our result agrees with the c.f.p. predictions in that point.

Also the corresponding q-distribution, shown in Fig. 25, has its maximum at q = 0 and thus confirms a dominant L = 0 contribution. In Fig. 26 we present again the recoil momentum distribution of the 3.9 MeV level together with a result from the (π^-, γ) measurement of Ref. 60 [61] where the recoil momentum distribution was calculated from the observed Doppler-broadening of the corresponding γ-ray. The curve from the (π^-, γ) results of Ref. 61 is slightly broader (HWHM $\sim$105 MeV/c) than the one measured in this (π^-, 2n) experiment, the HWHM being about 85 MeV/c. However, considering the completely different methods of the two experiments, the qualitative agreement is rather satisfactory. Both distributions are considerably narrower than that obtained by Kossler et al. [59], which was also calculated from the observed Doppler-broadening of the γ-ray with a HWHM of $\sim$140 MeV/c.

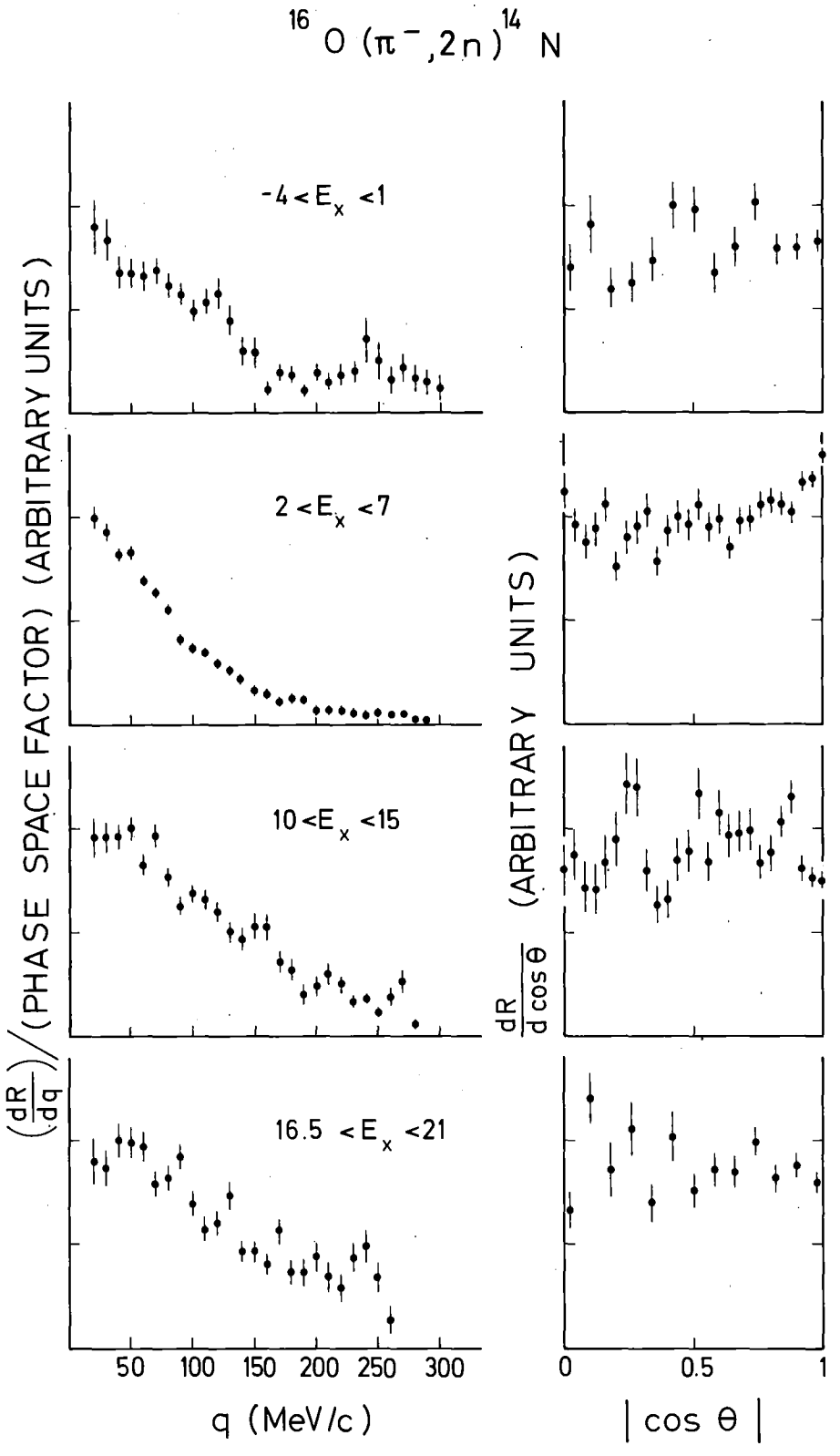

Fig. 25: q- and θ-distributions for different regions in excitation energy of ^{14}N. All data points refer to measurement I.

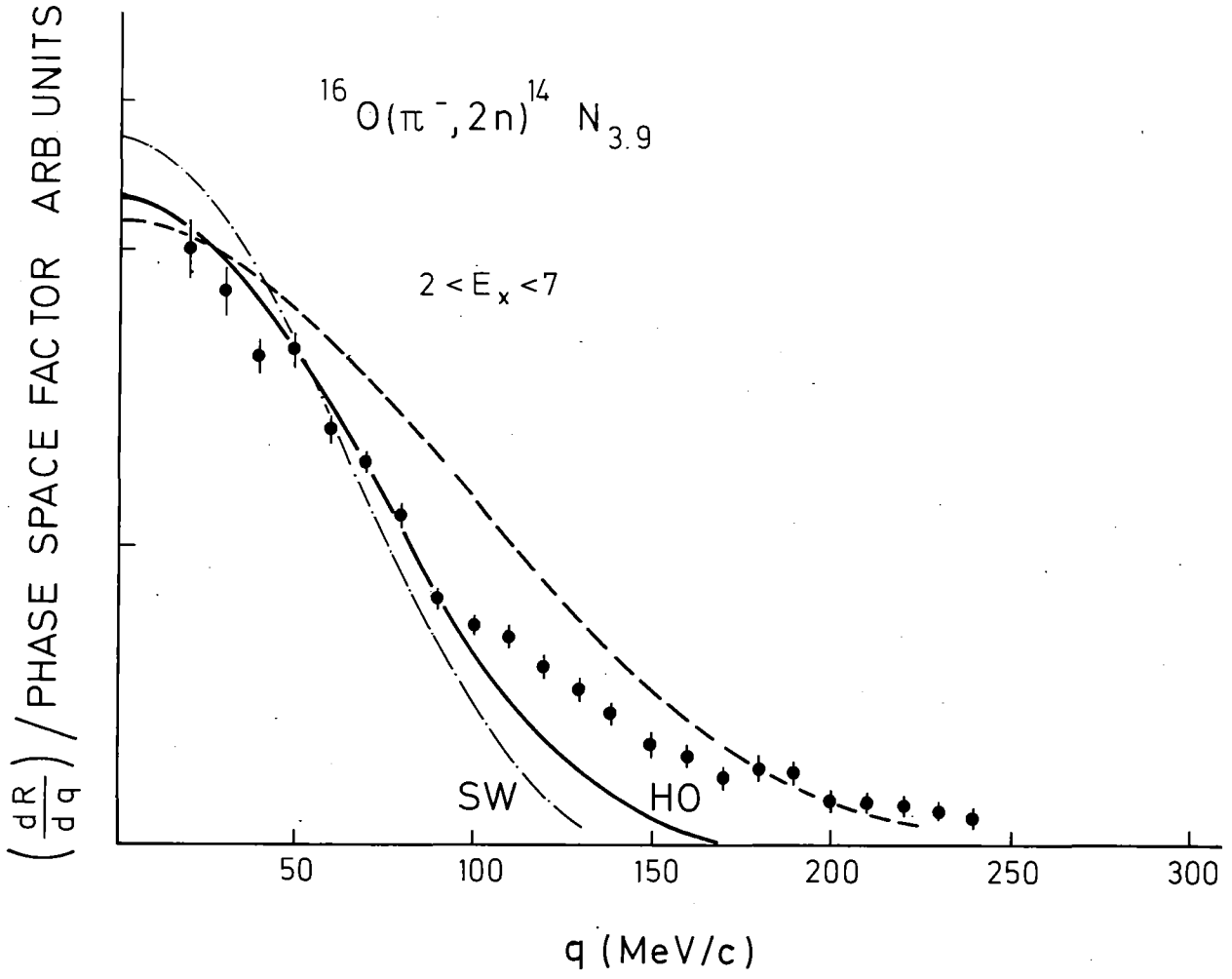

Fig. 26: Measured q-distribution for the transition to the second excited state of ^{14}N. The dashed curve has been taken from the (π^-,γ) measurement of Ref. 60 [61]. The solid and dot-dashed curves are calculated for 2S-motion in a harmonic oscillator (HO) and a square well (SW) potential, respectively. See also text.

Fig. 26 also shows two theoretical curves. One is the absolute value squared of the Fourier transform of a 2S (N = 1, L = 0) wave function calculated for a harmonic oscillator potential [10,33]:

$$\left|\Phi_{2S}(q)\right|^2 = \text{const.}\ (1-\frac{2}{3}\ \frac{q^2}{q_0^2})^2\ \exp.\ (-\frac{q^2}{q_0^2}).$$

q_0 is related to the harmonic oscillator length parameter $r_0 = (\frac{\hbar}{m_N\omega})^{0.5}$ by the expression $q_0 r_0 = \hbar$.

r_0 is related to the nuclear r.m.s. radius and has been taken from electron scattering data [62]: $r_0 = 1.76$ fm. In our case m_N has to be replaced by μ, the reduced mass of a deuteron and of the remaining ^{14}N, $\mu \simeq 1.75\ m_N$, and r_0 has to be changed accordingly. In this way we obtained a value for the parameter q_0 of $q_0 = 148.4$ MeV/c and using q_0 the solid curve in Fig. 26 was calculated. Up to about 100 MeV/c the agreement between the calculated curve and the experimental result is surprisingly good if one considers that the curve is based on simple assumptions and neglects the relative motion of the two nucleons as well as distortion effects.

Deviations for high values of q can be due to admixtures from surrounding $\Lambda = 2$ levels in the relatively wide window $2 \leq E_X \leq 7$. In principle, the distortions are expected to be most important for nucleon pairs from the inner region of the nucleus. This also would alter the q-distribution, presumably to the most significant extent for high recoil momenta.

The second calculated curve in Fig. 26 is a 2S Fourier transform squared for a square well potential [63]

$$\left|\Phi_{2S}(q)\right|^2 = \text{const.}\ \frac{(\cos qR + \frac{\beta}{q}\sin qR)^2}{(\alpha^2-q^2)^2 \cdot (\beta^2+q^2)^2} \quad .$$

For R, the joining point of the interior (spherical Bessel fuction) and exterior solutions (spherical Hankel function) we selected R = 3.5 fm ($\simeq 1.4\ A^{1/3}$). β is connected with the binding energy of the pair [64]

$$\beta = \sqrt{\frac{2\mu(|B| + E_x)}{\hbar^2}} = 1.51\ \text{fm}^{-1},$$

μ being the same reduced mass as before. α fixes the energy eigenvalue and is obtained by graphical or numerial solution from [64] $\alpha R \cot(\alpha R) = -\beta R$.
For the 2S state we obtain $\alpha = 1.5656\ \text{fm}^{-1}$.

It is clear from Fig. 26 that the square well solution with these parameters gives a poorer fit to our data than the harmonic oscillator solution. The calculated width is narrower than the experimental one which may be due to neglecting the contribution of the relative motion of the two nucleons (see discussion of ^{6}Li q-distribution and Ref. 18).

It should be mentioned that the q-distribution measured by us is in good agreement with the (π^+, 2p) result shown in Arthur's report [10].

The θ-distribution for the transition discussed here is shown in Fig. 25 and is consistent with a $\Delta L = 0$, $L_i = L_f = 0$ case in agreement with Koltun's selection rule.

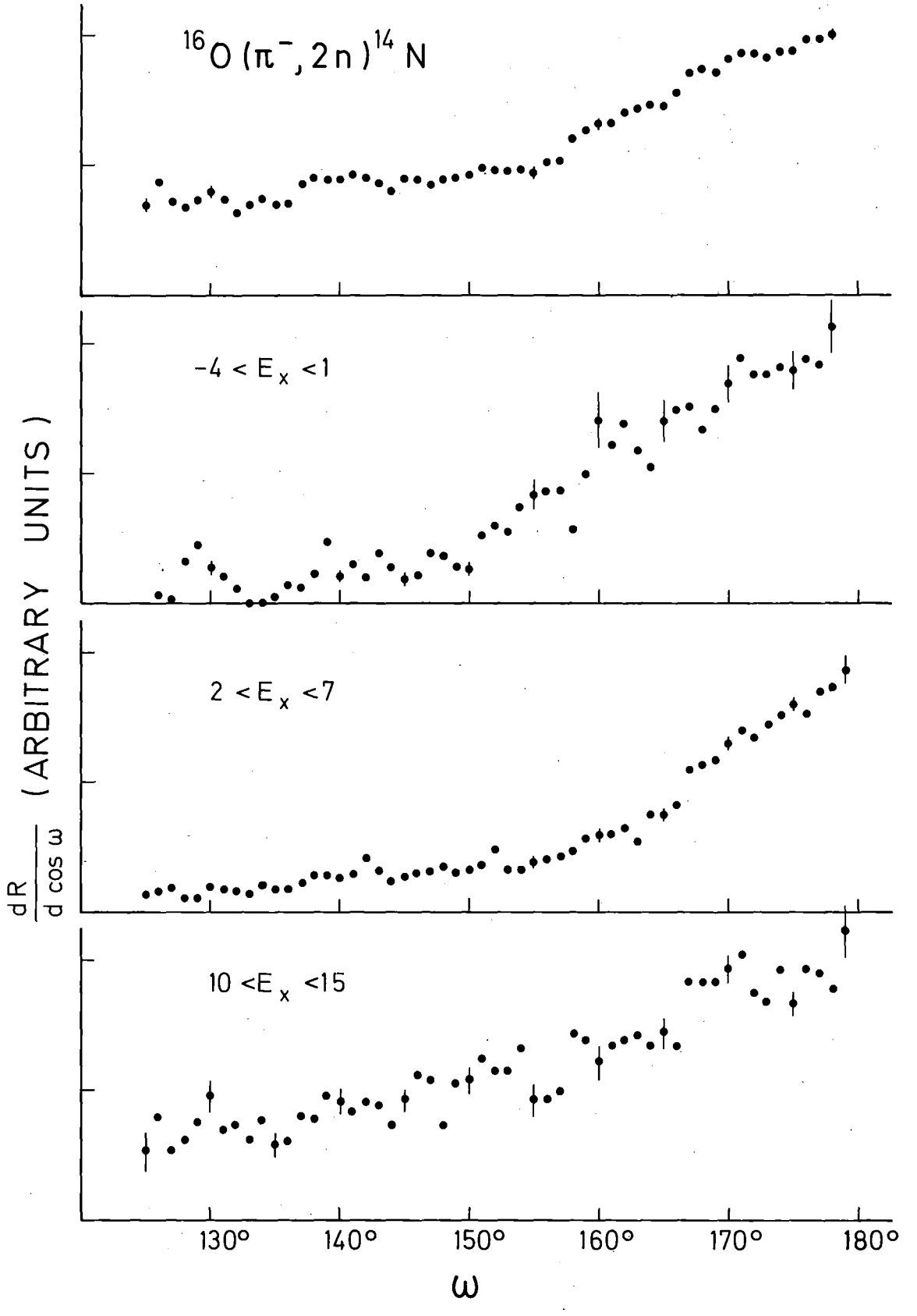

Fig. 27: ω-distributions integrated over all excitation energies (top) and for different regions in excitation energy of ^{14}N.

The ω-distribution, Fig. 27, is the result of joining the curves from the two measurements. It exhibits a clear peak at 180° verifying the quasi-free reaction mechanism. From the decrease of the distribution with decreasing angle ω we conclude that the number of events below ω = 125° is rather small. Our total absolute rate for ω > 125° and $1 \leq E_x \leq 7$ is $2.5 \pm \begin{smallmatrix}1.5\\0.75\end{smallmatrix}$ % per stopped pion. This value lies between the two reported values from the (π^-, γ) measurements, 1.8 % [59] and 4.8 ± 0.9 % [60].

Other levels at low excitation energy

Apart from the 3.9 MeV transition Cohen and Kurath [15] predict only one other Λ = 0 transition to the first excited state at 2.3 MeV (0^+, T = 1). From the (π^-, γ) measurements [59,60] it is known that this transition is much weaker than that to the 3.9 MeV level. This is in accord with our spectrum although we cannot separate these levels.

The ground state transition is predicted to be Λ = 2 in both c.f.p. calculations [15,16], with almost exactly the same strength as the 3.9 MeV level. In our excitation energy spectrum of measurement I and without restriction in recoil momentum (see Fig. 24, upper part) the ground state is much weaker than the 3.9 MeV state. This suppression is at least partly due to geometrical favoring of Λ = 0 transitions. The Λ = 2 assignement of the ground state transition is consistent with our data because its contribution is greater in the spectrum restricted to higher values of q (q > 110 MeV/c), Fig. 24, and even more so in the spectrum from measurement II, shown in Fig. 28. This measurement covered recoil momenta in the range 80 MeV/c

$\lesssim q \lesssim 350$ MeV/c and thus emphasized much more the $\Lambda = 2$ transitions.

The q-distribution of the ground state region, shown in Fig. 25, is strongly influenced by events from the dominating transition at 3.9 MeV, particularly for small recoil momenta. It is, however, considerably wider (HWHM $\simeq$ 140 MeV/c) than that of the 3.9 MeV level. This indicates the $\Lambda = 2$ contribution. Obviously, also the 1S x 1d combination might be of some importance.

The ω-distribution for the ground state events, shown in Fig. 27, exhibits a clear 180° correlation.

The excitation spectrum of measurement II, shown in Fig. 28, shows that the dip between the peak at 4 MeV and the structure around 11 MeV is filled, indicating possible excitation around 7 MeV. This would be in agreement with a Cohen and Kurath [15] prediction of a strong $\Lambda = 2$, $T = 0$ transition to an excitation energy of 7 MeV. In this context it should be mentioned that according to both (π^-, γ) measurements [59,60] the level at 5.1 MeV $(2^-, T = 0)$, which would be a possible candidate, is only weakly populated.

The most obvious difference between the excitation spectra of the two measurements, Figs. 24 and 28, is the much higher yield around 11 MeV found in measurement II. The respective structure may contain more than one peak although this is not very well established. Because of the clear enhancement of this structure with a high value of q a strong $\Lambda = 2$ contribution can be assigned

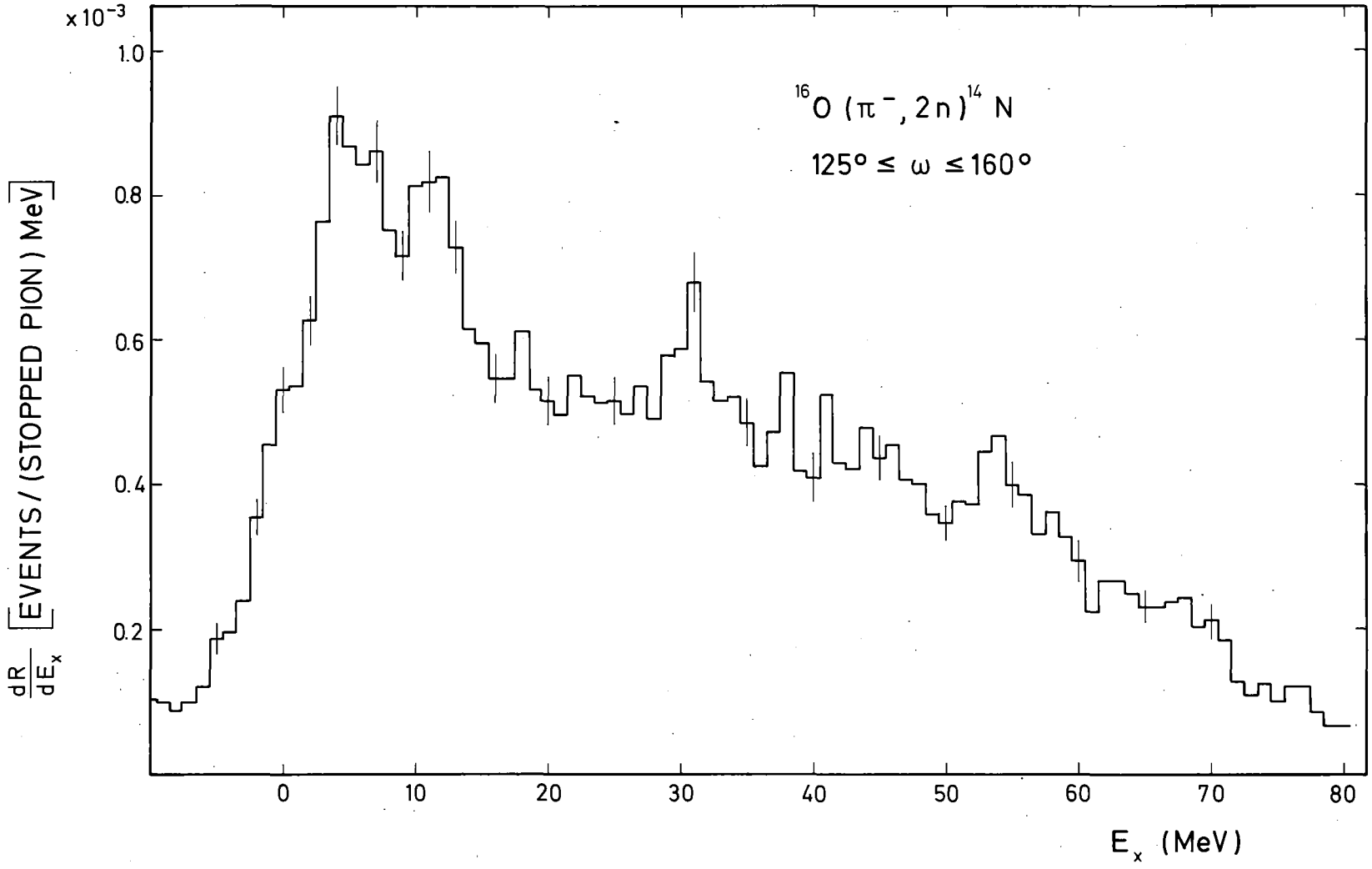

Fig. 28: Excitation energy spectrum of ^{14}N from measurement II integrated over all recoil momenta.

to these transitions. This is consistent with the c.f.p. calculations [15,16], since both of them have the absolutely highest factors for $\Lambda = 2$ in the region 9.5-11.5 MeV excitation energy.

The q-distribution for this excitation energy region, shown in Fig. 25, has its maximum at $q = 0$ and a width of about 130 MeV/c. It indicates an important $L = 0$ part. If the c.f.p. predictions are correct in so far as there are no $\Lambda = 0$ transitions in the vicinity, we may observe a 1S x 1d case here (see Appendix A, p. 10 and 12 for a similar case in ^{12}C). However, this $l = 2$ would be somewhat unexpected because of the required spatial correlation between the two nucleons.

In Figs. 29 and 30 we show, for completeness, some neutron energy and relative momentum distributions, respectively, for regions of low excitation energy. Data points from both measurements, I and II, are given separately. The neutron energy spectra show a symmetric peak which becomes slightly broader in the case of measurement II (smaller angles ω).

According to Fig. 2 in Chapter II, one expects the relative momentum distributions to be located at smaller p for smaller ω (increased q). For an equal window in q and increasing average q the p-distributions should also become broader. These features are well established by our experimental results; see Fig. 30.

Because of the larger ω-region covered the $\Lambda = 0$ preference is less stringent for ^{16}O. Therefore, it

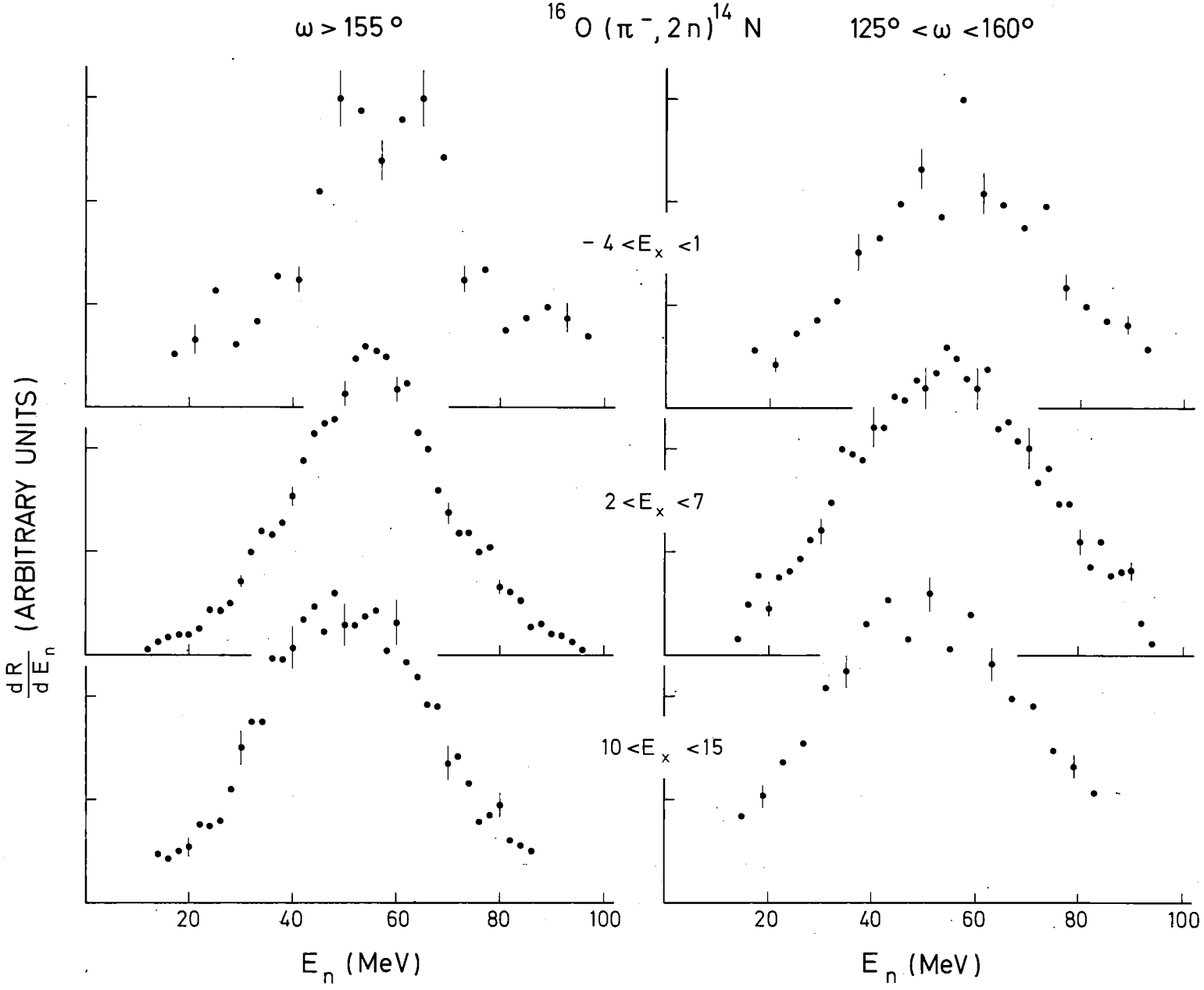

Fig. 29: E_n-distributions for different regions in excitation energy of ^{14}N. Data points from the two measurements are given separately.

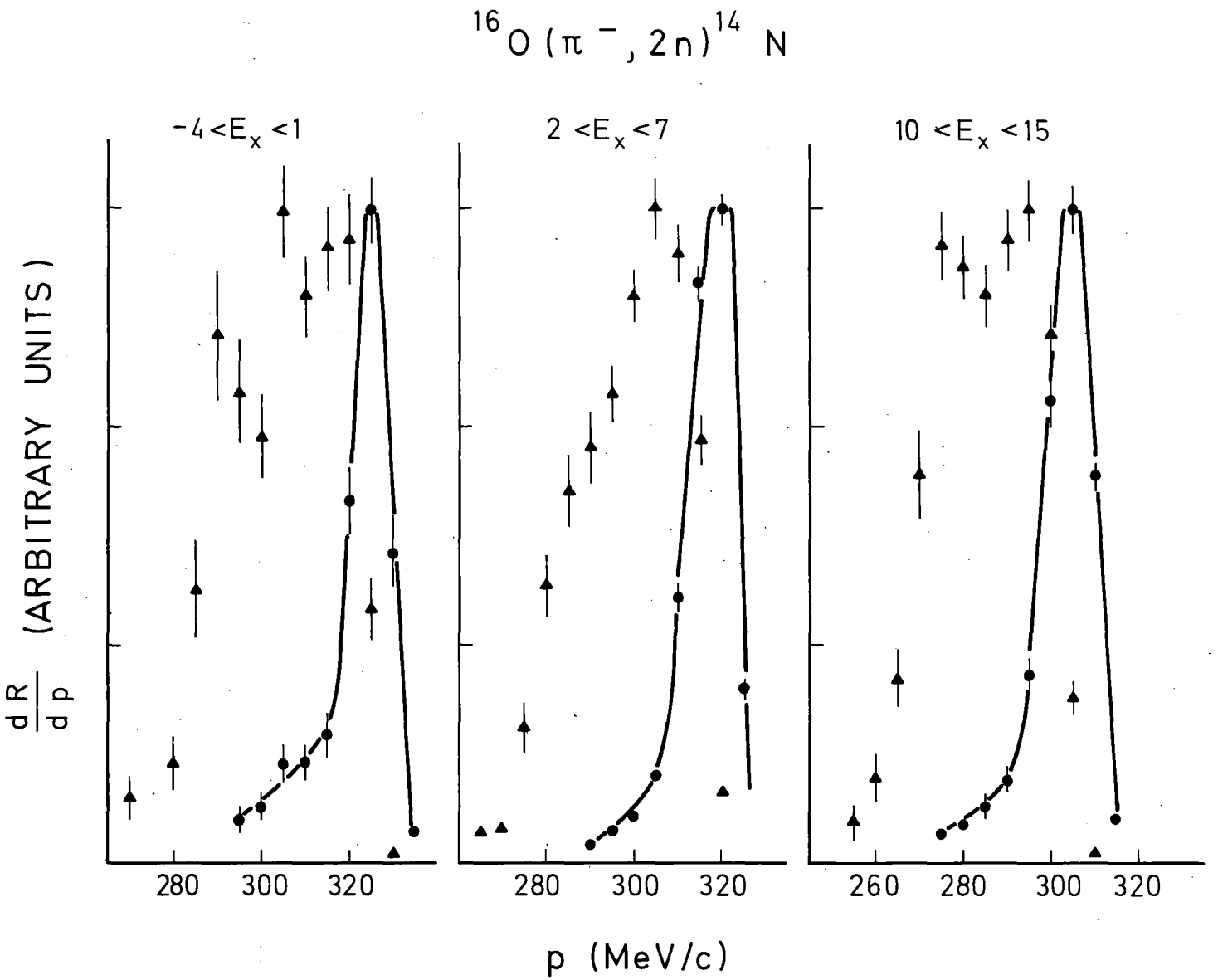

Fig. 30: p-distributions for different regions in excitation energy of ^{14}N. Points are from measurement I, triangles from measurement II (see also text). The solid line is just a guide to the eye.

seems more appropriate than in case of the other target nuclei to make a comparison between theoretical predictions (c.f.p. calculations [15,16]) and experimental results for the ratio of $\Lambda = 2$ to $\Lambda = 0$ transitions. Such a comparison is given in the following table:

Λ	c.f.p. strength prediction [15] (predicted E_x)		(π^-,2n) absolute rate per stopped pion, $\omega > 125^o$, $E_n > 15$ MeV (E_x-window)
0	2.7	(3.6 MeV)	2.55 % ($1 \leq E_x \leq 7$)
2	2.7	(0.0 MeV)	0.45 % ($-4 \leq E_x \leq -1$) *)
(T=1)	12.7	(9.5 MeV)	
2			2.45 % ($8 \leq E_x \leq 15$)
(T=0)	6.6	(10.15 MeV)	

Some remarks are necessary before conclusions can be drawn on the basis of the table. First, the windows in excitation energy are of different widths and, therefore, there are different contributions from other levels to the given absolute rates. Second, because of a broader ω-distribution for the third window ($8 \leq E_x \leq 15$, see Fig. 27) some events are not included there.
Despite these remarks, the table above shows that the ratio of $\Lambda = 2$ to $\Lambda = 0$ transition strength is suppressed in the (π^-, 2n) results compared to the Cohen and Kurath [15] prediction. For equal c.f.p. the $\Lambda = 0$ transition strength seems to be enhanced by a factor of the order of 5 with respect to $\Lambda = 2$ in case of the ^{16}O (π^-, 2n) ^{14}N reaction.

*) The number of events in this E_x window has been doubled to get the absolute rate.

This conclusion is consistent with the more tentative result indicated in Appendix A on the general weakness of $\Delta = 2$ transitions in the nuclei ^{9}Be, ^{10}B and ^{12}C where, however, the measurement was restricted to $\omega > 145^{o}$.

In Appendix A a striking similarity is reported between single and two-nucleon separation energies in ^{9}Be, ^{10}B, ^{12}C and ^{14}N obtained from (p, 2p) and (π^-, 2n) measurements, respectively. The most strongly populated two-hole states seem to have a separation energy higher by a factor of 1.62 than that of the most strongly populated single-hole states. Here the separation energy of the two-hole states in defined as $E_s = E_x + M_B - M_A + m_d$. M_A and M_B are the masses of the target and residual nucleus. m_d is the mass of the free deuteron. For ^{16}O the most strongly populated level in ^{14}N at 3.9 MeV has a separation energy of 24.7 MeV. This value is well in line with some of the strongly populated levels in the other nuclei; see Fig. 11 in Appendix A. The ^{16}O (p, 2p) ^{15}N reaction, on the other hand, has shown two levels having the same strong population at approximately 12 and 18.5 MeV separation energy [65], corresponding to $p_{1/2}^{-}$ and $p_{3/2}^{-}$-removal, respectively. Scaling by the factor 1.62 yields our two-nucleon separation energy to lie exactly in the middle between the two single-nucleon separation energies, as if it were a $p_{3/2}^{1}\ p_{1/2}^{1}$-removal. The 3.9 MeV level in ^{14}N is known to have a strong $(p_{3/2}^{-1}\ p_{1/2}^{-1})$-configuration [66] and thus the separation energies mentioned above furnish a striking confirmation of the multiplication factor 1.62 connecting single and two-nucleon removal.

High E_x region:

Around 18 MeV the excitation spectra of measurement I, Fig. 24, seem to show a peak which is, however, not reproduced by the result of measurement II, Fig. 28. A confirmed peak at that position could be assigned to a Cohen and Kurath prediction for a $\Lambda = 2$, $T = 1$ transition [15]. Some additional structure may also exist around 30 MeV excitation energy as can be seen in the spectrum of measurement II, Fig. 28.

The structure at high excitation energies immediately leads to the question of the contribution of quasi-free 2-nucleon processes accompanied by the emission of at least one s-shell nucleon. A comparison of the excitation spectra of the two measurements shows that the ratio of events with $E_x > 15$ MeV to events with smaller E_x increases with smaller values of ω. As ω and q are correlated, one could take this as an evidence for the importance of quasi-free processes at high excitation energies. For these processes the q-distribution will become broader with increasing excitation energy and, correspondingly, the ω-distributions will be wider.
But also for non-quasi-free events, like emission of several nucleons, rather wide or even isotropic ω-distributions are expected. As these events result in a high excitation energy, they would also produce the effect indicated above.

Apart from some possible structure around 30 MeV, the data of measurement II show a rather striking excitation energy distribution if one restricts q to relatively

small values, such as $q < 210$ MeV/c. This is shown in Fig. 31. Then the excitation energy region from 20-75 MeV appears as a very broad maximum with possible structure consisting of wide peaks. The same data with $q \cdot 250$ MeV/c, also shown in Fig. 31, do not show such a broad maximum. The spectrum decreases rather smoothly with increasing excitation energy except for the possible peak around 30 MeV.

Comparison with other reactions and theory:

A comparison of our total excitation spectrum from measurement I with the $(\pi^+, 2p)$ results [9,10] shows qualitative agreement within the experimental uncertainties. This proves the similarity of the reaction mechanism. Due to the somewhat different kinematics most of the distributions in different variables can not be compared directly. However, we have already mentioned the good agreement of the q-distributions for the low-excitation energy region (around the 3.9 MeV level) measured in our experiment and the $(\pi^+, 2p)$ case [10].

Kopaleishvili et al. [21] made a theoretical prediction of the excitation spectrum in the $(\pi^-, 2n)$ reaction, neglecting the distortions and taking the asymptotic approximation for the final state NN interaction. None of their excitation spectra displayed fits our data well. Their prediction for S-absorption and $q < 100$ MeV/c can be directly compared with our spectrum (Fig. 24, bottom). It clearly underestimates the contribution of the 3.9 MeV level and predicts too much strength at 12 MeV and 18 MeV.

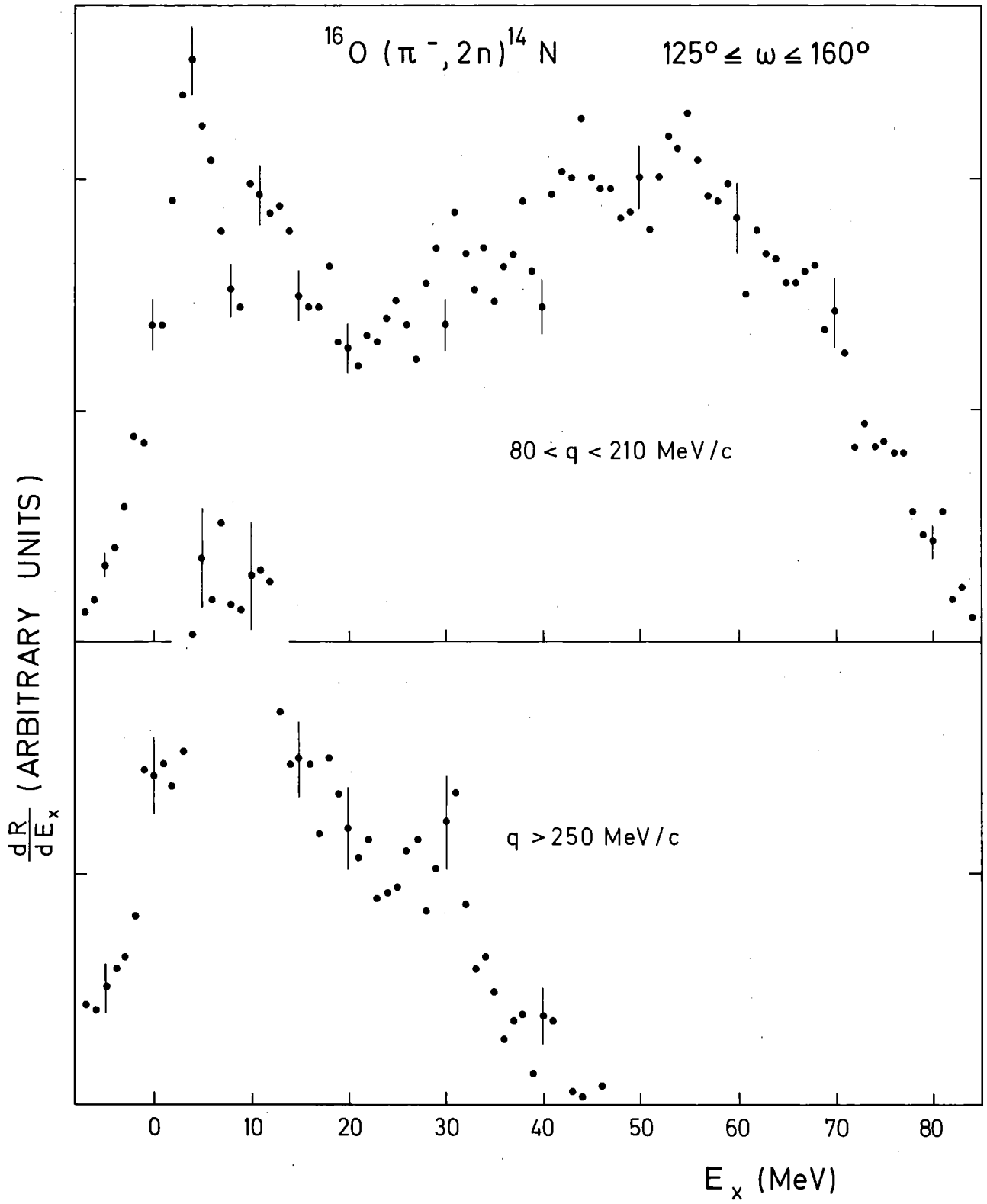

Fig. 31: Excitation energy spectra of ^{14}N from measurement II. Top: events with low recoil momenta. Bottom: events with high recoil momenta.

In any case, the conclusion of the authors of Ref. 21 saying that the available data give preference to S-absorption has to be put in doubt for the following reason. The argument was based on a comparison between the calculated predictions for S- and P-absorption (both with $q < 50$ MeV/c) and the (π^-, γ) result of Kossler et al. [59] who, evidently, integrated over all allowed recoil momenta. It is common belief that, apart from the very light nuclei, absorption from the atomic 2P orbit is the most important term for nuclei with $A \lesssim 20$. Therefore, it would be interesting to have corresponding theoretical predictions on the excitation energy, which are not restricted to $q < 50$ MeV/c.

Already an earlier paper by Kopaleishvili et al. [22] contained predictions on the transition strength for certain levels. The calculation was done for S-absorption and there was no restriction as regards q. For ^{16}O a comparison with our data yields that the theory gives too little strength for the 3.9 MeV level relative to the 0 MeV and 12 MeV regions.

Weber [67] carried out a three-body partial wave analysis in treating the final state of the $(\pi^-, 2n)$ reaction. He considered only S-absorption so that a detailed comparison does not seem meaningful. In their final paper Morris and Weber [28] treat 2P-absorption but do not include ^{16}O.

Other reactions that lead to the same residual nucleus and can therefore be compared with the $(\pi^-, 2n)$ result are the quasi-elastic deuteron knockout (p, pd) and the two nucleon pickup reactions (d, α) and (p, ^3He).

In a recent measurement performed at E_p = 75 MeV the ^{16}O (p, pd) ^{14}N reaction [68] was investigated. The resulting excitation spectrum is similar to ours obtained in measurement I. The dominating peak found by these authors corresponds to the second excited level at 3.9 MeV. A somewhat smaller contribution was due to the transition to the ground state and to the first excited state. There was also some evidence for peaks occuring around 7 MeV and 11.5 MeV. The measurement was performed for small recoil momenta in the vicinity of q = 0. Our results are in accord with this (p, pd) measurement.

When comparing with two nucleon pickup reactions such as (d, α) or (p, ^3He) it should be kept in mind that the presence of only one fast particle in their final state implies much less freedom in the range of q which can be studied.

Fleming et al. [66] have measured the $^{16}O(p,^3He)^{14}N$ reaction at 54 MeV and found the strongest excitation at 3.95 MeV followed by 7.03 MeV, 0 MeV and 2.3 MeV. A comparison between their measured angular distribution and a DWBA calculation confirmed the dominance of L = 2 for the ground state and 7 MeV transitions. This is consistent with our observation that their relative strength increases with larger q. The (p,^3He) result mentioned also reveals considerable excitation in the region 9-11 MeV, which is similar to our result.

In another more recent (p,^3He) measurement performed by Hoot et al. [69] at E_p = 40 MeV only transitions

leading to the ground, first and second excited states were investigated. For the 3.95 MeV level these data seem to indicate the presence of a much stronger L = 2 component than is given by the c.f.p. calculation. We have no supporting indication.

The $^{16}O(d,\alpha)^{14}N$ result found by van der Woude and de Meijer [70] at E_d = 40 MeV shows high yields at excitation energies of 0, 3.95, 7.06 and 11.04 MeV. The corresponding transitions are predominantly L = 2, 0,2 and 2, respectively. This result is in good agreement with the Cohen and Kurath predictions [15] as well as with the interpretation of our data.

V. 4. ^{9}Be, ^{10}B, ^{12}C

Results on these three target nuclei are given in Appendix A. They have been cited several times here and no additional comments will be made.

V. 5. ^{14}N

Some results on ^{14}N as the target were published in Ref. 71. In connection with the comparison of single nucleon- and two-nucleon separation energies ^{14}N is mentioned in Appendix A too. Some additional remarks are presented below.

The first concerns the absolute rates which are not given in Ref. 71. For the transition to the first excited state in ^{12}C at 4.44 MeV ($0 \leq E_x \leq 7$) we obtain a rate of 7^{+4}_{-2} % per stopped pion. This is in agreement with a result

published recently of a (π^-,γ) measurement [72] quoting a rough estimate of 10 ± 5 %. On account of our restriction $\omega > 145^o$ we missed a small number of events.

The same (π^-,γ) measurement [72] has yielded the recoil momentum distribution for the transition to the first excited state of ^{12}C at 4.44 MeV. It was calculated from the observed Doppler-broadening of the corresponding decay γ-ray. The HWHM of their curve of about 165 MeV/c is significantly larger than ours, see Ref. 71. A similar case of discrepancy occurs for the $^{16}O(\pi^-,2n)^{14}N_{3.9}$ transition, see V. 3. No explanation can be recognized for the time being.

In Fig. 32 we show again the measured q-distribution for the $^{14}N(\pi^-,2n)^{12}C_{4.44}$ transition. It is compared with some theoretical curves based on a simple model. The expressions for the 2S Fourier transforms squared for the harmonic oscillator (HO) and the square well (SW) potentials were given in V. 3. in connection with the $^{16}O(\pi^-,2n)^{14}N_{3.9}$ transition. Here we also include the 1S function in case of the HO potential. We used the following parameters for the $^{14}N(\pi^-,2n)^{12}C_{4.44}$ transition. For the square well function we use:

$R = 3.5$ fm, $\alpha = 1.5339$ fm^{-1}, $\beta = 1.1813$ fm^{-1}, $\mu = 1607.7$ MeV/c^2.

For the harmonic oscillator functions we have taken r_0 from electron scattering data [62], $r_0 = 1.67$ fm, resulting in $q_0 = 154.7$ MeV/c for the Fourier transform. The reduced mass μ has been taken into account.

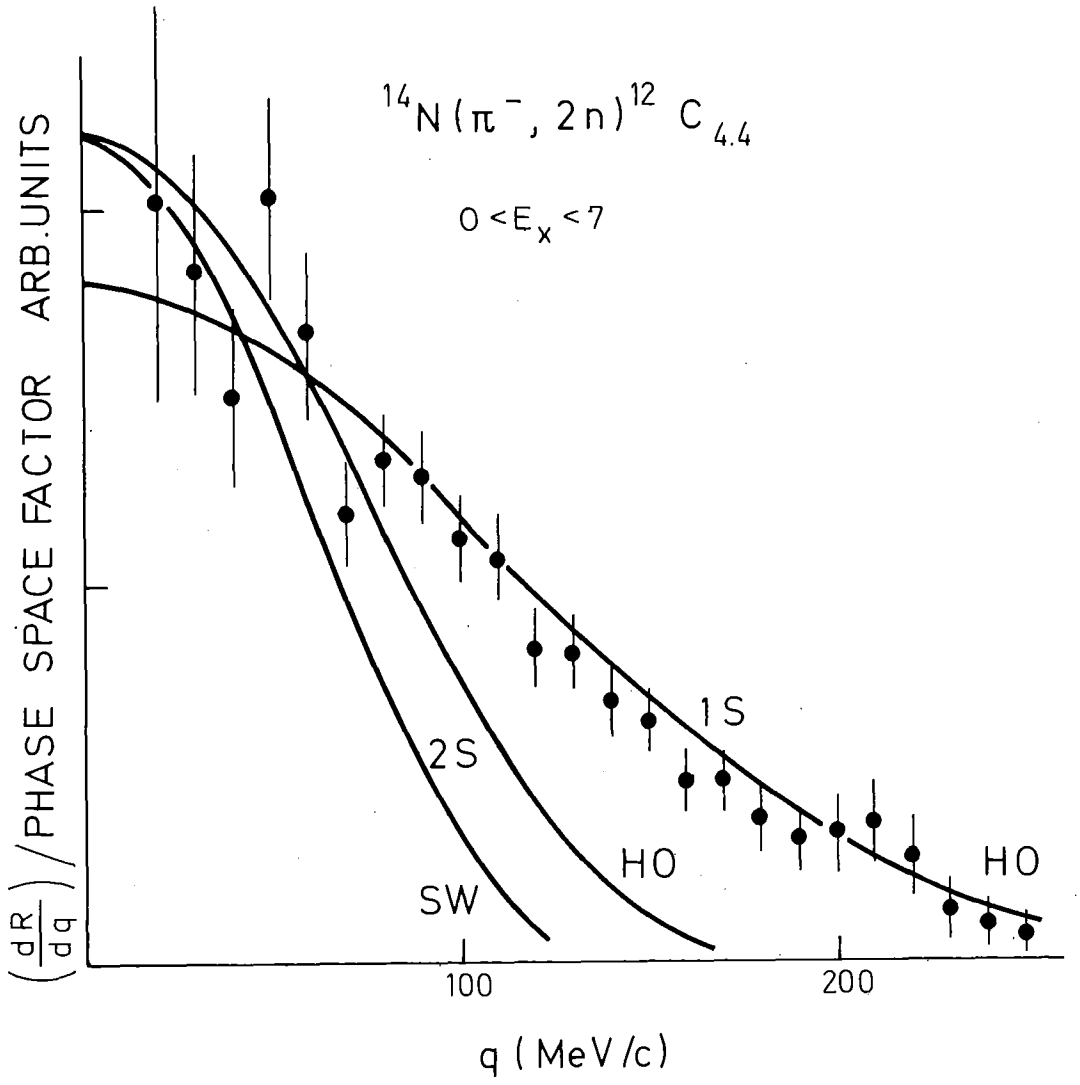

Fig. 32: Recoil momentum distribution for the transition to the first excited state of ^{12}C. The solid curves correspond to the 1S or 2S motion of the c.m. of the two nucleons. They have been calculated for a square well potential (SW) as well as for a harmonic oscillator (HO). See also text.

Both 2S functions are much too narrow to reproduce our data. The measured distribution is clearly wider than that of the 3.9 MeV level in ^{14}N, despite a separation energy smaller by 10 MeV.

The harmonic oscillator 1S momentum distribution, also shown in Fig. 32, is simply proportional to exp $(-q^2/q_0^2)$ with the same q_0 as above (related to electron scattering data). It

fits the data surprisingly well. Assuming that this agreement is not fortuitous, it would mean a relative 2s motion of the pair; see II. 5. This, however, is somewhat unexpected because high relative momenta p are favored in this process and this 2s implies a smaller average p between the two nucleons than the 2S x 1s case. Also the latter seems to be the favorite case; see the transitions to $^{4}He_{g.s.}$ or $^{14}N_{3.9}$ and the conclusions reached in Appendix A.

VI. SUMMARY AND CONCLUSIONS

Results have been reported on the first systematic, kinematically complete (π^-,2n) measurement covering the most important nuclei of the 1p-shell with statistics and energy resolution comparable to or better than available (π^+,2p) results.

The importance of the direct quasi-free reaction mechanism has been established most clearly and convincingly for the events leading to low excitation energies in the residual nucleus. This has been demonstrated by many distributions in several different variables, like neutron energy, recoil momentum or angle spanned by the two neutron momenta. Distributions in relative momentum of the two neutrons emitted and in the angle spanned by this momentum and the momentum of the c.m. of the two neutrons have been presented for the first time.

The structure observed at low excitation energies could be attributed to known levels or groups of levels. In general, the predictions for two nucleon removal according to existing c.f.p. calculations agree rather well with the data as far as the predicted excitation energies are concerned.

When comparing the experimental rates for specific transitions with the magnitudes of the c.f.p. one should keep in mind that the c.f.p. contain pure nuclear structure information, independent of the reaction mechanism. In addition, for different total orbital angular momenta Λ of the two nucleons favoring of certain recoil momenta due

to geometry has to be taken into account. Most of the data, but especially those from ^{16}O where the usual geometrical restriction imposed on large recoil momenta has been bypassed by an additional measurement, indicate a considerably smaller $\frac{\Lambda = 2}{\Lambda = 0}$ ratio of the rates than predicted by the c.f.p. calculation by Cohen and Kurath.

The measurement made with ^{16}O as the target nucleus and with opening angles $125^{o} \leq \omega \leq 160^{o}$ showed an excitation spectrum quite different from the 'normal' case of back-to-back emission. It contains valuable information on $\Lambda \neq 0$ transitions. More such measurements are encouraged which should cover smaller angles and use different target nuclei. Unfortunately, these measurements have the experimental drawback of much smaller yields.

We tried to shed some light on the questions of population of deep lying two-hole states (s^1p^1- and s^2-removal) reached in a direct quasi-free reaction. For ^{6}Li and ^{7}Li as target nuclei such highly excited states are clearly observed in the residual nuclei. They correspond to removal of at least one s-shell nucleon. If the range of certain kinematical variables is restricted, there seem to be broad structures at high excitation energies also for the heavier nuclei. Still the question of contribution from non-quasi-free processes leading to these high excitation energies has to remain open, at least in quantitative terms. Assuming an isotropic distribution in angle ω for these non quasi-free events, the measured absolute rates in our ω-range are too big to be in line with these processes constituting the dominant contribution.

In the relatively few cases where theoretical predictions directly related to pion absorption can be compared with our results any agreement found seems to be more accidental than due to a refined treatment of all important aspects.

In some cases we compared measured recoil momentum distributions with simplified theoretical predictions. We made use of the momentum space wave functions for the absorbing quasi-deuteron moving in either a harmonic oscillator or a square well potential. The necessary parameters were fixed according to electron scattering data and binding energies. Considering the neglect of several effects that can change the q-distributions, like rescattering or distortion, the agreement with the data is surprisingly good although it is far from being perfect.

In accordance with the picture of a quasi-free absorption mechanism we observe a systematic change of the average recoil momentum with the separation energy of the pair. This is summarized in Fig. 33 for the most prominent $\Lambda = 0$ transitions leading to low excited states. Some of them can be contaminated by small $\Lambda = 2$ contributions but the general trend is established. The case of ^{14}N leading to the first excited state of ^{12}C at 4.44 MeV seems to be exceptional. It may indicate a 1S motion of the c.m. of the pair whereas 2S is usually observed for low E_x $\Lambda = 0$ transitions.

Except for ^{14}N, comparison of our excitation spectra with the corresponding $(\pi^+,2p)$ results yields good agreement within experimental uncertainties. This indicates a very similar reaction mechanism. The two reactions are

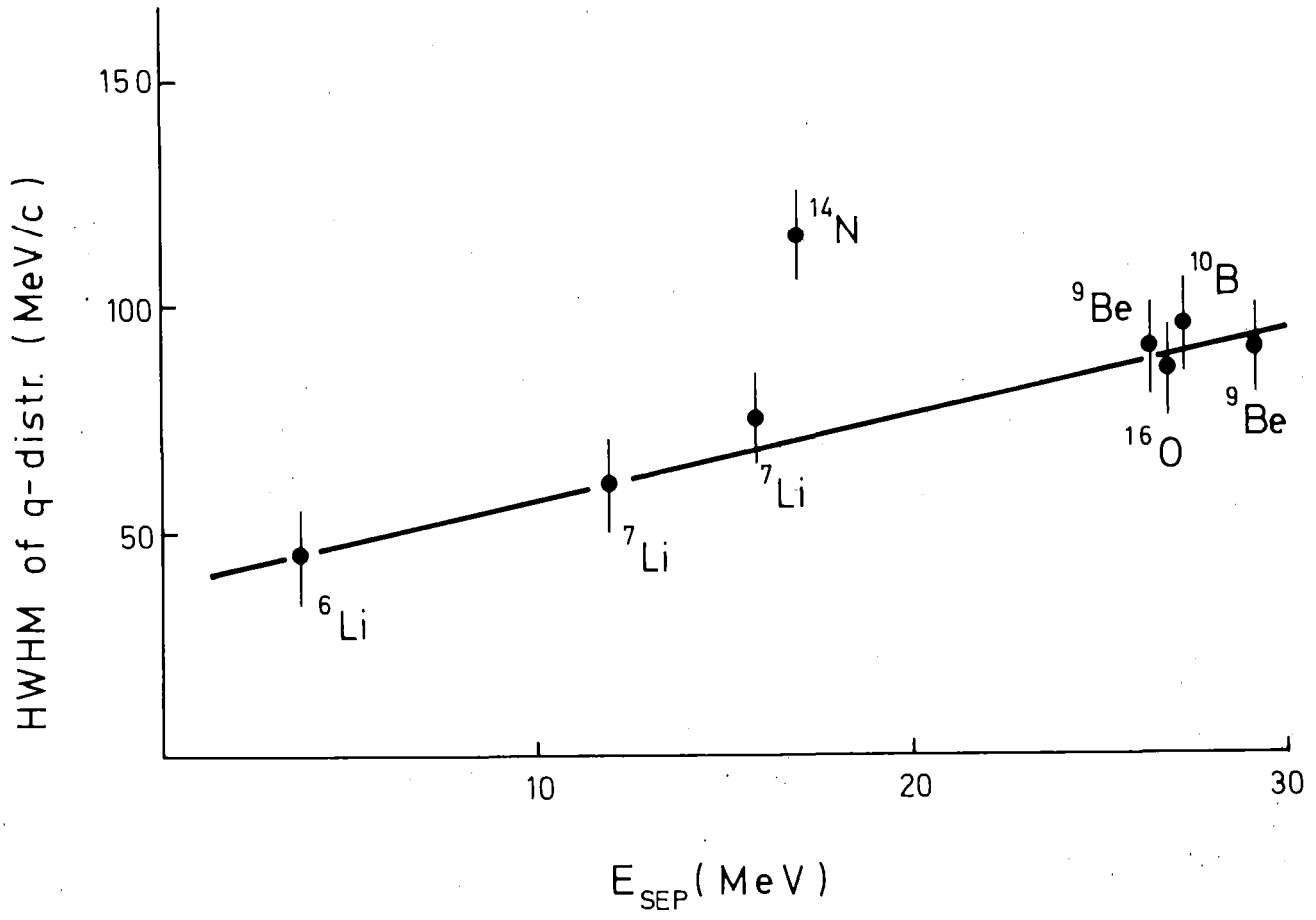

Fig. 33: Width of the q-distributions of the most prominent Λ=0 transitions as a function of the pair separation energy.

connected via charge symmetry. However, the result above is far from being trivial for the following reasons. First, the initial quantum state of the pion is, in principle, different because the π^+ are in flight whereas the π^- are stopped and absorbed from the atomic orbit. This should have an influence on the transitions observed. Second, the mean free path of the pion decreases quite rapidly with increasing pion energy (at least for $E_\pi \lesssim 100$ MeV). Therefore, π^+-absorption should be more a surface phenomenon than π^--absorption. Different parts of the 2-nucleon

wave function should be selected and this in turn would affect the q-distributions measured. Also the excitation spectrum might be influenced. Evidently, differences can be expected already for the π^- data, depending on whether the pion is absorbed from the S- or P-orbit.

More detailed measurements could perhaps reveal differences between $(\pi^+,2p)$ and $(\pi^-,2n)$.

Apart from the special cases of the cluster-type nuclei ^{6}Li and ^{7}Li we found that most of the strongly populated p-shell two-hole states induced by pion absorption have the same separation energies varying within a few MeV only. In addition, for the heavier nuclei of the 1p-shell starting with ^{9}Be, a remarkable correlation was found between these two-hole separation energies and the separation energies of the strongly populated single-hole states reached by (p,2p) reactions. From this we conclude that the two nucleons selected by the pion are in a closely correlated state in the sense of a definite overlap of their wave functions. It does not necessarily imply short range correlations in the usual sense.

REFERENCES

[1] K.A. BRUECKNER ET AL., Phys. Rev. 84 (1951) 258.

[2] M.G. HUBER, Annales de Physique 5 (1970) 239.

[3] S. OZAKI ET AL., Phys. Rev. Letters 4 (1960) 533.

[4] H. DAVIES ET AL., Nucl. Phys. 78 (1966) 663.

[5] M.E. NORDBERG ET AL., Phys. Rev. 165 (1968) 1096.

[6] F. CALLIGARIS ET AL., Nucl. Phys. A 126 (1969) 209.

[7] D.L. CHESHIRE AND S.E. SOBOTTKA, Nucl. Phys. A 146 (1970) 129.

[8] R.L. BURMAN AND M.E. NORDBERG, Jr., Phys. Rev. Letters 21 (1968) 229.

[9] J. FAVIER ET AL., Nucl. Phys. A 169 (1971) 540.

[10] E.D. ARTHUR ET AL., Phys. Rev. C 11 (1975) 332.
E.D. ARTHUR, Los Alamos Report No. LA-5230-T, 1973.

[11] T. ERICSON, Phys. Letters 2 (1962) 278.

[12] D.S. KOLTUN, Advances in Nucl. Phys. Vol. 3 (1969) 71.

[13] J. HÜFNER, Phys. Reports 21 (1975) 1.

[14] T.A. BRODY AND M. MOSHINSKY, Tables of Transformation Brackets, Universidad de Mexico (1961) and References therein.

[15] S. COHEN AND D. KURATH, Nucl. Phys. A 141 (1970) 145.

[16] V.V. BALASHOV ET AL., Nucl. Phys. 59 (1964) 417.

[17] Y. SAKAMOTO, Nucl. Phys. 87 (1966) 414.

[18] Y. SAKAMOTO ET AL., Phys. Rev. C 11 (1975) 668.

[19] D.S. KOLTUN, Phys. Rev. 162 (1967) 963.

[20] T.I. KOPALEISHVILI, Sov. J. of Nuclei and Particles 2 (1973) 87.

[21] T.I. KOPALEISHVILI ET AL., Sov. J. of Nucl. Phys. 15 (1972) 629.

[22] T.I. KOPALEISHVILI ET AL., Phys. Letters 22 (1966) 181.

[23] N.F. GOLOVANOVA AND N.S. ZELENSKAJA, Sov. J. of Nucl. Phys. 8 (1969) 158.

[24] K.N. CHUNG ET AL., Z. f. Physik 240 (1970) 195.
K.N. CHUNG ET AL., Phys. Letters 29 B (1969) 265.

[25] R.I. JIBUTI AND T.I. KOPALEISHVILI, Nucl. Phys. 55 (1964) 337.

[26] IL TONG-CHEON, Phys. Rev. 166 (1968) 1051; Phys. Rev. 158 (1967) 900; Phys. Letters 26 B (1968) 549.

[27] H. GARCILAZO AND J.M. EISENBERG, Nucl. Phys. A 220 (1974) 13; References to older articles by J.M. Eisenberg et al. can be found therein.

[28] J.W. MORRIS, JR. AND H.J. WEBER, Annals of Physics 79 (1973) 34; References to older articles by the authors can be found therein.

[29] F. HACHENBERG ET AL., Phys. Letters 66 B (1977) 425.

[30] J.M. EISENBERG ET AL., Phys. Rev. C 11 (1975) 1048 and references therein.

M. DILLIG, Lettere al Nuovo Cimento 10 (1974) 4.

[31] S.G. ECKSTEIN, Phys. Rev. 129 (1963) 413.

[32] D.S. KOLTUN AND A. REITAN, Phys. Rev. 141 (1966) 1413.

[33] D.D. KOLTUN AND A. REITAN, Phys. Rev. 155 (1967) 1139.

[34] T.I. KOPALEISHVILI AND I.Z. MACHABELI, Nucl. Phys. A 160 (1971) 204.

[35] T.I. KOPALEISHVILI, Nucl. Phys. B 1 (1967) 335.

[36] W. ELSAESSER AND J.M. EISENBERG, Nucl. Phys. A 144 (1970) 441.

[37] R.S. KAUSHAL AND Y.R. WAGHMARE, Nucl. Phys. A 144 (1970) 449.

[38] B. KOBER, Diplomarbeit, University of Karlsruhe (1972).

[39] F. TAKEUTCHI ET AL., Large-area position-sesitive time-of-flight counters for neutrons and charged particles, CERN preprint, 1 July 1975.

[40] R.J. KURZ, UCRL-11339 (1964).

[41] P. KITCHING ET AL., Phys. Rev. C 11 (1975) 420 and references therein.

[42] P.G. ROOS ET AL., Nucl. Phys. A 257 (1976) 317 and references therein.

[43] D. MILJANIĆ ET AL., Nucl. Phys. A 215 (1973) 221 and references therein.

[44] A.K. JAIN ET AL., Nucl. Phys. A 216 (1973) 519 and references therein.

[45] R. HAGELBERG ET AL., Nucl. Phys. A 207 (1973) 366.

[46] W. DOLLHOPF ET AL., Phys. Letters 58 B (1975) 425.

[47] E. VELTEN, Ph. D. thesis, University of Karlsruhe (1970) and references therein.

[48] D. VINCIGUERRA ET AL., Lettere al Nuovo Cimento 14 (1975) 333 and references therein.

[49] Energy levels of ^{4}He, Nucl. Phys. A 206 (1973) 1;
^{5}He, ^{7}Li, ^{8}Be, ^{10}B, Nucl. Phys. A 227 (1974);
^{12}C, Nucl. Phys. A 248 (1975) 1;
^{14}N, Nucl. Phys. A 152 (1970) 42.

[50] J.W. WATSON ET AL., Nucl. Phys. A 172 (1971) 513.

[51] C. RUHLA ET AL., Phys. Letters 6 (1963) 282.

[52] M. JAIN ET AL., Nucl. Phys. A 153 (1970) 49.

[53] P.G. ROOS ET AL., Phys. Rev. Letters 22 (1969) 242.

[54] T.I. KOPALEISHVILI AND I.Z. MACHABELI, Sov. J. of Nucl. Phys. 4 (1967) 27.

[55] B.K. JAIN AND B. BANERJEE, Il Nuovo Cimento 69 A (1970) 419.

[56] G. ALBERI AND L. TAFFARA, Il Nuovo Cimento 58 B (1968) 441.

[57] Y.C. TANG ET AL., Phys. Rev. 123 (1961) 548.

[58] J. CERNY ET AL., Phys. Rev. 152 (1966) 950.

[59] W.J. KOSSLER ET AL., Phys. Rev. C 4 (1971) 1551.

[60] H.D. ENGELHARDT ET AL., Nucl. Phys. A 258 (1976) 480.

[61] C.W. LEWIS AND H. ULLRICH, private communication.

[62] L.R.B. ELTON, Nuclear Sizes, Oxford university press, 1961.

[63] Y. SAKAMOTO AND F. TAKEUTCHI, private communication.

[64] L.I. SCHIFF, Quantum Mechanics, Third ed., Mc Graw-Hill, p. 83-88.

[65] TH.A.J. MARIS in Proc. of the fifth Int. Conf. on High-Energy Physics and Nuclear Structure, Uppsala 1973, G. TIBELL ed., p. 356.

[66] D.G. FLEMING ET AL., Nucl. Phys. A 162 (1971) 225.

[67] H.J. WEBER, Annals of Physics 57 (1970) 322.

[68] J.Y. GROSSIORD ET AL., Phys. Rev. C 15 (1977) 843.

[69] C.G. HOOT ET AL., Nucl. Phys. A 203 (1973) 339.

[70] A. VAN DER WOUDE AND R.J. DE MEIJER, Nucl. Phys. A 258 (1976) 199.

[71] B. BASSALLECK ET AL., Phys. Letters 65 B (1976) 128.

[72] C.E. STRONACH ET AL., Phys. Rev. C 15 (1977) 984.

EUROPEAN ORGANIZATION FOR NUCLEAR RESEARCH

A P P E N D I X A

TWO-NEUTRON EMISSION INDUCED BY STOPPED π^- ON ^{9}Be, ^{10}B, AND ^{12}C *)

B. Bassalleck, W.-D. Klotz, F. Takeutchi**), and H. Ullrich

Kernforschungszentrum und Universität Karlsruhe
Institut für Experimentelle Kernphysik, Fed. Rep. Germany
and CERN, Geneva, Switzerland

and

M. Furić***)

CERN, Geneva, Switzerland

ABSTRACT

The $(\pi^-,2n)$ process has been studied in a kinematically complete experiment on three neighbouring 1p-shell nuclei. Distributions of excitation energy of the residual nuclei, of recoil momentum, of the angle between the emitted neutrons, and the angle between the sum and the difference of the neutron momenta have been measured. From the excitation spectra a striking analogy with (p,2p) data has been found in the region of p-shell nucleon removal. The possibility of s-shell nucleon removal has been investigated. The data are compared with theoretical predictions.

Nucleon reaction $(\pi^-,2n)$ on ^{9}Be, ^{10}B, and ^{12}C, E = 0 measured rate (En_1,En_2,ω); excitation spectra for residual nuclei deduced, recoil momentum distributions extracted.

Geneva - 28 March 1977

(Submitted to Physical Review)

*) Work supported in part by the Bundesministerium für Forschung and Technologie of the Federal Republic of Germany.

**) Present address: Department of Physics, Kyoto Sangyo University, Kamigamo-Motoyama, Kyoto, Japan.

***) On leave of absence from Institute R. Bošković, Zagreb, Yugoslavia.

1. INTRODUCTION

In light nuclei the pion absorption with the subsequent back-to-back emission of a nucleon pair proceeds very strongly via the quasi-free mechanism. The coincident detection and energy measurement of both nucleons permit a complete determination of the kinematical properties for the absorbing pair. This offers an excellent opportunity to study separation energies, momentum distributions, and angular momenta of the two nucleons involved[1]. Such experiments are also expected to yield information about the πNN interaction itself, and its dependence on the different quantum states of the NN-combinations inside nuclei.

The theoretical treatment of the pion absorption in nuclei presents a major problem. The following aspects have to be taken into account simultaneously: a) short-range correlations between the nucleons in the initial state; b) the interaction between three and more particles in the final state; c) a proper description of the pion absorption dynamics; and, d) realistic wave functions for the absorbing nucleus. So far only two published calculations include (a), (b), and (c). They differ in the approach to the final state. While Morris and Weber[2] use the coupled channel method with realistic interactions, Garcilazo and Eisenberg[3] solve the Faddeev equation with separable potentials. However, experimentally observable features such as excitation spectra of residual nuclei and momentum distributions are strongly influenced by (d). Consequently our data will be compared with calculations using more realistic nuclear wave functions. We use results of Kopaleishvili et al.[4] who consider only the nucleon-nucleon interaction in the final state, but include (c) and (d). In addition, we use the tabulated coefficients of fractional parentage (c.f.p.) for the two-nucleon removal of Cohen and Kurath[5] (CK) and of Balashov et al.[6] (BBR).

On the experimental side, the results with best energy resolution until recently could be obtained with $(\pi^+,2p)$ measurements[7,8]. In most cases, however, the insufficient energy resolution or inadequate statistics hampered the identification of the discrete final states. The resolution of the existing $(\pi^-,2n)$ measurements[9,10] was at least a factor of 3 lower than that of the $(\pi^+,2p)$ experiments. Owing to charge symmetry $(\pi^-,2n)$ and $(\pi^+,2p)$ reactions should lead to identical states in the same residual nucleus if the quasi-free mechanism is the dominant one and if the kinematical conditions are identical for both experiments. The latter condition is not fulfilled *a priori*, since $(\pi^+,2p)$ studies are performed with pions in flight, while in $(\pi^-,2n)$ experiments pion absorption occurs "at rest". This causes a difference not only in pion energy but possibly also in the pion angular momentum relative to the nucleon pair. A comparison between $(\pi^+,2p)$ and $(\pi^-,2n)$ measurements with equivalent accuracy can therefore test the basic assumptions on the mechanism, and also investigate the influence of the

initial pion state on the experimental results, especially on the excitation spectra. A difference between the two reactions had been already reported for the target ^{14}N [11].

In the $(\pi^-,2n)$ reactions on 1p-shell nuclei, strong peaks observed in the excitation spectra for the residual nuclei are so far mainly attributed to nucleon removal from the p-shell. Only for the lithium targets has a large contribution from the s-shell nucleons also been identified[7,10,12]. Evidence for the two-hole states in the p-shell and, separately, in the s-shell was reported in the reaction $^{12}C(\pi^-,2n)^{10}B$ [9]. However, the peak due to the holes in the s-shell was not observed in an experiment with higher resolution on the analogous $(\pi^+,2p)$ reaction[7].

In our experiment we use large-area position-sensitive neutron counters with subnanosecond time resolution. They allow the study of the $(\pi^-,2n)$ reaction with energy resolution[13] comparable to or better than that of the existing $(\pi^+,2p)$ data. At the same time, these counters offer rather large solid angles. The targets ^9Be, ^{10}B, and ^{12}C were used to search systematically for the evidence of the inner shell absorption in the nuclei close to the lithium isotopes. Where possible, we have made comparisons with existing $(\pi^+,2p)$ data and with theoretical predictions.

2. CONCEPTS RELEVANT FOR DATA INTERPRETATION

Figure 1 shows the kinematical variables which are used. In the case of the absorption of stopped π^- followed by a three-body disintegration, there are three independent variables. For a given excitation energy of the residual nucleus E_x, p, and q are related by the energy conservation. So the combinations like q and ω, or q and θ, together with E_x, form a complete set of variables to describe the kinematics. The importance of the θ distributions has been pointed out by Koltun[14].

In the quasi-free description of the $(\pi^-,2n)$ reaction, we assume that the pion is absorbed by a neutron-proton pair in the target. In the initial state, the angular momentum of the centre of mass of the pair and of each nucleon with respect to the centre of mass of the target, are L, ℓ_1, and ℓ_2, respectively. The total angular momentum Λ is written as $\Lambda = \ell_1+\ell_2 = L+\ell$, where ℓ denotes the relative angular momentum of the nucleons.

In the following we assume that the pion is mainly absorbed by a pair in relative s-state, i.e. $\ell = 0$, and we have $L = \Lambda$. For p^2 removal, i.e. for the removal of two nucleons from the p-shell, we have $\ell_1 = \ell_2 = 1$ and therefore $L = 0$ or 2, and in both cases the parity of the residual state is the same as that of the target. It should be noted that the n-p pair can be in a spin triplet, isospin singlet, or a spin singlet, isospin triplet state. For L = 0 the energy

conservation in the shell model allows the admixture of the following two combinations:

$$\text{a) } 2S\ (\mathcal{N} = 1,\ L = 0) \times 1s\ (n = 0,\ \ell = 0)$$

$$\text{b) } 1S\ (\mathcal{N} = 0,\ L = 0) \times 2s\ (n = 1,\ \ell = 0)\ ,$$

where $\mathcal{N}$ and n are the principal quantum numbers associated with the c.m. motion and the relative motion of the two nucleons, respectively. In contrast to the $(\pi,2N)$ reactions, (b) is suppressed in the case of two-nucleon transfer or quasi-free deuteron knockout reactions, because the removed nucleon pair is not in the lowest energy state. For $\Lambda = 2$, under the assumption of $\ell = 0$, there is only one combination possible:

$$\text{c) } 1D\ (\mathcal{N} = 0,\ L = 2) \times 1s\ (n = 0,\ \ell = 0)\ ^{*)}\ .$$

For the removal of an s-p pair, we have $L = 1$, and the possible combination is

$$\text{e) } 1P\ (\mathcal{N} = 0,\ L = 1) \times 1s\ (n = 0,\ \ell = 0)\ .$$

The parity of the residual state is different from that of the target nucleus. For the removal of an s^2 pair, we have $L = 0$, and the only possible combination is:

$$\text{f) } 1S\ (\mathcal{N} = 0,\ L = 0) \times 1s\ (n = 0,\ \ell = 0)\ .$$

The parity of the residual state is again the same as that of the target.

The q-distribution for a given residual state is dominated by L and $\mathcal{N}$, and is essentially the absolute value squared of the c.m. wave function of the two nucleons in the momentum space. In Fig. 2 we show two measured q-distributions for different n-p pairs with similar separation energies. They are compared with simplified calculations for different $\mathcal{N}$ and L carried out with a square well potential and the corresponding separation energies. It should be mentioned that for the case of $L = 0$, the width of the distribution is dominated by the separation energy of the pair in the target. Large separation energies correspond to wider distributions.

For the interpretation of the experimentally obtained q-distributions, the following should be considered:

---

*) For the geometrical reason stated later, this component is suppressed. In this case, the admixture of the component (d), $1S\ (\mathcal{N} = 0,\ L = 0) \times 1d\ (n = 0,\ \ell = 2)$, may become important.

i) So as to detect mainly the quasi-free events, our counters are placed at $\omega \sim 180°$, and hence small q is favoured. Levels corresponding to $L \neq 0$ (especially to L = 2) transitions are therefore suppressed in the excitation spectra. In the case of $\Lambda = 2$ transitions, component (d) involving 1S may become more important. However, as 1S also shows a wide q-distribution, we expect a wide distribution for $\Lambda = 2$ for any admixture of (c) and (d).

ii) The shape of the q-distributions can be modified owing to various effects. The distribution for $L \neq 0$ is expected to be zero at q = 0, but the distortion effects caused by initial- and final state interactions tend to fill this dip. Also, if the pions are preferentially absorbed at the nuclear surface, or if the emitted nucleons originating from the inner regions undergo stronger distortions, the contribution of the wave function of the c.m. of the pair at small radii is suppressed. Hence in the resultant q-distributions, the peak position shifts towards small q for $L \neq 0$, and the width becomes smaller for L = 0 [15].

If the process is dominated by short-range correlations, the large-p components of the initial state play the important role. As by energy conservation, large p is related to small q, this effect will enhance the small-q components and hence will have the same result as the preceding effect.

3. EXPERIMENTAL SET-UP AND DATA HANDLING

Negative pions of 70 MeV from the CERN Synchro-cyclotron (SC) low-energy pion channel were stopped in targets of 3-5 g/cm^2 thickness. The experimental set-up is shown in Fig. 3. All counters were plastic scintillators.

The pion stop trigger was obtained from counters I and II before the degrader, counter III and the hodoscope, between the degrader and the target, in coincidence, and counter V in anticoincidence. Counter II, with the dimensions 12 cm × 10 cm × × 1 cm, had a pair of twisted-strip light-guides, two RCA 8850 photomultipliers, and was used as the start counter for the two neutron time-of-flight counters. The time resolution of this counter for 2 MeV pulses was 300 psec. The pulse height of counter III was used to determine the pion stopping point in the target in the beam direction. The hodoscope strips, of 2 cm width each, mounted on Philips 1110 phototubes, served to fix the stopping point in the target in the horizontal direction, perpendicular to the beam. Counter IV was a plastic scintillator of 0.5 mm thickness; it enabled us to reject those pions which stopped in the hodoscope.

The two outgoing neutrons were detected in coincidence with a pair of large-area, position-sensitive, time-of-flight counters, placed 4.5 m from the target. The angle between the centres of the counters was 160°, thus covering an ω-range

from 140° to 180°. The sensitive volume of one neutron counter is 2 m wide × 48 cm high × 9 cm thick, covering a solid angle of 47 msr at a distance of 4.5 m from the target.

To localize the neutron impact point vertically, the counter is subdivided into eight bundles of scintillators, each of 6 cm height. In order to improve the time resolution by localizing the impact point in depth, it is also subdivided into six layers of 1.5 cm thickness each. In total, each counter consists of 48 rods, made of NE 110 plastic scintillator and assembled as indicated in Fig. 3. The development and testing of a prototype counter has been described previously[16]. Two adjacent bundles are viewed by a 56 DVP photomultiplier at each end. The position information along the counter is taken from the time difference between the two photomultipliers. A total of 30 small phototubes (Philips 1110) on each counter show the pattern of the rods that have given a signal for each event.

The time-of-flight information, time difference between the photomultipliers on both sides, pulse heights of the 56 DVP's, and pattern information of all phototubes as well as hodoscope information and counter III pulse-height, were written on tape, event by event, via a CAMAC system and a PDP 8L on-line computer. The pulse-height information from the neutron counters was later used to set a threshold, in the off-line program, and also to remove the residual walk of the ORTEC 473 constant-fraction discriminators used.

A typical time resolution of a neutron counter is 800 psec for 20 MeV electron equivalent pulses, including start counter resolution. This resulted in an excitation energy resolution ΔE_x of 3-6 MeV FWHM, depending on pulse-height threshold, flight path, and on E_x. This resolution is at least a factor of 3 better than in previous $(\pi^-,2n)$ measurements.

All data were written on magnetic tape and analysed using the CERN CDC 7600. In the off-line analysis, a sufficiently high pulse-height threshold (4-5 MeV electron equivalent) was set to get a uniform efficiency over the whole counter by taking into account the light attenuation in the rods[16]. The efficiency correction was made with the Kurz code[17], which had been tested on the prototype counter in an independent efficiency measurement. All distributions shown are corrected for this effect. Usually, neutrons with kinetic energy below 15 MeV were rejected. Also events from the last 12 cm on each side of the counters were not accepted because of non-uniformity in the effective light-propagation velocity. If the first layer had triggered, and if the measured pulse height and kinetic energy were in a certain relation, then the event was assigned to a charged particle and was rejected. The data have also been corrected for geometrical acceptance in our ω-range between 145° and 180°. The corresponding correction function has been determined for our geometry with high statistical accuracy using a Monte Carlo simulation program.

Within the experimental limitations (E_{kin} > 15 MeV, ω > 145°) our data are therefore free of geometrical bias and can be directly compared with theory. The recoil momentum distributions shown are obtained by dividing the corrected rate by the three-body phase-space factor. For the θ-distributions, q has been restricted to values where there is no reduction in phase space caused by our restricted ω-range. In all figures, the errors given are statistical.

In principle, all our data are available as a function of three independent parameters, as described in Section 2. For practical reasons, however, only one- and two-dimensional distributions are given in this paper.

4. RESULTS AND DISCUSSION -- LOW E_x REGION

4.1 Beryllium-9

So far, the only attempt to study the $^9Be(\pi^-,2n)^7Li$ reactions has been made by Calligaris et al.[10]. Their statistics were poor, however, being based on a total of 145 events, and it was therefore interesting to repeat the measurement with better statistics and good resolution.

Our observed excitation spectrum of the residual ^7Li nucleus is shown in Fig. 4. The spectrum shows a maximum at about 10 MeV and then decreases slowly with increasing excitation energy. The ground state ($3/2^-$) and the 0.48 MeV first excited state ($1/2^-$) are weakly populated. In the α-α-n cluster picture for the ^9Be target, the transition to these levels corresponds to a removal of the weakly bound neutron and a proton from one of the α clusters. The weak rate is therefore probably explained by the rather large distance between the proton and the neutron which absorb the pion. The recoil momentum distribution corresponding to these levels is shown in Fig. 5. It indicates a predominant contribution of L = 0; the half-width is, however, relatively large (∿ 120 MeV/c) for this pair separation energy (see Section 2). It is larger than the corresponding width for higher levels, described later, which have higher separation energy. This fact again supports the assumption of a large distance between the absorbing nucleons and the cluster picture of the ground state of the target nucleus and the two lowest levels of ^7Li.

In the excitation spectrum in Fig. 4 two large peaks in the region between 7 MeV and 11 MeV are visible. As the number of known levels in this region is small, they can be attributed to the levels at 7.47 MeV ($5/2^-$, T = ½) and 10.25 MeV ($3/2^-$, T = ½). Balashov et al.[6] predict by far the largest spectroscopic factor for the Λ = 0 transition to the members of a $^{2T+1,2S+1}L = {}^{2,4}P$ triplet at about 8-11 MeV. According to Barker[18], the level at 7.47 MeV ($5/2^-$) seems to be the lowest member of this triplet. These facts lead to the conclusion that this transition corresponds to the removal of a spin triplet (T = 0) n-p pair from the

target nucleus. The $\Delta T = 0$ transition is confirmed by the fact that this level is populated in the $^{9}Be(p,^{3}He)^{7}Li$ reaction ($\Delta T = 0,1$) at $E_p = 43.7$ MeV, whereas the mirror level at 7.21 MeV in ^{7}Be is not seen in the $^{9}Be(p,t)^{7}Be$ reaction ($\Delta T = 1$) under the same conditions[19].

The energy of the $3/2^-$ member of the $^{2,4}P$ triplet is calculated to be between 8 MeV and 11 MeV[20]. According to Ajzenberg-Selove and Lauritsen[21] the 10.25 MeV level is the only $3/2^-$ member of the triplet. Then the large population (seen in Fig. 4) comparable to that of the 7.5 MeV level agrees with the prediction of Balashov et al.[6]. Furthermore, the recoil momentum distributions corresponding to these peaks, shown in Fig. 5 , are rather similar. They both indicate a strong $L = 0$ component, and the half-width is about 90 MeV/c, which is smaller than the width of the q-distribution for the ground and first excited levels already mentioned. Therefore this is in agreement with the $\Lambda = 0$ prediction.

Besides the $1/2^-$ member of the $^{2,4}P$ triplet, Balashov et al. predict a large spectroscopic factor also for $[21]^{2}P$ levels at E_x about 16-18 MeV (the numbers in the bracket correspond to the Young scheme). However, except for the 16.8 MeV level, no level is experimentally well established (see Ref. 21), and at the same time no other distinct peak is seen in our excitation spectrum. Therefore, a further comparison of the result with the c.f.p. calculation is difficult.

In conclusion, the largest rates come from the transition to $^{2,4}P$ levels, and the transitions to the ground and first excited states are weak. The analog $(\pi^+,2p)$ reaction on the same target has been investigated by Favier et al.[7]. Their excitation energy spectrum seems to be similar to ours within their experimental resolution.

4.2 Boron-10

Data on the pion-induced two-nucleon emission with ^{10}B as a target nucleus were obtained for the first time. Figure 6 shows the excitation spectra. Since the residual nucleus ^{8}Be is particle unstable, the four-body break-up contribution in the excitation spectrum is possible even in the ground-state region. In the spectrum without q-windows, two main peaks can be observed at approximately 3 MeV and 19 MeV excitation energy. The momentum distributions for these peaks are shown in Fig. 7. The distribution for the peak at 3 MeV is $\sim$ 150 MeV/c wide. We conclude that it is dominated by a $\Lambda \neq 0$ component. The observed large width of the 3 MeV peak in the excitation energy spectrum can be at least partially explained by the known width of this level in ^{8}Be. The momentum distribution shown in Fig. 7 for the peak around 19 MeV is narrow and it has its maximum in the vicinity of zero momentum, indicating mainly $L = 0$. In Fig. 6 the excitation spectrum restricted to large q-values is also given. It indicates that the broad peak around

19 MeV is a superposition of three peaks at 17, 19, and 22 MeV. The splitting is not visible in the excitation spectrum for low q-values, where only the 19 MeV peak persists. This suggests $\Lambda \neq 0$ for the peaks at 17 and 22 MeV. In the lower curve of Fig. 6 there is also a weak peak visible at 10 MeV, which for the same reasons should correspond to $\Lambda \neq 0$.

The levels with large c.f.p. are also indicated in Fig. 6. When comparing the experimental results with the c.f.p. calculations, several remarks are important. The correspondence between the theoretical and known experimental levels is not completely established, especially in the region of higher excitations. In Fig. 6 the position of the levels is given according to the calculations. The $L = 2$ transitions are suppressed in our geometry, as discussed previously. The $\Delta T = 1$ transitions can appear only at higher excitations since all the known $T = 1$ levels in ^{8}Be are above 16 MeV.

At $E_x \sim 3$ MeV both theories[5,6] predict $\Lambda = 2$ contributions in agreement with our data. The calculations differ in the strength for $\Lambda = 2$ transitions to the level at 10 MeV. Cohen and Kurath expect this level to be less populated than the one at 3 MeV, while Balashov et al. predict the opposite. In the region above 16 MeV, strong $\Delta T = 0$, $\Lambda = 0$ transitions are predicted by both Cohen and Kurath and by Balashov et al. which agree with the position of the largest experimental peak at 19 MeV. A $\Delta T = 0$, $\Lambda = 2$ transition is also expected in both calculations at somewhat lower energy than the $\Lambda = 0$ contribution, in agreement with our indication for a level at 17 MeV. None of the $\Delta T = 0$, $\Lambda = 2$ calculations can explain the observed indication of a level around 22 MeV.

Cohen and Kurath expect two $\Delta T = 1$, $\Lambda = 2$ contributions which agree with the excitations at 17 and 22 MeV. It should be noted that only $\Delta T = 1$ calculation explains the excitation around 22 MeV. The largest $\Delta T = 1$, $\Lambda = 0$ transition strength is expected for the level at $\sim$ 18 MeV, in accordance with the position of the main observed peak. However, another $\Delta T = 1$, $\Lambda = 0$ transition, weaker in intensity, is expected around 22 MeV. The middle spectrum in Fig. 6, which emphasizes $\Lambda = 0$ transitions, does not confirm this.

The indication of wide structure at higher energies will be discussed later. The comparison with $(\pi^+,2p)$ or (p,pd) data is not possible, owing to lack of such measurements.

The following summary can be made. In the excitation spectrum of ^{8}Be a $\Lambda = 2$ transition to $E_x \sim 3$ MeV and a $\Lambda = 0$ transition to $E_x \sim 19$ MeV are well identified. Evidence for transitions to additional levels exists at 10, 17 and 22 MeV; $\Lambda = 2$ is assigned to all the corresponding transitions as a dominant component. The isospin assignment for the absorbing nucleon pair is difficult above $E_x \sim 16$ MeV, where $\Delta T = 1$ becomes possible in addition to $\Delta T = 0$. Cohen and

Kurath suggest $\Delta T = 1$ for the $\Lambda = 2$ transition to 22 MeV excitation. For the transition to E_x = 17 MeV and 19 MeV, both isospin values for the nucleon pair are possible.

4.3 Carbon-12

Carbon-12 has often been used as target for $(\pi^-,2n)$ reactions[9,10,22,23] as well as for the analogous $(\pi^+,2p)$ reaction[7]. Ozaki et al.[22] and Nordberg et al.[23] show no excitation energy spectrum, whereas in the case of Calligaris et al.[10] the statistics are very poor. The measurement done by Cheshire and Sobottka[9] had rather bad energy resolution; besides a peak around 5 MeV, the excitation energy spectrum shows a peak around 38 MeV which they have attributed to removal of two s-shell nucleons.

Figure 8 shows our measured excitation energy distribution. Also indicated are levels with large c.f.p. according to calculations for two p-shell nucleon removal[5,6]. The spectrum is dominated by a large peak around 1 MeV, in addition to which there are three more peaks at about 4.5 MeV, 7 MeV, and 12 MeV. Also, there seems to be an indication of a somewhat broader peak at 21-22 MeV.

Cohen and Kurath predict large c.f.p. for transitions to the ground state (3^+, T = 0), first excited state (0.7 MeV, 1^+, T = 0), and second excited state (1.7 MeV, 0^+, T = 1). Our experimental result is compatible with this prediction, as the main contribution lies in the region of $E_x < 5$ MeV. The ground-state transition has $\Lambda = 2$, whereas the other two have $\Lambda = 0$. Our measured q-distribution for this lowest excitation energy range is shown in Fig. 9. It indicates some L = 0 contribution,+) but the width is significantly larger ($\sim$ 150 MeV/c) than for the targets ^{9}Be or ^{10}B for the same separation energy. As is known from a (π^-,γ) measurement[24], the first three excited states all contribute, and therefore our dominant peak around 1 MeV is very likely composed of ground state plus the first three excited states. Within our energy resolution we cannot give precise numbers for the relative contributions among them.

Also Balashov et al.[6] predict the major strength to be in the low excitation region ($E_x < 3$ MeV) and are thus in qualitative agreement with our result.

The structure around 4.5 MeV can be attributed to the 4.77 MeV level (3^+, T = 0) with some possible contribution from the 3.6 MeV level (2^+, T = 0) and from the levels around 5.1-5.2 MeV. According to the Cohen and Kurath prediction, there should be significant strength in this region for $\Lambda = 2$ transitions. Our measured q-distribution for this E_x part (Fig. 9), is very broad and of different shape than for pure L = 0. From this we conclude that a major $\Lambda = 2$ contribution is possible, in agreement with Cohen and Kurath.

+) For a pure L=2 the peak of the q-distribution would occur at a much greater value of q.

For the peaks above E_x = 6 MeV, no attempt at comparison with known levels has been made. However, it should be emphasized that Cohen and Kurath predict a very large c.f.p. for a $\Lambda = 2$, $\Delta T = 1$ transition to an excitation energy of 7.2 MeV. Indeed we observe a peak around 7 MeV whose q-distribution, shown in Fig. 9, is again very wide with the maximum close to zero momentum. If it is the predicted level, then, in view of the very large predicted c.f.p., it is suppressed compared to the observed $\Lambda = 0$ transition at about 1 MeV. The peak around 12 MeV and the broader structure around 21-22 MeV are discussed later in this paper, in connection with the possibility of s-shell nucleon removal.

The excitation spectrum of the $(\pi^+,2p)$ measurement of Favier et al.[7] is in rather good agreement with our excitation spectrum, proving the similarity of the reaction mechanism. Also the excitation spectra of both reactions for small q only (Fig. 8 and Ref. 7) are very similar: the spectra are essentially flat in the E_x-range 15-70 MeV.

Besides the comparison with $(\pi^+,2p)$, a comparison could be made with other reactions that lead to the same residual nucleus, such as (p,pd), (d,α), or $(p,{}^3He)$. The two-nucleon pick-up reactions (d,α) and $(p,{}^3He)$, however, are sensitive to larger recoil momenta q than the $(\pi^-,2n)$ process in our geometry.

A recent $^{12}C(p,pd)^{10}B$ measurement[25] at E_p = 75 MeV has shown about equal population of ground state and first excited state, even at recoil momentum q = 0. Their experiment showed a smaller population of the second and third excited states, similar to our results. The higher excitation region has not been measured by these authors.

Among the numerous theoretical papers on π^- absorption there are only very few that contain a detailed prediction on the excitation energy spectrum that this reaction should produce. Kopaleishvili et al.[4] have calculated this distribution for ^{12}C, among other target nuclei, assuming absorption from the atomic s-orbit and neglecting the final-state nucleon-nucleus interaction. As they show a result only for q < 50 MeV/c, our excitation spectrum for small recoil momenta (Fig. 8), should be compared with their prediction. They agree in so far as the main strength is below 5 MeV.

The latest attempt to treat the complete three-body final-state system of the $(\pi^-,2n)$ reaction by solving the corresponding Faddeev equations is the one by Garcilazo and Eisenberg[3]. In Fig. 10 a comparison between our measured ω-distribution, integrated over all E_x values, and their prediction has been made. It shows that our distribution is rather flat in the ω-range covered, and disagrees with the predicted distribution, which is peaked at 180°. If we restrict our

data to small E_s values (see Fig. 16), then the ω-distribution is peaked at this angle , and thus is in better qualitative agreement with the prediction for two nucleons coming from the $1p_{3/2}$ shell[3]. But it should be also mentioned that the shape of this shown ω-distribution depends on the choice of the upper limit in E_s, i.e. the higher this limit the less pronounced the peak at 180° generally becomes. Therefore we would like to emphasize the necessity of theoretical efforts giving more detailed excitation spectra with angular and recoil momentum distributions for certain ranges of excitation energy.

4.4 General remarks on the p-shell hole states

To discuss the systematic trends of the p-nucleon removal in different targets, the separation energy of the neutron-proton pair is more relevant than the excitation energy in the residual nuclei. In Fig. 11 our results are presented in the way that the strongly populated residual levels for ^{9}Be, ^{10}B, and ^{12}C, and also for ^{14}N [11] are indicated as a function of E_s, the separation energy of a free deuteron*). It is surprising to find that for all these targets, the peaks are nearly at the same position, namely at $E_s \sim 26$ MeV. A comparison of the energies of our $(\pi^-,2n)$ peaks and the peaks from (p,2p) results[26] as shown in Fig. 11, reveals a certain similarity between them. If the scale of the single-nucleon separation energy is expanded by almost a factor of 2 with respect to the two-nucleon separation energy, this similarity becomes obvious, and does not seem to be only fortuitous. This can be understood considering that the proton and the neutron in the same orbit are strongly correlated and can absorb the pion, whereas the correlation is weak between two nucleons from different orbits. Best agreement between the separation energies in Fig. 11 could be achieved with a multiplication factor of 1.62. It is also important to use the separation energy for the free deuteron to get this agreement.

About the quantum state of the absorbing pair the following can be said. For $\Lambda = 0$, the two components a) 2S ($\mathcal{N} = 1$, $L = 0$) × 1s ($n = 0$, $\ell = 0$) and b) 1S ($\mathcal{N} = 0$, $L = 0$) × 2s ($n = 1$, $\ell = 0$) may contribute, as has been mentioned in Section 2. For the transitions to which the c.f.p. calculations predict strong $\Lambda = 0$ contributions, such as the 7.5 MeV and 10.3 MeV levels in ^{7}Li, or the 19 MeV level in ^{8}Be, the experiment shows that the width of the corresponding q-distributions is as small as 80-90 MeV/c. This is much smaller than the width for $\Lambda = 2$ transition. In Fig. 2 a comparison with calculated q-distributions for 1S and 2S transitions is made, which shows that the above mentioned $\Lambda = 0$ transitions are closer to the 2S distribution. Therefore, the combination (a),

---

*) E_s is given by: $E_s = E_x + M_B - M_A + m_d$. Where M_A and M_B are the masses of the target and recoil nucleus, and m_d is the mass of the free deuteron.

corresponding to the pion absorption by a pair in a relative 1s-state, seems to be favoured compared to (b), i.e. 2s absorption.

According to our observations, for equal c.f.p., $\Lambda = 2$ transitions are generally weaker than $\Lambda = 0$ transitions. It has already been mentioned that the $L = 2$, $\ell = 0$ component of the $\Lambda = 2$ transition is suppressed in our geometry. Apparently also the second component $L = 0$, $\ell = 2$ does not appear strongly. We conclude, therefore, that the absorption by a pair in the relative d-state ($\ell = 2$) is less favoured than in the s-state ($\ell = 0$).

It should be mentioned, however, that we observe a clear though not very strong transition at 7 MeV in the residual nucleus ^{10}B, which corresponds probably to the absorption of a pair in a relative d-state, provided our attribution to a predicted $\Lambda = 2$ state is correct. The corresponding q-distribution is given in Fig. 2. It agrees with the schematically calculated distribution for a 1S-state.

5. RESULTS AND DISCUSSION -- HIGH E_x REGION

On the lithium isotopes two well-separated big peaks are observed in the excitation energy spectra obtained in the $(\pi^-,2N)$ reactions, one peak around E_x = 0-4 MeV and the other around 30 MeV [7,10,12]. The latter peak, which has more than twice the area of the former one, is interpreted as s-shell nucleon removal[7,12]. In the $^{12}C(\pi^-,2n)^{10}B$ measurement of Cheshire and Sobottka, the reported peak corresponding to s^2 removal at $E_x \sim 38$ MeV [9] is comparable in size to the p^2-removal, i.e. the ratio of s- to p-removal is smaller than in the lithium isotopes. Therefore it is interesting to look at s-nucleon removal with targets in the mass number range between lithium and carbon.

It is worth while to mention the results from (p,2p) [26] and (p,d) [27] experiments on single s-nucleon removal involving the same targets. In the corresponding separation energy spectra, a peak which is $\sim$ 20-30 MeV wide occurs at a one-nucleon separation energy of 27-34 MeV, depending on the target. In the (p,d) results, there is even some structure in this broad peak. From the analogy between p^{-1} peaks in (p,2p) results and p^{-2} peaks in $(\pi^-,2n)$ results mentioned earlier, we expect s^2-removal to appear at considerably higher E_s than one-nucleon removal. In addition, the peak should be wide, with possible fine structure.

Our excitation spectra are shown in Figs. 4, 6, 8. None of these spectra show such a clear and distinct peak at higher E_x as was observed in ^6Li or ^7Li. In ^{12}C we cannot confirm the separated s^{-2} peak, reported by Cheshire and Sobottka. This is in spite of the fact that our experimental set-up covers a much ω-range.

Because of the large separation energies of s-shell nucleons, one expects wide q-distributions for the corresponding peaks. In order to be more sensitive

to those states, we show in Fig. 12 the excitation spectra for events with large recoil momentum for ^{9}Be, ^{10}B, and ^{12}C, respectively. From these spectra several observations can be made. Although there is no broad, dominant peak at higher separation energies, we observe many events in this region. It should also be kept in mind that owing to the energy threshold of 15 MeV for one neutron, the high E_x-region is already somewhat suppressed. Apart from the structure at small excitation energies discussed in Section 4, structures at higher energies are visible. In the ^{12}C spectrum we recognize a peak at $E_s \sim 36.5$ MeV, followed by a dip at 42 MeV; in the case of ^{9}Be there are one or two peaks around 36 MeV and a dip at 43 MeV, and in ^{10}B a peak at 40 MeV and a dip at 45 MeV.

For the peaks just mentioned, q- and θ-distributions are shown in Fig. 13. The q-distributions are relatively wide (compared, for instance, with the 10.5 MeV peak in ^{9}Be); they increase towards q = 0 and thus indicate L = 0 dominance. The interpretation of these three narrow peaks is not simple. As the separation energies are slightly too high for p^2-removal, they might be contributions from sp-removal. The q-distributions, however, do not support this picture.

In the higher excitation-energy region, it can be expected that the contribution of mechanisms other than quasi-free 2N absorption becomes important. In fact, Favier et al.[7] estimate that in their ω-range, which is comparable to ours, half the events are due to other processes. On the other hand, our observed structure in the high excitation-energy region seems to support the quasi-free 2N process.

In order to investigate the relative contributions of these two processes, a comparison of separation energy spectra with different windows in ω and in q is shown in Figs. 14 and 15. From this comparison several remarks can be made: in the spectra with ω-windows (Fig. 14), it can be seen that for ^{9}Be, up to $E_s \sim$ $\sim$ 35 MeV, the ω-distribution is decreasing with decreasing ω, whereas beyond this point it is rather flat. For ^{12}C the distribution becomes flat at E_s = 30-37 MeV, and beyond this energy range the distribution is slightly increasing. The ^{10}B target seems to be exceptional. The ω-distribution is decreasing everywhere, although its inclination changes at $E_s \sim 34$ MeV.

In the spectra with q-windows (Fig. 15), it can be seen that the q-distribution changes rather drastically at $E_s \sim 48$ MeV for ^{12}C. Below this energy the distribution is decreasing with increasing q, whereas beyond this point it is almost flat. An indication of the same behaviour is observed in ^{9}Be. The target ^{10}B is again very different. The region where the q-distributions are decreasing continues up to $E_s \sim 70$ MeV. The sudden change of the q-distribution mentioned above can be understood if it is postulated that, at this separation energy, s^2-removal replaces p^2-removal. In the latter case, according to our observation, the

dominant transitions come from 2S ($\mathcal{N}$ = 1, L = 0), showing a narrow q-distribution. In the case of s^2-removal, however, only transitions corresponding to 1S ($\mathcal{N}$ = 0, L = 0) are allowed. This causes a considerably wider q-distribution, in addition to the widening of the q-distribution owing to the larger separation energy.

The processes other than the quasi-free 2N absorption are expected to produce distributions that do not critically depend on the target nucleus, if the mass is similar. In the separation energy spectra for q-windows as well as for ω-windows, ^{10}B is very different from the other targets. This difference can also be seen in the ω distributions for the range of separation energies between 48 MeV and 70 MeV, as shown in Fig. 16. It seems therefore not very likely that processes other than quasi-free 2N absorption are dominant in this energy range.

This conclusion is also supported by the absolute rates. In Table 1 the integrated rates per stopped pion for the low E_s-region as well as for the high E_s-region are given for all three target nuclei. The numbers correspond to the ω-range from 145° to 180°. In the low E_x-region the observed ω-distributions are strongly peaked at 180° and hence our set-up covers nearly all events. This is certainly no longer the case in the high E_x-region, because there the ω-distributions are much wider. An isotropic ω-distribution, however, can be excluded, because in this case the extrapolated rates per stopped pion integrated over all the ω-range would far exceed 100%. A non-isotropic ω-distribution can in turn be more easily explained by direct processes.

6. CONCLUSIONS

It was shown that for all three targets, ^{9}Be, ^{10}B, ^{12}C, studied in our experiment, the prominent peaks in the low excitation-energy region can be attributed to known levels, and that their population is in a qualitative agreement with the c.f.p. calculations for the p-shell nucleons.

In these target nuclei, as well as in ^{14}N, a surprising similarity has been found between the systematics of the two-nucleon separation energy E_s of the two-hole states strongly populated in the (π^-,2n) reaction, and the one-nucleon separation energy of the single-hole states observed in the (p,2p) reaction. This could be explained by a strong correlation between proton and neutron in the same orbit.

For the p^2-removal, the small width of the q-distributions for Λ = 0 transitions and the general weakness of Λ = 2 transitions seem to indicate that the pion absorption by a nucleon pair in relative 1s-state is favoured compared to the 2s- as well as the 1d-states.

Relatively high rates have been observed for the transitions leading to high separation energies. Although no quantitative conclusion on the relative

contribution of s^2-removal and non-quasi-free 2N processes could be made, the absolute rate corresponding to this E_s region in our ω-range, as well as the structure observed in the excitation spectra, seem to support the importance of the s^{-2} process.

A comparison between our excitation spectra and those from the low-energy $(\pi^+,2p)$ reaction shows that, within the experimental precision, the relative population of the residual levels is very similar in these reactions. For the nuclei studied here, we conclude therefore that the relative population does not depend on whether the pion is absorbed from atomic orbits or in flight.

Acknowledgements

We would like to express our thanks to all the members of the SC group for their collaboration, and in particular to Dr. E.G. Michaelis, who also carefully read the manuscript.

Table 1

Integrated rates per stopped pion for different E_s-regions. The numbers are corrected with respect to geometrical efficiencies in the ω-range between 145° and 180°.

	E_s < 35 MeV	E_s > 35 MeV
^{9}Be	14.5%	22%
^{10}B	12.5%	16%
^{12}C	10%	16%

REFERENCES

1) T. Ericson, Phys. Letters 2, 278 (1962).

2) J.W. Morris and H.J. Weber, Ann. Phys. (USA) 79, 34 (1973).

3) H. Garcilazo and J.M. Eisenberg, Nuclear Phys. A220, 13 (1974).

4) T.I. Kopaleishvili, I.Z. Machabeli and M.Sh. Chachkhunashvili, Soviet J. Nuclear Phys. 15, 629 (1972).

5) C. Cohen and D. Kurath, Nuclear Phys. A141, 145 (1970).

6) V.V. Balashov, A.N. Boyarkina and I. Rotter, Nuclear Phys. 59, 417 (1964).

7) J. Favier, T. Bressani, G. Charpak, L. Massonnet, W.E. Meyerhof and Č. Zupančič, Nuclear Phys. A169, 540 (1971).

8) E.D. Arthur, W.C. Lam, J. Amato, D. Axen, R.L. Burman, P. Fessenden, R. Macek, J. Oostens, W. Shlaer, S. Sobottka, M. Salomon and W. Swenson, Phys. Rev. C 11, 332 (1975).

9) D.L. Cheshire and S.E. Sobottka, Nuclear Phys. A146, 129 (1970).

10) F. Calligaris, C. Cernigoi, I. Gabrielli and F. Pellegrini, Nuclear Phys. A126, 209 (1969).

11) B. Bassalleck, H.D. Engelhardt, M. Furić, E.L. Haase, W.D. Klotz, C.W. Lewis, F. Takeutchi and H. Ullrich, Phys. Letters 65B, 128 (1976).

12) R.L. Burman and M.E. Nordberg, Jr., Phys. Rev. Letters 21, 229 (1968).

13) B. Bassalleck, D. Engelhardt, M. Furić, W.-D. Klotz, C.W. Lewis, F. Takeutchi and H. Ullrich, Meson-Nuclear Physics 1976 (eds. P.D. Barnes et al.) (AIP, New York, 1976), p. 272.

14) D.S. Koltun, Phys. Rev. 162, 962 (1967).

15) Y. Sakamoto, P. Cüer and F. Takeutchi, Phys. Rev. C 11, 668 (1975).

16) F. Takeutchi, B. Kober and E.L. Haase, Large-area, position-sensitive time-of-flight counters for neutrons and charged particles, CERN preprint, 1 July 1975, presented at the Journées d'étude de physique nucléaire à moyennes énergies, IPN, Orsay, 1975.

17) R.J. Kurz, UCRL-11339 (1964).

18) F.C. Barker, Nuclear Phys. 83, 418 (1966).

19) C. Détraz, J. Cerny and R.H. Pehl, Phys. Rev. Letters 14, 708 (1965); J. Cerny, C. Détraz and R.H. Pehl, Phys. Rev. 152, 950 (1966).

20) S. Meshkov and C.W. Ufford, Phys. Rev. 101, 734 (1956).

21) F. Ajzenberg-Selove and T. Lauritsen, Nuclear Phys. A227, 1 (1974).

22) S. Ozaki, R. Weinstein, O. Glass, E. Lock, L. Neimala and A. Wattenberg, Phys. Rev. Letters 4, 533 (1960).

23) M.E. Nordberg, K.F. Kinsey and R.L. Burman, Phys. Rev. 165, 1096 (1968).

24) H.O. Funsten, W.J. Kossler and C.E. Stronach, Bull. APS 17, Ser. 2, 464 (1972).

25) J.-Y. Grossiord, Thesis, Université de Lyon (1976).

26) G. Jacob and A.J. Maris, Rev. Mod. Phys. 38, 121 (1966), and references therein.

27) B. Fagerström and J. Källne, Phys. Scripta 8, 14 (1973).

Figure captions

Fig. 1 : Kinematical variables used in the text.

Fig. 2 : Recoil momentum distributions as measured for the 10.5 MeV level in ^{7}Li (○), and for the 7 MeV level in ^{10}B (●). The curves correspond to 1S, 2S, and 1D c.m. states and are calculated in the same manner as described in Ref. 15. A square well potential has been used, and the parameter in the n-p relative wave function is chosen according to the electron scattering data.

Fig. 3 : Experimental set-up. For details see text.

Fig. 4 : Excitation energy spectrum for the residual nucleus ^{7}Li. Upper curve: all data; lower curve: events with $q < 100$ MeV/c.

Fig. 5 : q- and θ-distributions for three peaks in the E_x spectrum of ^{7}Li. For the θ-distributions, q has been restricted to less than 220 MeV/c, 210 MeV/c, and 200 MeV/c from top to bottom.

Fig. 6 : Excitation energy spectrum for the residual nucleus ^{8}Be. Upper curve: all data; middle curve: events with $q < 100$ MeV/c; lower curve: events with $q > 140$ MeV/c. Results of c.f.p. calculations from Ref. 5 (CK) and Ref. 6 (BBR) are indicated on top of the figure. For (CK) the solid lines refer to $T = 0$ and dashed lines to $T = 1$. For (BBR), solid lines refer to $\Lambda = 2$, $T = 0$, and the dashed line to $\Lambda = 0$, $T = 0$.

Fig. 7 : q- and θ-distributions for two peaks in the E_x-spectrum of ^{8}Be. For the θ-distributions, q has been restricted to less than 190 MeV/c and 170 MeV/c for the lower and higher E_x-window, respectively.

Fig. 8 : Excitation energy spectrum for the residual nucleus ^{10}B. Upper curve: all data; lower curve: events with $q < 100$ MeV/c. Results of c.f.p. calculations from Ref. 5 (CK) and Ref. 6 (BBR) for $T = 0$ (solid lines) and $T = 1$ (dashed lines) are indicated on top of the figure.

Fig. 9 : q- and θ-distributions for three peaks in the E_x spectrum of ^{10}B. For the θ-distributions, q has been restricted to less than 180 MeV/c, 170 MeV/c, and 165 MeV/c from top to bottom.

Fig. 10 : Measured (●) ω-distribution from the reaction $^{12}C(\pi^-,2n)^{10}B$, integrated over all E_x, compared with the theoretical prediction (curve) of Ref. 3 with correlation parameter $r_c = 0.6$ fm. The two distributions have been normalized at 180°.

Fig. 11 : Comparison of separation energies for the removal of one (dashed lines) and two (solid lines) nucleons for the three targets measured in this experiment and for ^{14}N from Ref. 11.

Fig. 12 : Comparison of E_s spectra with q > 140 MeV/c for the three targets. E_x scales are also shown.

Fig. 13 : q- and θ-distributions for three peaks in the intermediate E_x-region. For the θ-distributions, q has been restricted to less than 160 MeV/c.

Fig. 14 : Separation energy spectra for different ω-windows for the three targets. Curves I to V correspond to windows in (-cos ω) of 0.820-0.856; 0.856-0.892; 0.892-0.928; 0.928-0.964, and 0.964-1.00, respectively.

Fig. 15 : Separation energy spectra for different q-windows for the three targets.

Fig. 16 : Comparison of ω-distributions for the three targets, for small and large separation energies.

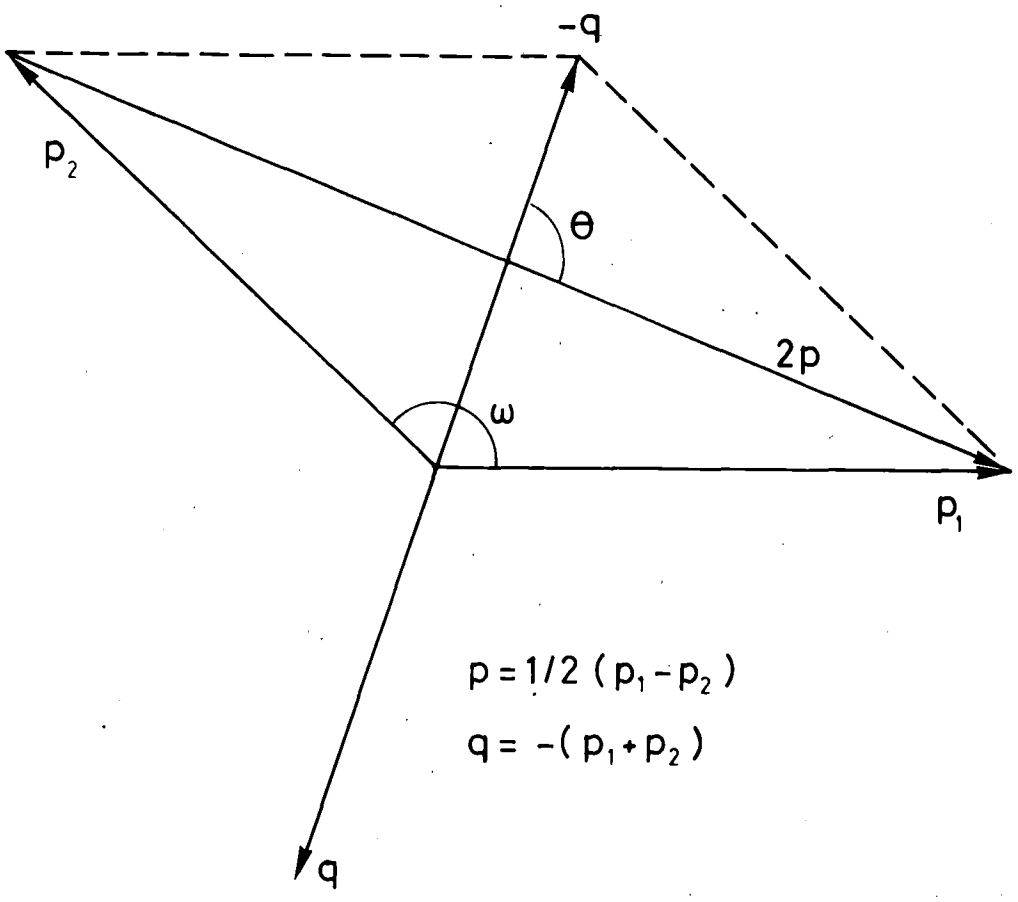

Fig. 1

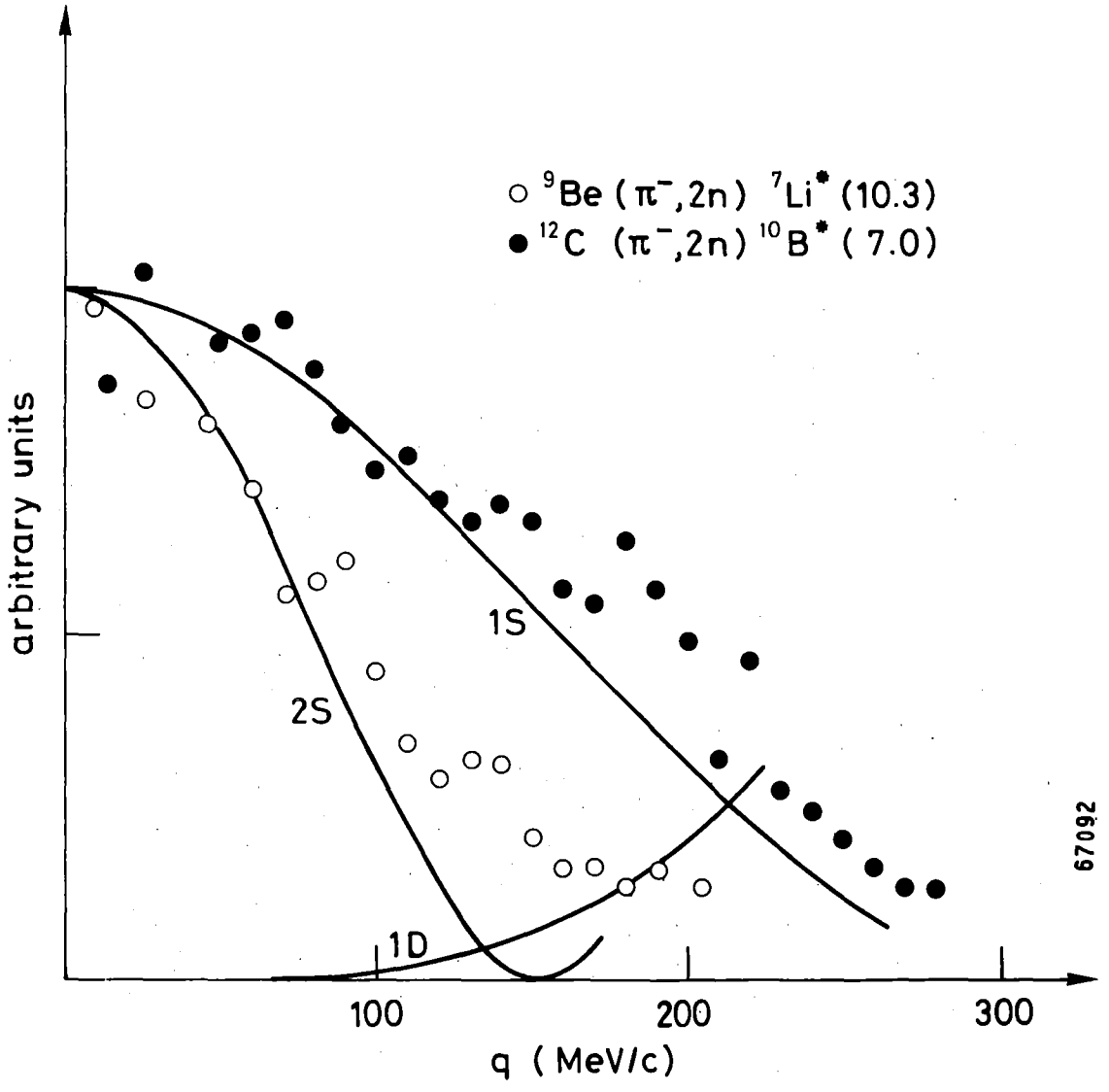
○ ^{9}Be (π^-,2n) ^{7}Li* (10.3)
● ^{12}C (π^-,2n) ^{10}B* (7.0)
arbitrary units
1S
2S
1D
100
200
300
q (MeV/c)
67092

Fig. 2

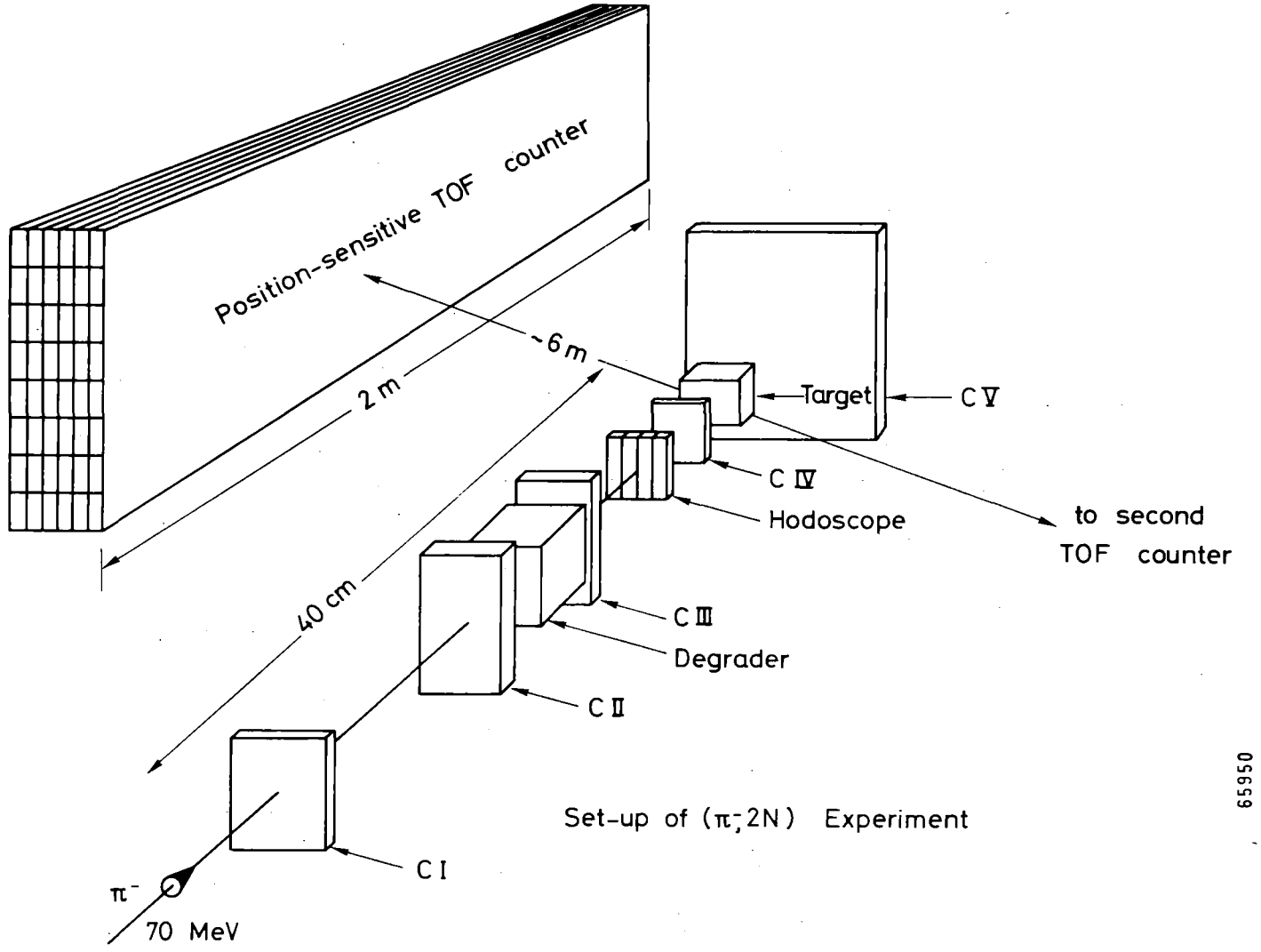

Set-up of (π⁻,2N) Experiment

Fig. 3

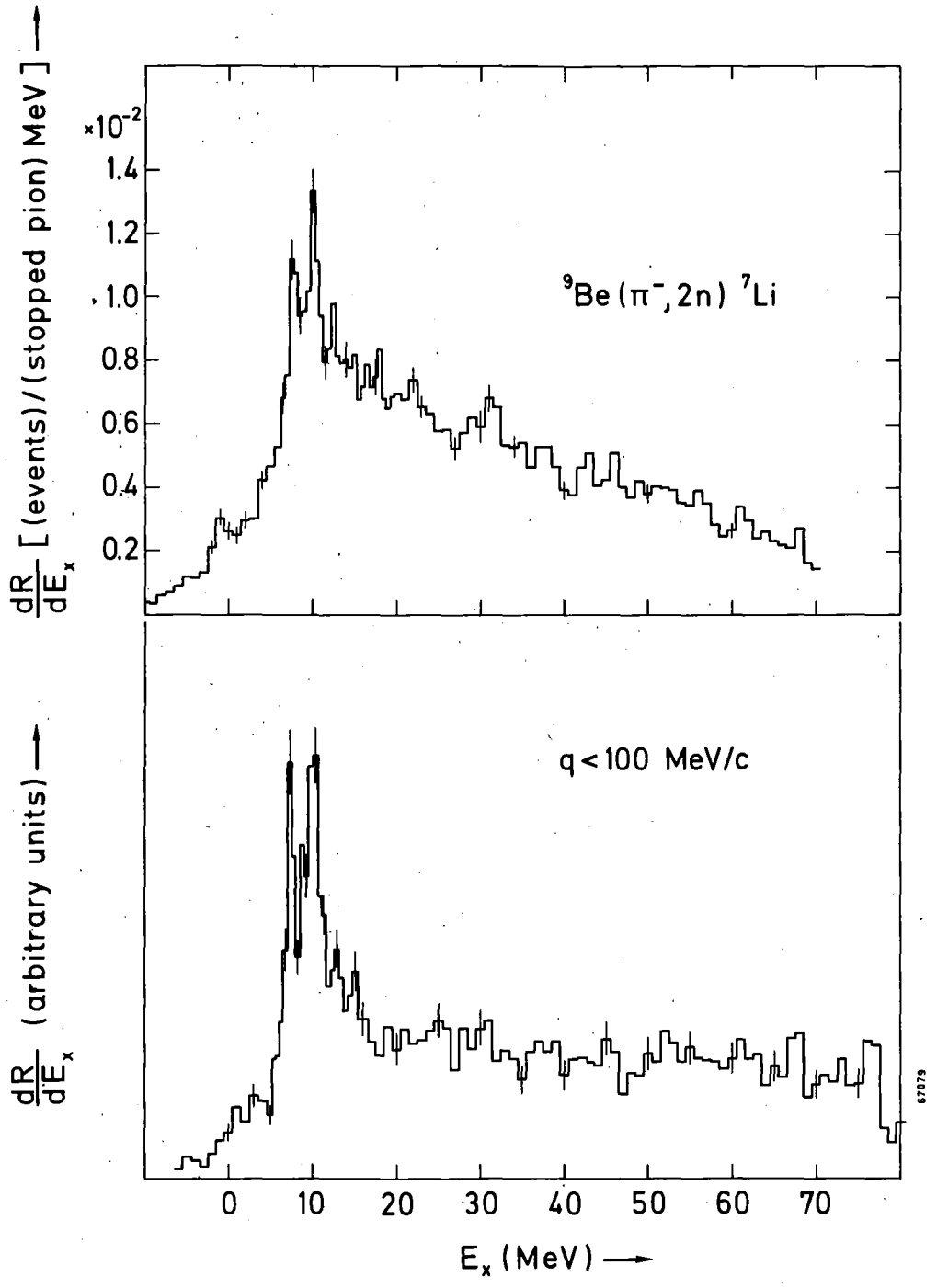
$\frac{dR}{dE_x}$ [(events)/(stopped pion) MeV] ⟶
×10⁻²
1.4
1.2
1.0
0.8
0.6
0.4
0.2
⁹Be(π⁻, 2n) ⁷Li
q < 100 MeV/c
$\frac{dR}{dE_x}$ (arbitrary units) ⟶
0
10
20
30
40
50
60
70
E_x (MeV) ⟶
67079

Fig. 4

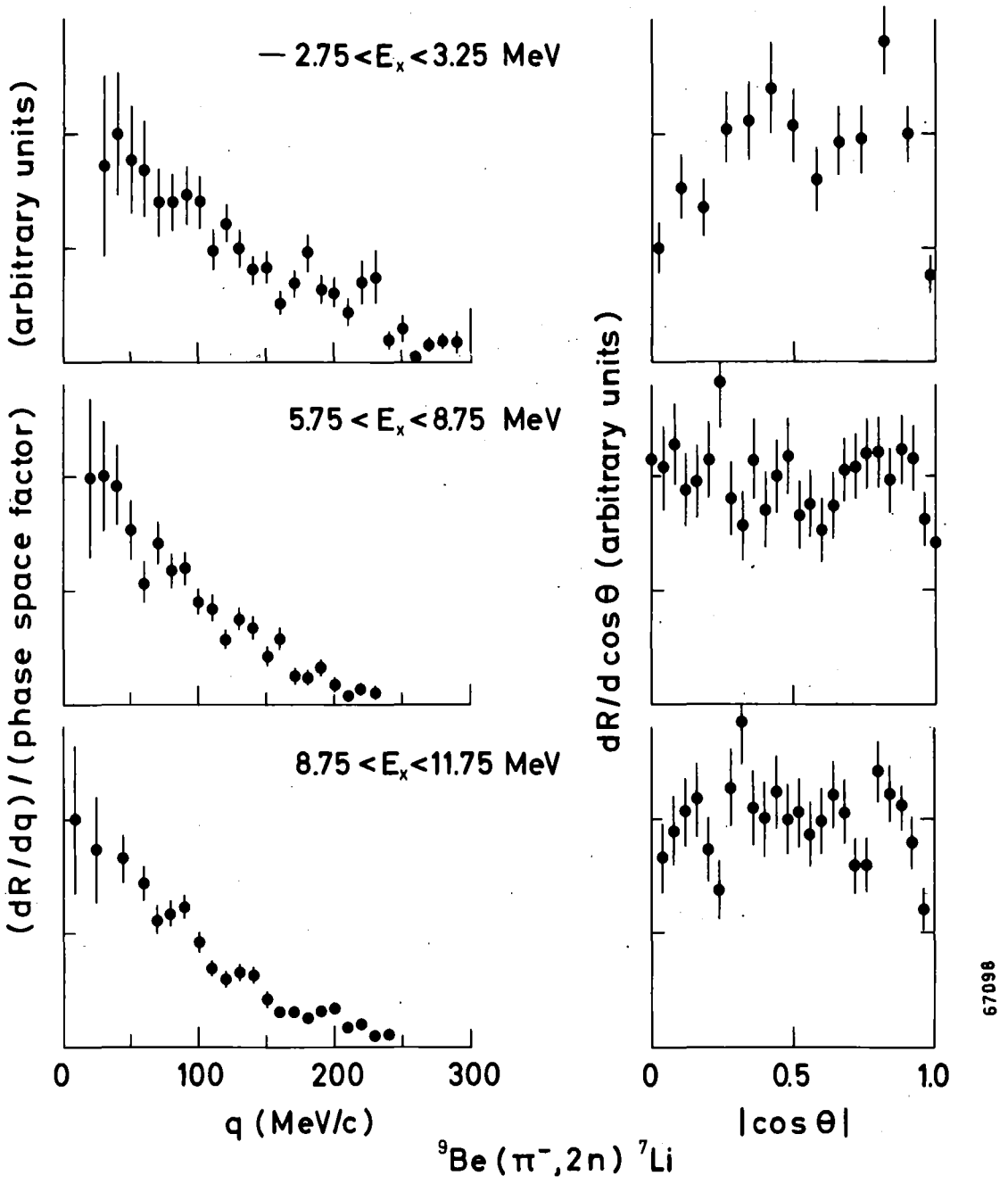
— 2.75<E$_x$<3.25 MeV
5.75 < E$_x$ < 8.75 MeV
8.75 < E$_x$ < 11.75 MeV
(dR/dq) / (phase space factor) (arbitrary units)
dR/d cos θ (arbitrary units)
0
100
200
300
q (MeV/c)
0
0.5
1.0
|cos θ|
^{9}Be (π$^-$, 2n) ^{7}Li
67098

Fig. 5

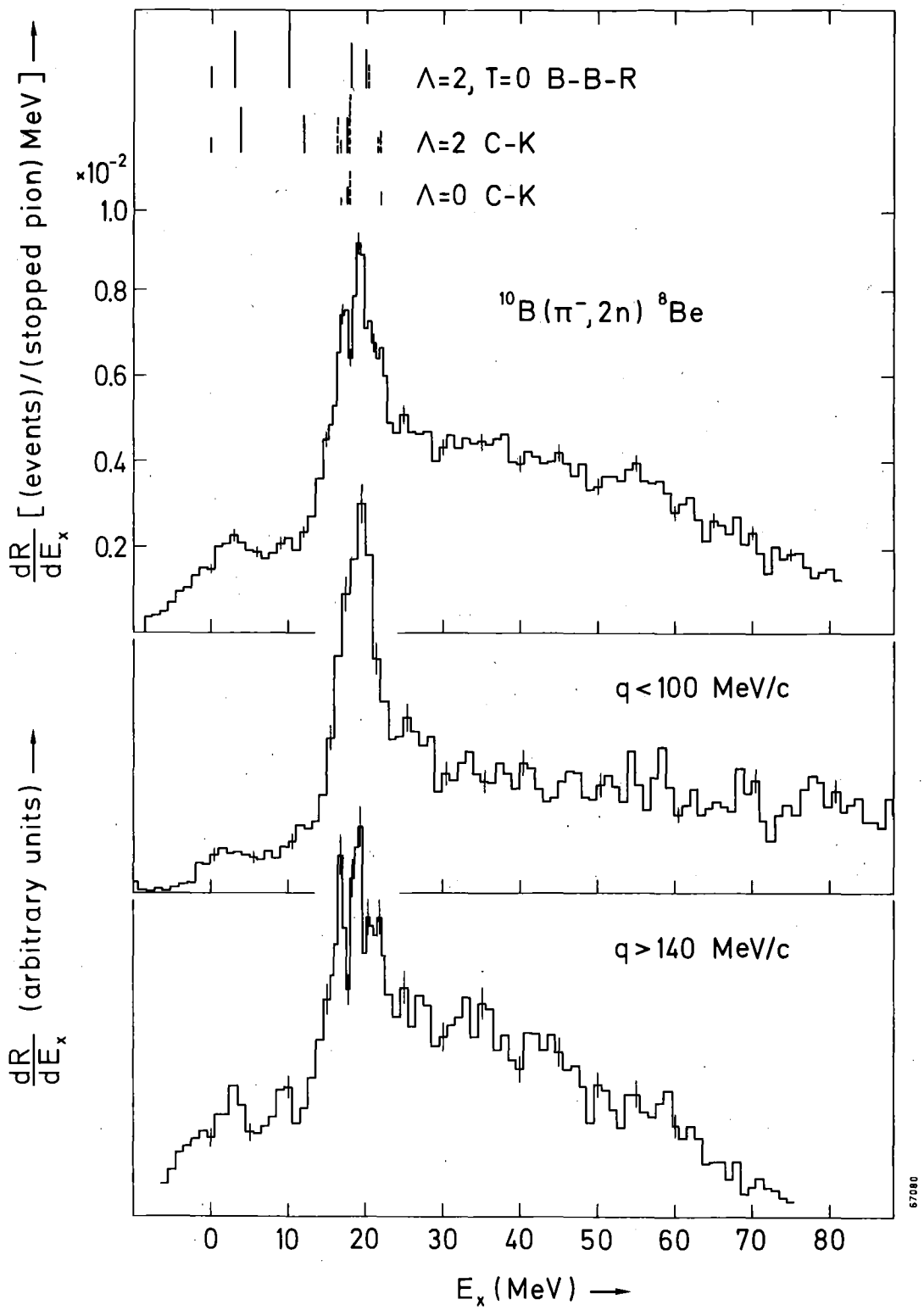
Λ=2, T=0 B-B-R
Λ=2 C-K
Λ=0 C-K
×10⁻²
1.0
0.8
0.6
0.4
0.2
¹⁰B(π⁻,2n) ⁸Be
dR/dE_x [(events)/(stopped pion) MeV] →
q<100 MeV/c
q>140 MeV/c
dR/dE_x (arbitrary units) →
0
10
20
30
40
50
60
70
80
E_x (MeV) →
67080

Fig. 6

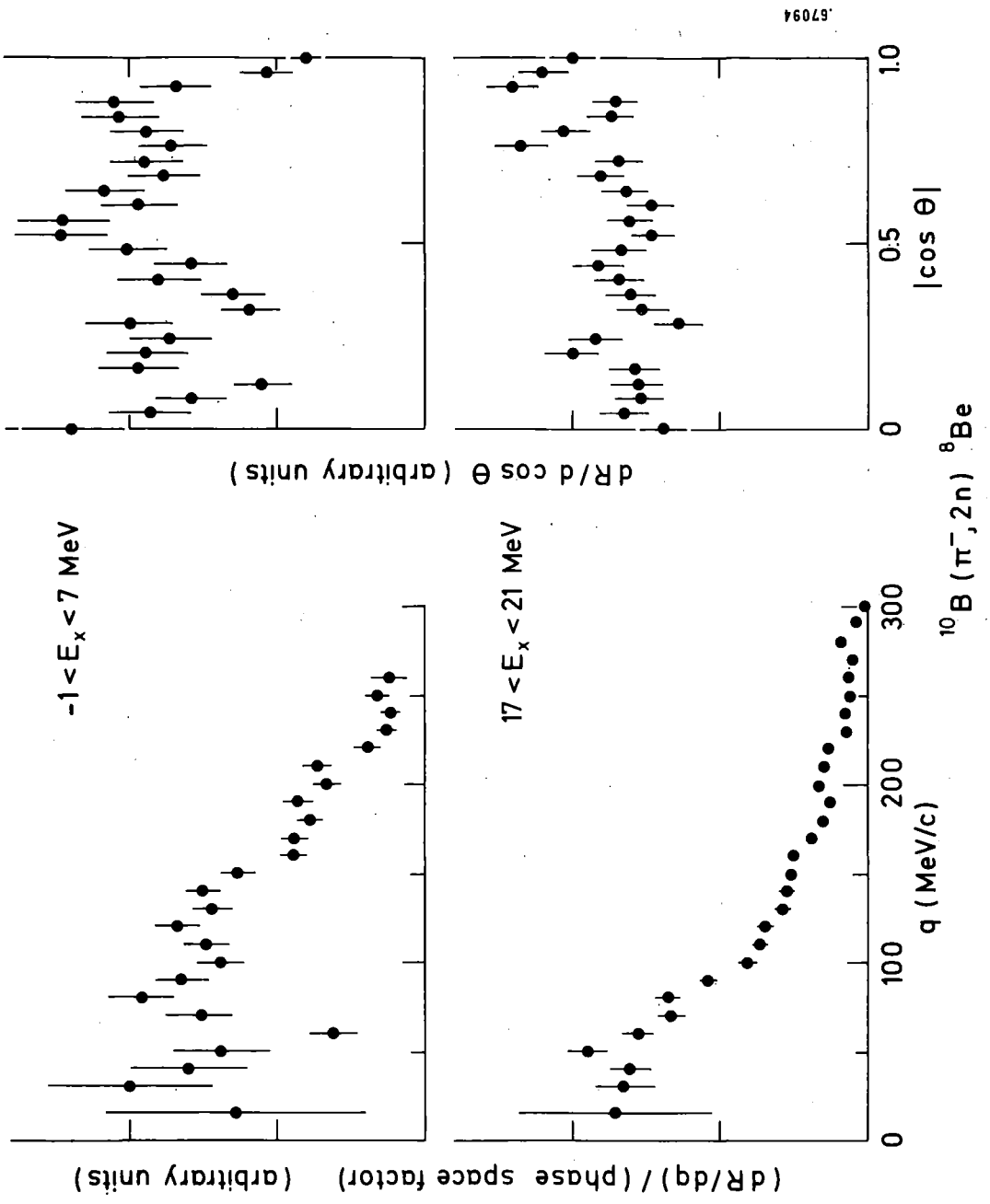
.67094
dR/d cos Θ (arbitrary units)
0
0.5
1.0
|cos Θ|
^{10}B (π$^-$, 2n) ^{8}Be
17 < E$_x$ < 21 MeV
-1 < E$_x$ < 7 MeV
(dR/dq) / (phase space factor) (arbitrary units)
0
100
200
300
q (MeV/c)

Fig. 7

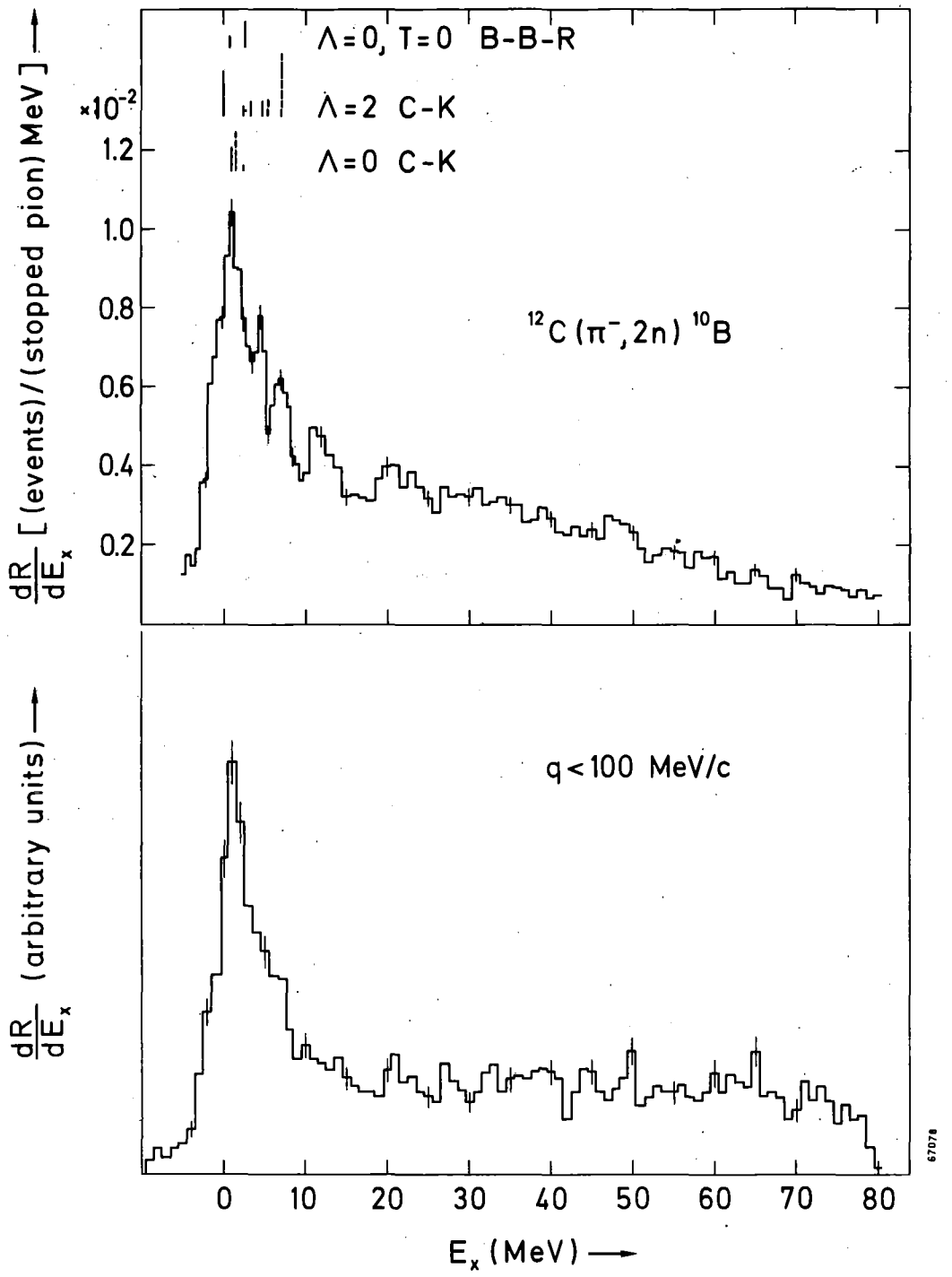
Λ=0, T=0 B-B-R
Λ=2 C-K
Λ=0 C-K
×10⁻²
1.2
1.0
0.8
0.6
0.4
0.2
dR/dE_x [(events)/(stopped pion) MeV]
¹²C (π⁻, 2n) ¹⁰B
q<100 MeV/c
dR/dE_x (arbitrary units)
0
10
20
30
40
50
60
70
80
E_x (MeV)
67078

Fig. 8

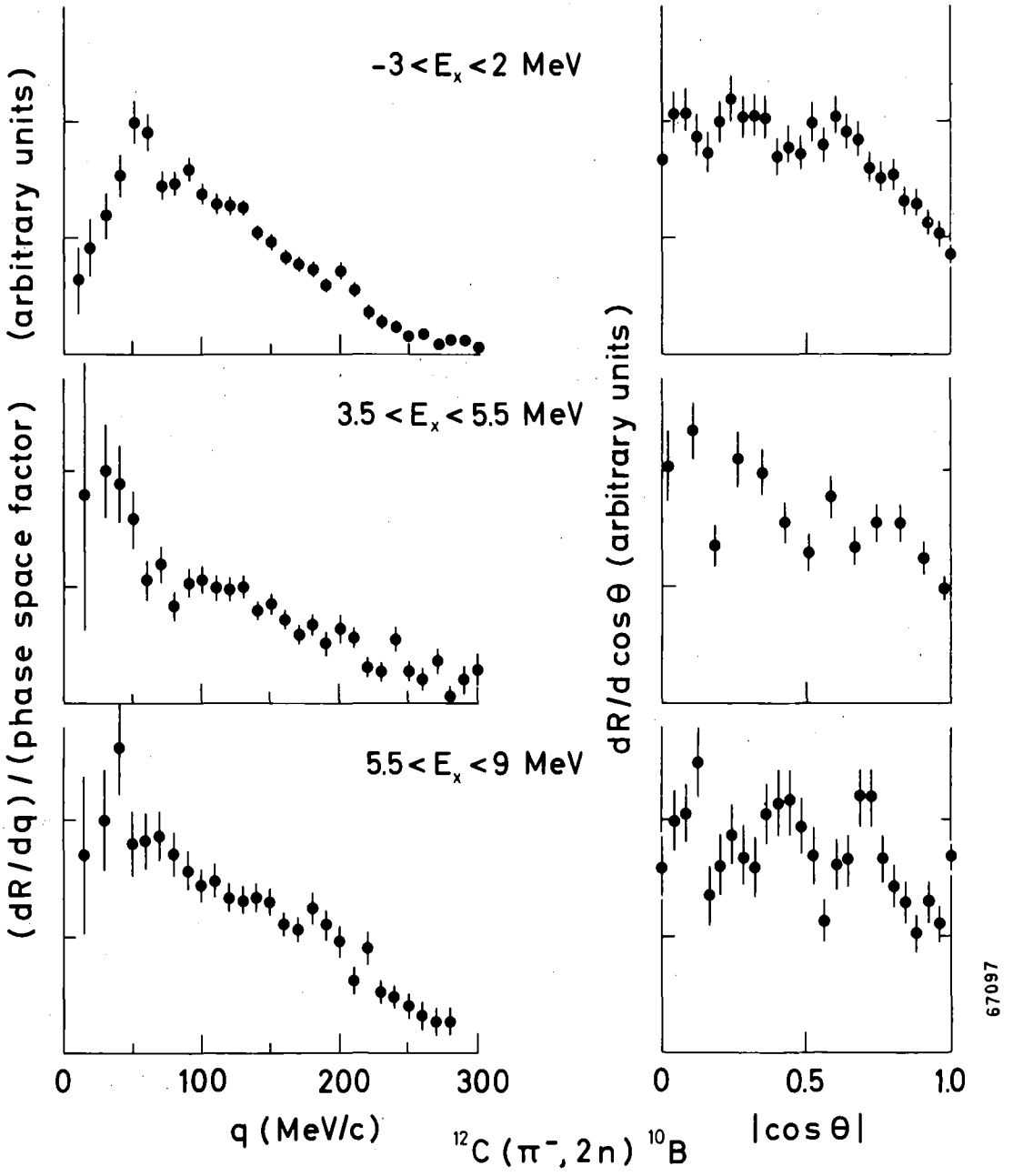
-3 < E_x < 2 MeV
3.5 < E_x < 5.5 MeV
5.5 < E_x < 9 MeV
(dR/dq) / (phase space factor)
(arbitrary units)
dR/d cos θ (arbitrary units)
0
100
200
300
q (MeV/c)
0
0.5
1.0
|cos θ|
12C (π⁻, 2n) 10B
67097

Fig. 9

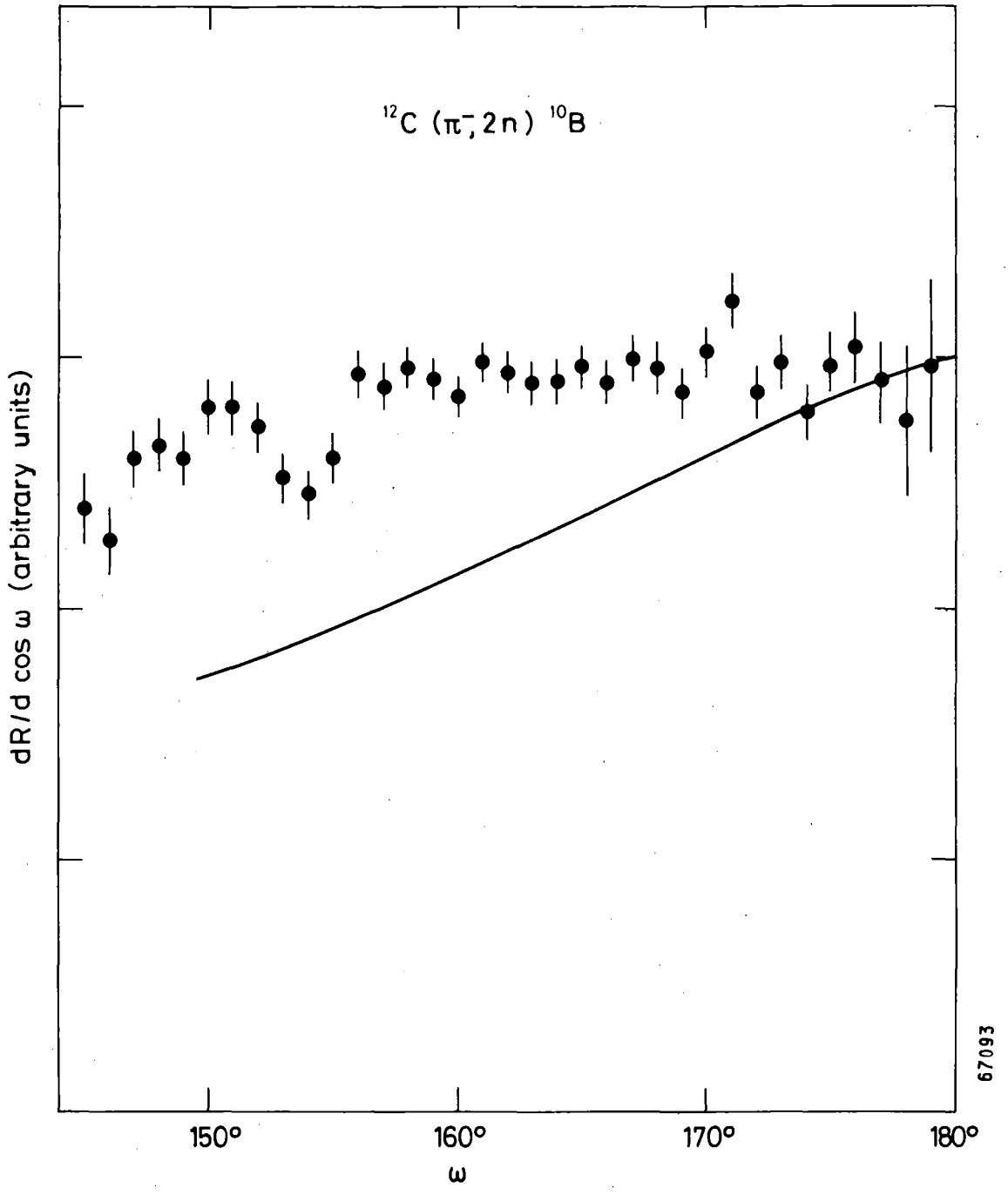

Fig. 10

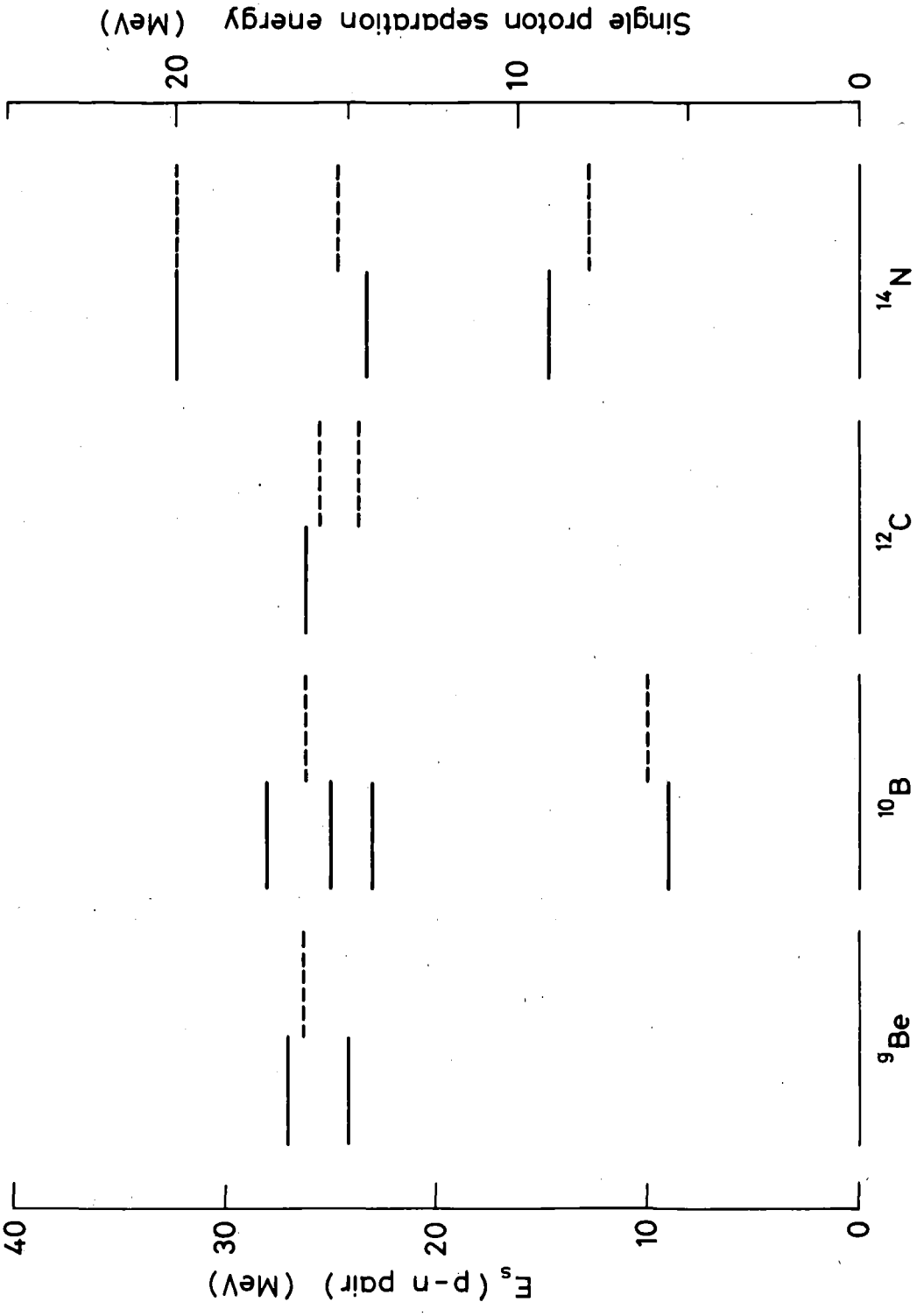
Single proton separation energy (MeV)
20
10
0
^{14}N
^{12}C
^{10}B
^{9}Be
E_s (p-n pair) (MeV)
40
30
20
10
0

Fig. 11

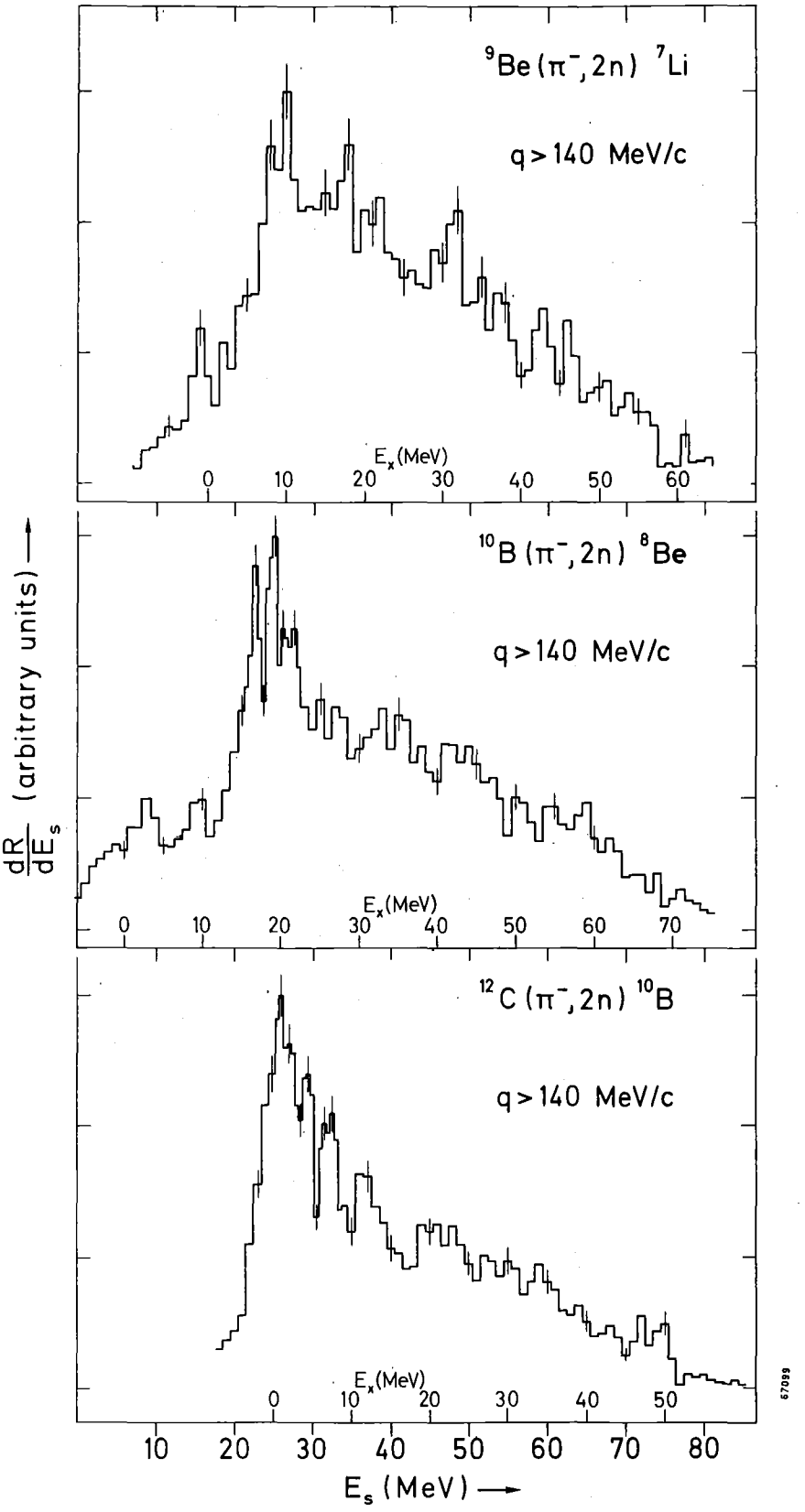
$^{9}Be(\pi^-,2n)\ ^{7}Li$
q > 140 MeV/c
E_x(MeV)
0 10 20 30 40 50 60
$^{10}B(\pi^-,2n)\ ^{8}Be$
q > 140 MeV/c
E_x(MeV)
0 10 20 30 40 50 60 70
$^{12}C(\pi^-,2n)\ ^{10}B$
q > 140 MeV/c
E_x(MeV)
0 10 20 30 40 50
$\frac{dR}{dE_s}$ (arbitrary units) →
10 20 30 40 50 60 70 80
E_s (MeV) →
67099

Fig. 12

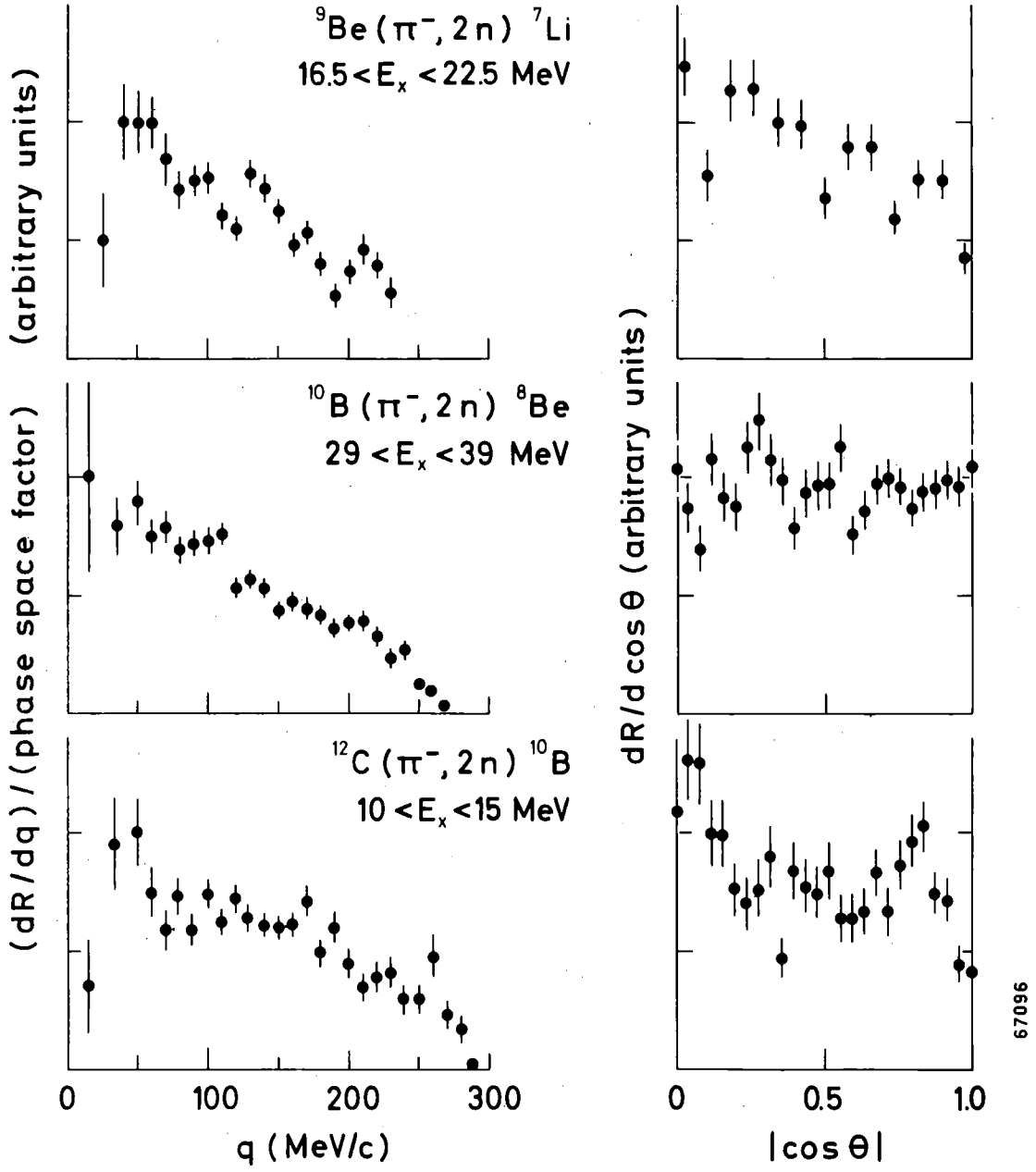
^{9}Be (π⁻, 2n) ^{7}Li
16.5 < E_x < 22.5 MeV
^{10}B (π⁻, 2n) ^{8}Be
29 < E_x < 39 MeV
^{12}C (π⁻, 2n) ^{10}B
10 < E_x < 15 MeV
(dR/dq) / (phase space factor) (arbitrary units)
dR/d cos θ (arbitrary units)
0
100
200
300
q (MeV/c)
0
0.5
1.0
|cos θ|
67096

Fig. 13

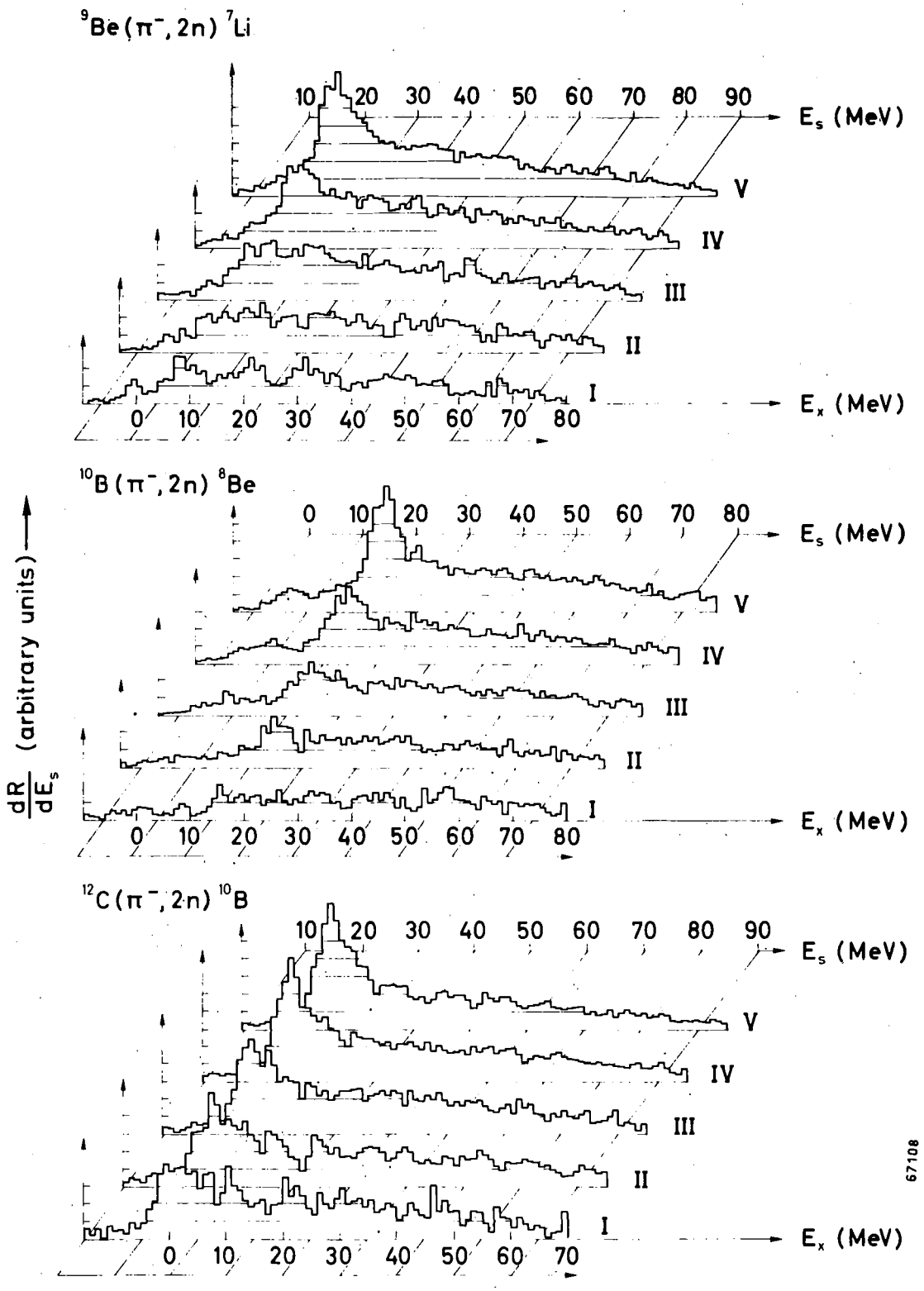
$^{9}Be(\pi^-, 2n)\,^{7}Li$
$^{10}B(\pi^-, 2n)\,^{8}Be$
$^{12}C(\pi^-, 2n)\,^{10}B$
$\frac{dR}{dE_s}$ (arbitrary units)
E_s (MeV)
E_x (MeV)
I
II
III
IV
V
67108

Fig. 14

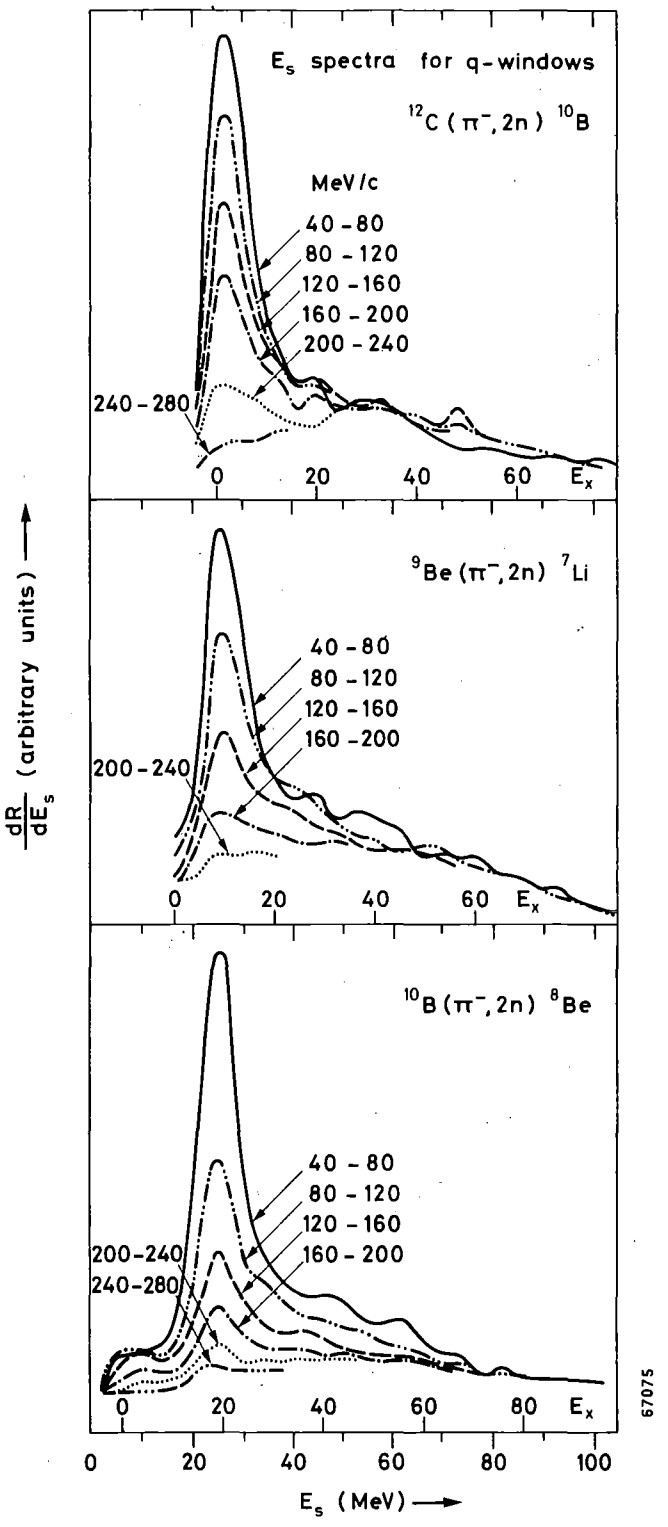
E_s spectra for q-windows
$^{12}C(\pi^-, 2n)\ ^{10}B$
MeV/c
40 - 80
80 - 120
120 - 160
160 - 200
200 - 240
240 - 280
0 20 40 60 E_x
$^{9}Be(\pi^-, 2n)\ ^{7}Li$
40 - 80
80 - 120
120 - 160
160 - 200
200 - 240
0 20 40 60 E_x
$^{10}B(\pi^-, 2n)\ ^{8}Be$
40 - 80
80 - 120
120 - 160
160 - 200
200-240
240-280
0 20 40 60 80 E_x
0 20 40 60 80 100
E_s (MeV) ⟶
$\frac{dR}{dE_s}$ (arbitrary units) ⟶
67075

Fig. 15

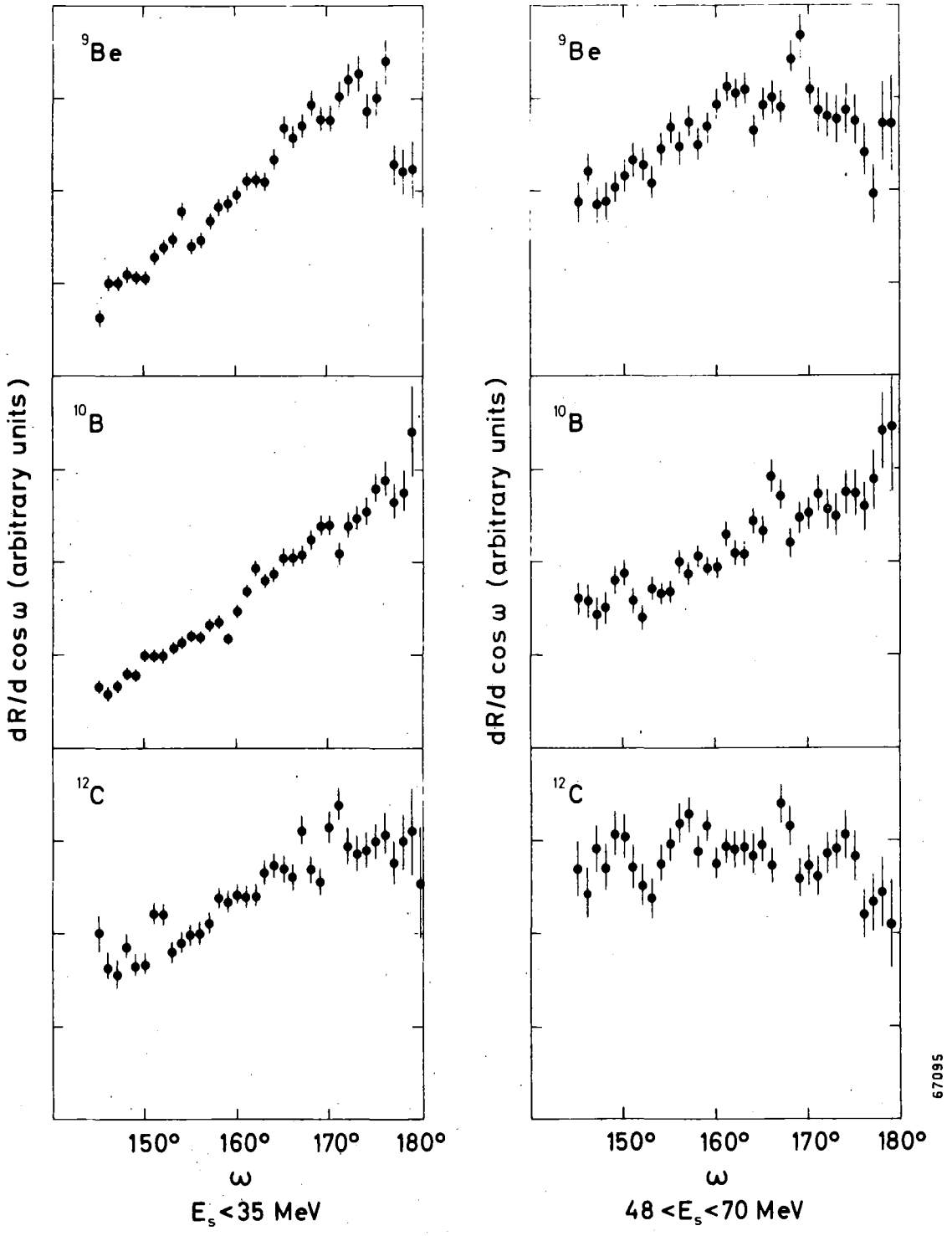
^{9}Be
^{10}B
^{12}C
dR/d cos ω (arbitrary units)
150°
160°
170°
180°
ω
E_s<35 MeV
48 <E_s<70 MeV
67095

Fig. 16